Diss. ETH No. 22381

RISK IN COMPLEX NETWORKS

A thesis submitted to attain the degree of

DOCTOR OF SCIENCES of ETH ZURICH

(Dr. sc. ETH Zurich)

presented by

VITOR HUGO LOUZADA PATRICIO

MSc in Bioinformatics, University of São Paulo

born on 15.09.1986

citizen of
Brazil

accepted on the recommendation of

PROF. DR. HANS JÜRGEN HERRMANN, examiner

PROF. DR. DIDIER SORNETTE, co-examiner

PROF. DR. JOSE S. ANDRADE JR., co-examiner

2014

para Helen,

A fool and his head are soon parted.
— KLINGON PROVERB [1].

Acknowledgements

Dear God,

Herewith I submit for publication my doctoral thesis entitled "Risk in Complex Networks" where I address how to convert three years of results, learning, suffering, and fun into a meaningful document that I am grateful, and glad, to have finished[1].

This thesis contains numerous co-authors which actively helped me to be here today, but unfortunately listing all of them would easily reach my page limit. I could not however miss the opportunity to leave a special thanks to Helen, who took care of me at home, Nuno, Tomassini, and Soares, who guided me at work, my lab mates (Trivik, Dominik, Nicolas, Ilias, Julian, Ryuta, Miller, Farhang, Roman Mani, Jens-Daniel, Katerina, Fabrizio, Gautam, Kornel, Roman Vetter, Konstantin, Alessandro, Felipe, Klara, Fabio Daolio, Hygor, Eduardo, and Heitor, here ordered based on their seats position), who guaranteed my sanity, my family, who I love so much, and the 50% discount products at Coop, who kept me going.

I would therefore appreciate if you could consider this work for publication.

Yours Sincerely,
The Author

Zusammenfassung

Naturkatastrophen, Finanzkrisen und Ausbrüche von Epidemien werden gemeinhin als Ereignisse betrachtet, deren Auswirkungen durch frühe Identifikation potentieller Gefahren gemildert werden könnten. Allerdings mangelt es Risikoeinschätzungsstudien an einheitlichen Methoden. In dieser Doktorarbeit verwenden wir eine einheitliche theoretische Grundlage, nämlich Netzwerktheorie, um scheinbar unterschiedliche Anwendungen in der wirklichen Welt zu behandeln. Wir vereinfachen diese Systeme, erfassen dabei immernoch ihre wichtigsten Eigenschaften und stellen neue Methoden vor, um Einblicke in ihr Verhalten zu gewinnen. Wir erwarten, dass unsere Herangehensweise auch auf andere Gegebenheiten ausgedehnt werden kann. Insbesondere stellen wir komplexe Systeme entweder als statische oder dynamische Netzwerke dar; dabei ist bei ersteren das Augenmerk auf die Risiken bestimmter Wechselwirkungsmuster gerichtet und bei letzteren auf die zeitliche Entwicklung dieser Wechselwirkungen. Was statische Netzwerke betrifft, stellen wir zwei neue Methoden zur Optimierung von Stabilitätsrisiken vor — eine, die auf schnelle Optimierung, und eine andere, welche auf räumlich eingebettete Netzwerke abzielt. Wir studieren das Synchronisationsverhalten dynamischer Netzwerke in der Gegenwart desynchronisierender Agenten. Des weiteren wird die Zerbrechlichkeit der Synchronisation zweier gekoppelter Netzwerke betrachtet, die durch ein neuartiges Atemverhalten überraschen. Die Grenze zwischen Dynamik und Statik ist jedoch nicht klar gezogen, sodass wir hier nicht nur beide Rahmenwerke getrennt gründlich untersuchen, sondern auch das Wechselspiel zwischen statischen und dynamischen Eigenschaften betrachten.

Summary

Natural catastrophes, financial crisis, and diseases outbreaks have all been considered as outcomes whose impact could be mitigated through the early identification of potential threats. Risk analysis studies however lack common techniques. In this thesis we make use of a common theoretical foundation, network theory, to deal with apparently distinct real applications. We simplify the systems, still grasping the most relevant features, and propose new techniques to get insights on their behavior, and expect that our approach could be extended to other situations as well.

In particular, we represent complex systems either as static or dynamic networks, the former focusing on the risk of certain interaction patterns and the latter on the time evolution of these interactions. For static networks, we propose two new methods of robustness risk optimization, one focusing on fast optimization and the other on spatially embedded networks. For dynamic networks, we analyze the synchronization risk of networks upon the introduction of agents that try to break synchronization. Also, we analyze the synchronization fragility of two coupled networks, reporting a surprisingly new breathing behavior. The frontier between static and dynamic however is not clearly defined and here we study in depth not only both frameworks separately but also look at the interplay between static and dynamic features.

Sumário

Catástrofes naturais, crises financeiras e surtos epidêmicos são considerados processos cujos impactos podem ser atenuados através da identificação precoce de potenciais ameaças. Estudos de análise de risco, no entanto, carecem de técnicas similares. Nesta tese, fazemos uso de uma base teórica comum - a teoria de redes - para lidar com aplicações reais aparentemente distintas. Simplificamos os sistemas, ainda mantendo as características mais relevantes, e propomos novas técnicas para obter uma análise compreensiva de risco sobre problemas diversos, esperando que nossa abordagem possa ser extendida a outras situações.

Em particular, representamos os sistemas complexos como redes estáticas ou dinâmicas - no primeiro caso focando no risco de certos padrões de interação e, no segundo, na evolução temporal dessas interações. Em redes estáticas, propomos dois métodos para otimização do risco de robustez, um centrado em uma otimização rápida e outro em redes espaciais. Em redes dinâmicas, analisamos o risco de sincronização a partir da introdução de agentes que tentam quebrar a sincronia. Além disso, analisamos a fragilidade da sincronização de duas redes acopladas e descobrimos um comportamento de batimento nunca antes reportado. A fronteira entre estática e dinâmica, contudo, não está claramente definida e aqui estudamos em profundidade não só ambos os quadros separadamente, como também a interação entre eles.

Résumé

Les catastrophes naturelles, crises financières et épidémies sont considérées comme des évènements dont l'impact pourrait être atténué par une identification précoce des risques potentiels. Cependant les études d'analyses de risques manquent de techniques adaptées. Dans cette thèse nous utilisons un fondement théorique commun, la théorie des réseaux, pour traiter des applications réelles a priori distinctes. Nous simplifions les systèmes, conservant leurs propriétés les plus importantes, et proposons de nouvelles techniques pour découvrir leur fonctionnement. Nous nous attendons à ce que notre approche puisse également être étendues à d'autres situations.

En particulier, nous traitons les systèmes complexes soit comme des réseaux statiques, soit comme des réseaux dynamiques. Dans le premier cas, nous nous intéressons au risque associé à certains types d'interactions et dans le second à leur évolution dans le temps. La frontière entre statique et dynamique n'est cependant pas clairement définie. Ici nous étudions en profondeur non seulement les deux cadres séparément, mais également l'interaction entre les propriétés statiques et dynamiques.

Contents

List of publications

Related to this thesis

- Louzada, V. H. P., Araújo, N. A. M., Andrade, J. S. & Herrmann, H. J. *How to suppress undesired synchronization.* Sci. Rep. 2, 658 (2012) [2];

- Louzada, V. H. P., Daolio, F., Herrmann, H. J. & Tomassini, M. *Smart rewiring for network robustness.* J. Comp. Netw. 1, 150-159 (2013) [3];

- Louzada, V. H. P., Araújo, N. A. M., Andrade, J. S. & Herrmann, H. J. *Breathing synchronization in interconnected networks.* Sci. Rep. 3, 3289 (2013) [4];

- Louzada, V. H. P., Daolio, F., Herrmann, H. J. & Tomassini, M. *Generating Robust and Efficient Networks Under Targeted Attacks.* in Propag. Phenom. Real World Networks (Krol, D., Fay, D. & Gabrys, B.) (Springer, 2015) [5];

- Louzada, V. H. P., Araújo, N. A. M., Verma, T., Daolio F., Herrmann, H. J., & Tomassini, M. *Critical Cooperation Range to Improve Spatial Network Robustness.* PLoS ONE 10, *e*0118635 (2015) [6].

Other works

- Araújo, N. A. M., Louzada, V. H. P., Andrade Jr, J. S. & Herrmann, H. J. *Controlling Synchronization in Complex Networks.* in Int. Work. Phase Transition, Crit. Phenom. Relat. Top. Complex Networks 1 (2014) [7];

- Louzada, V. H. P., Lopes, F. M. & Hashimoto, R. F. *A Monte Carlo Approach to Measure the Robustness of Boolean Networks.* in BCB '12 Proc. ACM Conf. Bioinformatics, Comput. Biol. Biomed. $696 - 699$ (2012) [8].

List of Figures

Chapter 1

Introduction

Natural catastrophes, financial crisis, and diseases outbreaks have all been considered as outcomes whose impact could be mitigated through the early identification of potential threats [9–12]. Risk analysis studies however, despite their ubiquity, lack common background, techniques, or even vocabulary. Reports usually rely on specialized approaches, which prevents cooperation and the propagation of the "hard learned lessons" to other fields. In this thesis we make use of a common theoretical foundation, network theory, to deal with apparently distinct real applications. We simplify the systems, still grasping the most relevant features, and propose new techniques to get insights on their behavior, and expect that our approach could be extended to other situations as well.

Complex Networks are the physical interpretation of graph theory, the study of pairwise interactions between objects [13]. In simple terms *risk* is defined as an uncertain event that has an effect on at least one of the objectives of the system [14], a definition that is entangled with the concept of complexity. Apparent harmless events interacting to create a spectacular catastrophe have long been known in risk analysis, one example being the crash of the Concorde in 2000 in Paris: instead of revealing a single major cause, investigations concluded that a small series of errors were responsible for the only fatal accident in Concorde history [15].

The use of Complex Networks and Statistical Physics in general is a powerful way to understand risk [16, 17]. In Chapter 2 we introduce Complex Networks and some of its useful metrics on the study of risk. In particular, analysis of complex systems can be subdivided into static and dynamic

frameworks, the former dealing with the risk of certain interaction patterns and the latter on the time evolution of these interactions. The frontier between static and dynamic however is not clearly defined and, in what follows, we study in depth not only both frameworks separately but also look at the interplay between static and dynamic features.

A network is said static if none of its properties evolve in time. At first, this constraint might sound a bit too unrealistic, but this simplification is capable of yielding remarkable insights, specially when one considers a static network formed by the aggregation of several events on time [18]. That is exactly our approach in Chapters 3 and 4: information about flights, passengers, and airports over an entire year is totalized on a single network which represents an overall picture the World Air Transportation. From this, we can ask the following question: is there an intervention that reduces the risk of failure of this network? In Chapter 3 we focus on the fastest way that interventions can be performed to make the network more *robust*, i.e., less prone to major disruptions. In Chapter 4 we propose a method that improves network robustness while avoiding possible economic downsides of the interventions.

In opposition to purely static networks, in Chapters 5 and 6 we add a second theoretical layer to our models. We study dynamic networks in which their properties evolve according to the Kuramoto model of synchronization [19]. In this model, nodes change their characteristics according to their interactions in time and the entire system, under certain conditions, can achieve a self-emerging synchronized state, i.e., a common behavior emerges without the guidance of a central master. Chapter 5 deals with possible attacks that create a synchronization risk. Chapter 6 details how fragile synchronization is when not only one but two networks are interacting through a communication lag. Both chapters present a bridge between real applications that could benefit from our results, such as the biological challenges that some organisms, and our brain, have on transporting information from geographically apart locations.

Chapter 2

Networks & Robustness

*Correlation doesn't imply causation, but it does waggle its
eyebrows suggestively and gesture furtively while mouthing
"look over there".*

— RANDALL MUNROE.

2.1 Introduction

Networks are a useful tool to interpret physical systems [20, 21]. They are
built upon surprisingly simple elements: *nodes*, representing the most basic
elements of the model, and *links*, their interaction. For certain systems, it is
sometimes necessary to add some other simple features. Links, for instance,
can be *directed*, to represent the causality of the interaction, or *weighted*, to
represent its strength/importance. Nodes can also have weight, for the ele-
ment's strength, or be embedded in a certain metric space, such as geograph-
ical coordinates, to represent their localization. We show in Fig. 2.1 a simple
sketch of a network model depicting a typical draw of nodes and links. Some
other concepts and measures are necessary when analyzing networks, among
them,

- **Degree.** The degree of a node is the number of links attached to it.
  In most network studies, the degree distribution $P(k)$, the frequency of
  node's degree observed in a network, is thoroughly analyzed. In relation
  to a node i, the node at the opposite end-point of a link is called *neighbor*
  of i;

- **Distance.** In a simple network context, the distance between two nodes
  is defined as the smallest number of links necessary to connect them,
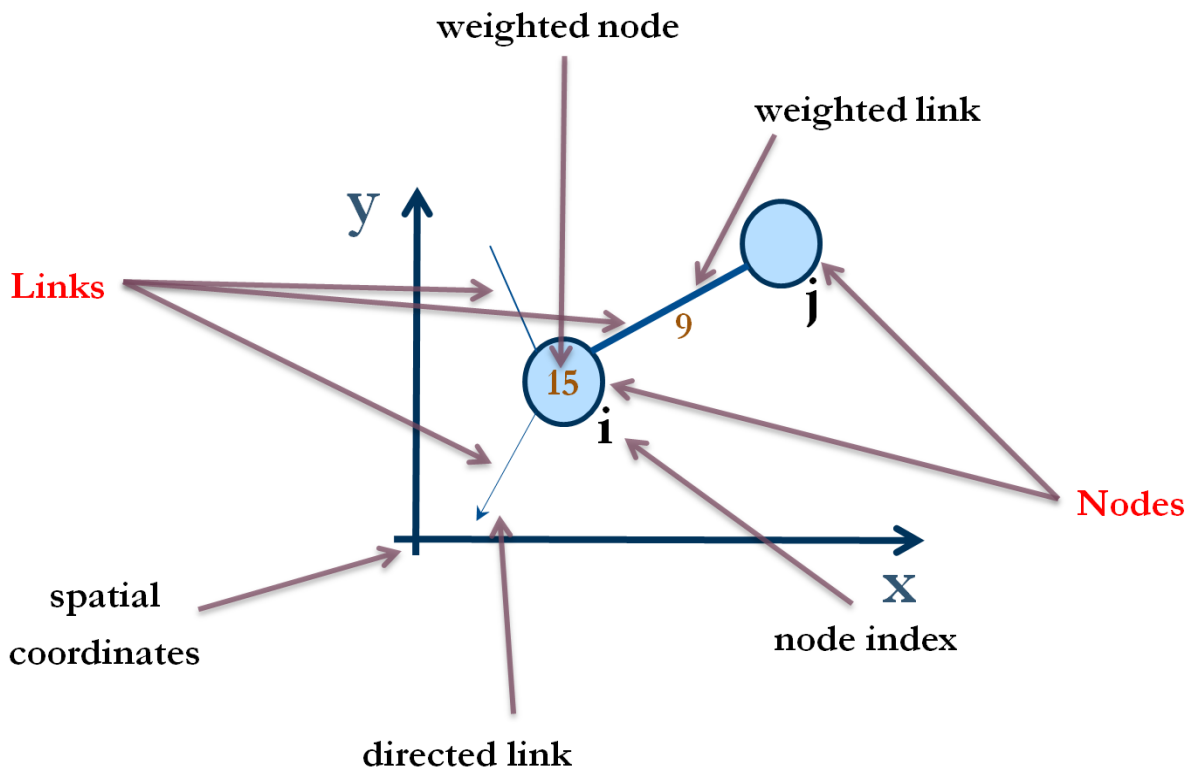
Figure 2.1 – **Properties of a network.** Networks mostly look like this, small circles with traces, the links, between them. Links can be of three types: weighted, directional, or plain simple. Nodes can also have weights and be embedded in a metric space.

creating the shortest path between two nodes. If networks are embedded in a metric space, distance is defined accordingly;

- **Clustering Coefficient** (CC). Measure of how nodes tend to cluster together. It is defined as the fraction of neighbors that are connected among themselves, averaged over all nodes [22];

- **Communities and Modularity** (M). Networks might be sub-divided in groups of nodes, called communities. Communities can be defined in several ways, but here we follow Ref. [23], which proposes a heuristic method to detect communities. This method defines the modularity (M) of a network as the density of links between communities of nodes as compared to the density within a community;

- **Assortativity** (a). Measure of how nodes of similar/disparate degrees are connected. It can be measured analytically with a degree-degree correlation (Newman's r coefficient [24], here called a coefficient to avoid confusion with other terms) or observed through a visual inspection of

4

a plot of the average neighbor's degree versus a nodes' degree [25].

The pattern in which links are distributed among nodes is called *network topology*. Variations of the topological structure are remarkably decisive to the network properties. To name a few topologies,

- **Lattice.** A regular lattice network, or grid, is a network that when embedded in an Euclidean Space $\mathbb{R}^d$ forms a regular tilling. Among many possibilities to form this tilling, a common instance is formed by placing nodes at the points in the plane with integer coordinates and connect nodes whenever the corresponding points are at distance 1. In this case, all nodes have the same degree equals $2d$;

- **Random (ER).** Also known as Erdős-Rényi networks [13]. In this topology, links are included between each pair of nodes with equal probability p, independently of the other links. For a large number of N nodes, the distribution of degrees is a Poisson distribution with average degree equals $(N-1)p$. ER networks exhibit a small average shortest path length along with a small clustering coefficient;

- **Small-world.** Networks where the average distance between two nodes scales with the logarithm of the number of nodes N. These networks have a small shortest path length, similarly to ER networks, but with a high clustering coefficient;

- **Scale-free.** Networks whose degree distribution follows a power law, $P(k) \approx k^{-\gamma}$. The range of γ is usually at $2 < \gamma < 3$ in which the the power law has a well-defined mean. In scale-free networks, nodes with a high degree are relatively common and are called *hubs*;

- **Barabási-Albert (BA).** Scale-free networks constructed through a preferential attachment mechanism [26]. Starting from a small set of connected nodes, new links are attached with higher probability to nodes of high degree, a rich-gets-richer strategy. For large N, we obtain a power law degree distribution with $\gamma = 3$.

Despite all these possible features, network models tend to be remarkably simple in their details. However, the joint combination of several simple interactions can give rise to properties that cannot be attributed to isolated relationships. If these properties are interesting, we label the underlying model as a *complex network*.

The simplified representation of complex systems as a network of nodes and links has provided important insights into the design of a variety of technical systems, such as power grids [27, 28], maritime commerce [29], communication networks [30–32], connected water reservoir [33], air transportation [34], and road networks [35]. Networks have helped to shed light into several macro-economics systems as well [18, 36, 37].

In opposition to technical systems, biological systems are constantly shaped by the forces of evolution. Hence, we can analyze the properties of such networks with the objective to understand better designs, diagnose possible problems, and uncover some remarkable new behavior. Many examples of past research about biological networks are present in the literature, in areas such as: protein interaction [38], gene regulatory networks [39, 40], metabolism [41], neuronal systems [42, 43], brain dynamics [44], and psychosis detection [45].

Networks have also been used to study the efficiency of the transference of information [46], resource allocation [47], hierarchy emergence [48], and synchronization [49–51]. A complete review of past and recent research on networks can be found in References [52], [53] and [54].

An important aspect of a network is the capability to withstand failures and fluctuations in the functionality of its nodes and links [55–57]. The design of networked infrastructures with these capabilities can be thought of as an optimization task. An early important work in this field is Albert et al. [21] where the authors showed by numerical simulations that scale-free networks, while they are robust against random removal of nodes, are much more vulnerable to the removal of nodes according to their degree. In other words, in a scale-free network if the nodes are removed in decreasing order of degree, starting with the most connected ones, then the network falls apart very quickly.

In Ref. [58], a procedure is described that successfully modifies scale-free networks so that the largest connected component still has a considerable size after several attacks targeted at the most connected nodes. This feature guarantees that there is at least one path connecting a large number of nodes after attacks and is considered an appropriate definition of robustness. A natural question that follows is the maintenance of network efficiency after attacks, i.e., a network is efficient in this sense if "good paths" among nodes do not cease to exist after several targeted failures. Using a consolidated definition of efficiency, we propose in this chapter an optimization procedure that mod-

ifies existing networks in order to improve their efficiency under targeted attacks.

2.2 Model

Our method is an extension of the work by Schneider et al. [58], who used a hill-climbing procedure to optimize robustness against targeted attacks. We modify this approach by adding a simulated annealing strategy [59] to avoid the search getting trapped in local maxima. Previous approaches have successfully used simulated annealing to increase network robustness [60]. Here however we extend our focus to the following objectives: Robustness, Efficiency, and a combined measure of both. We create three sets of networks optimized for these cost functions and compare their characteristics. In what follows, we describe the cost functions and the optimization procedure.

2.2.1 Network Robustness

The definition of network robustness might change according to a specific application. Previous work used the percolation threshold, the formation of long-range connectivity when links are randomly included, as a robustness measure [61,62]. This threshold identifies the formation of a giant connected component: below the threshold, it does not exist; while above it, there exists a giant component of the order of the system size. This measure however is a limited approach to study risk: it ignores the behavior before and after the connection event.

In this chapter, and in the entire thesis as well, we call an *attack* the removal of a node of the network, and the robustness we measure by the size of the largest connected component (LCC) of the network after this removal, as proposed by Schneider et al. [58]. Effectively, we observe the system during the entire process, not only at the critical threshold value. To quantify it, we proceed with a series of attacks and subsequently measure the robustness after each node removal. Hence, robustness R is defined as:

$$R = \frac{1}{N} \sum_{Q=1}^{N} S\left(\frac{Q}{N}\right) , \qquad (2.1)$$

where N is the number of nodes, Q is the number of nodes removed from the network, and $S(q)$ is the size of the LCC after a fraction $q = Q/N$ of

nodes is removed, considering that all incoming links are also removed from the network. The parameter R is contained in the interval $1/N \leq R < 0.5$, and is a measure for robustness: a small R is associated to a fragile network and a larger R to a robust one.

The attacks performed are targeted to the nodes with highest degree of the network: we find the most connected node, remove it, calculate $S(q)$, update the degrees, and find the new most connected node to repeat the process. In case two nodes have the same degree, we choose the one with the smallest index. The value R is therefore unique for each network.

2.2.2 Network Efficiency

One can think of network efficiency as a low cost of communication among its members. In this light, we relate efficiency with the shortest paths between all pairs of nodes, thus following Latora and Marchiori [46] who defined the network efficiency E as:

$$E = \sum_{\substack{i,j=1 \\ i \neq j}}^{N} \frac{1}{l_{ij}} \, , \tag{2.2}$$

where l_{ij} stands for the shortest path length between nodes i and j. If i and j belong to separate connected components of the network, we set $l_{ij} \to \infty$ to guarantee a consistent behavior of the cost function.

2.2.3 Network Integral Efficiency

Keeping in mind that we would like to keep the efficiency of networks after attacks, it is straightforward to modify the definition of E to account for this. Hence, we define Integral Efficiency $IntE$ as:

$$IntE = \frac{1}{N} \sum_{Q=1}^{N} E\left(\frac{Q}{N}\right) \, , \tag{2.3}$$

where $E(q)$ stands for the efficiency of the network after the removal of $q = Q/N$ nodes. Nodes are removed according to a targeted attack such as in Sec. 2.2.1. The value of $E(0)$ is the cost function E defined in Sec. 2.2.2. By choosing this quantity instead of E, which does not consider nodes removal in its definition, we try to avoid that the shortest paths among nodes increases after targeted attacks.

2.2.4 Optimization procedure

In their work, Schneider et al. [58] propose a simple hill-climbing search to modify the network topology in order to optimize the robustness R whilst keeping the degree of each node fixed. This restriction in often present in the modification of artificial systems, such as electric grids where constructing a receiver for a new power line in a station might be impractical. Hence, only swaps between lines (links in the network) are possible. A consequence of this restriction is that the underlying degree distribution of the network remains unchanged after swaps. Clearly, if we had no constraints on the degree distribution, we could design the topology starting from scratch with the robustness and efficiency as objectives in mind, obtaining different optimal topologies.

Next, we present an improved version of the optimization approach using simulated annealing and we describe it for any cost function F that changes after link modification:

1. **Initial State.** Let $G(N, E)$ be a network with $|N|$ nodes and $|E|$ links.

2. **Link swap.** Choose two pairs of links (i, j) and $(k, l) \in E$ randomly and create the network G^* by deleting the links (i, j) and (k, l), and adding the links (i, l) and (k, j).

3. **Acceptance probability**. Calculate the transition probability p of the system as:

$$
p = \begin{cases} \exp\left(-\dfrac{F(G) - F(G^*)}{T}\right) & \text{if } F(G^*) < F(G) \\ 1 & \text{if } F(G^*) \geq F(G) \end{cases}
$$

4. **Comparison**. Make $G = G^*$ with probability p, otherwise discard G^*. Return to Step 2.

This approach allows a network G^* with $F(G^*) < F(G)$ to be chosen with finite probability. By doing this, global minima could be reached and inferior local minima could be avoided. Notice that, for the three cost functions studied here, the value of $F(G)$ is unique for each network G. Furthermore, by decreasing the value of T according to the amount of link swaps executed, it is possible to decrease the acceptance ratio of worst networks when an optimum point is close. We decrease the temperature as function of the number
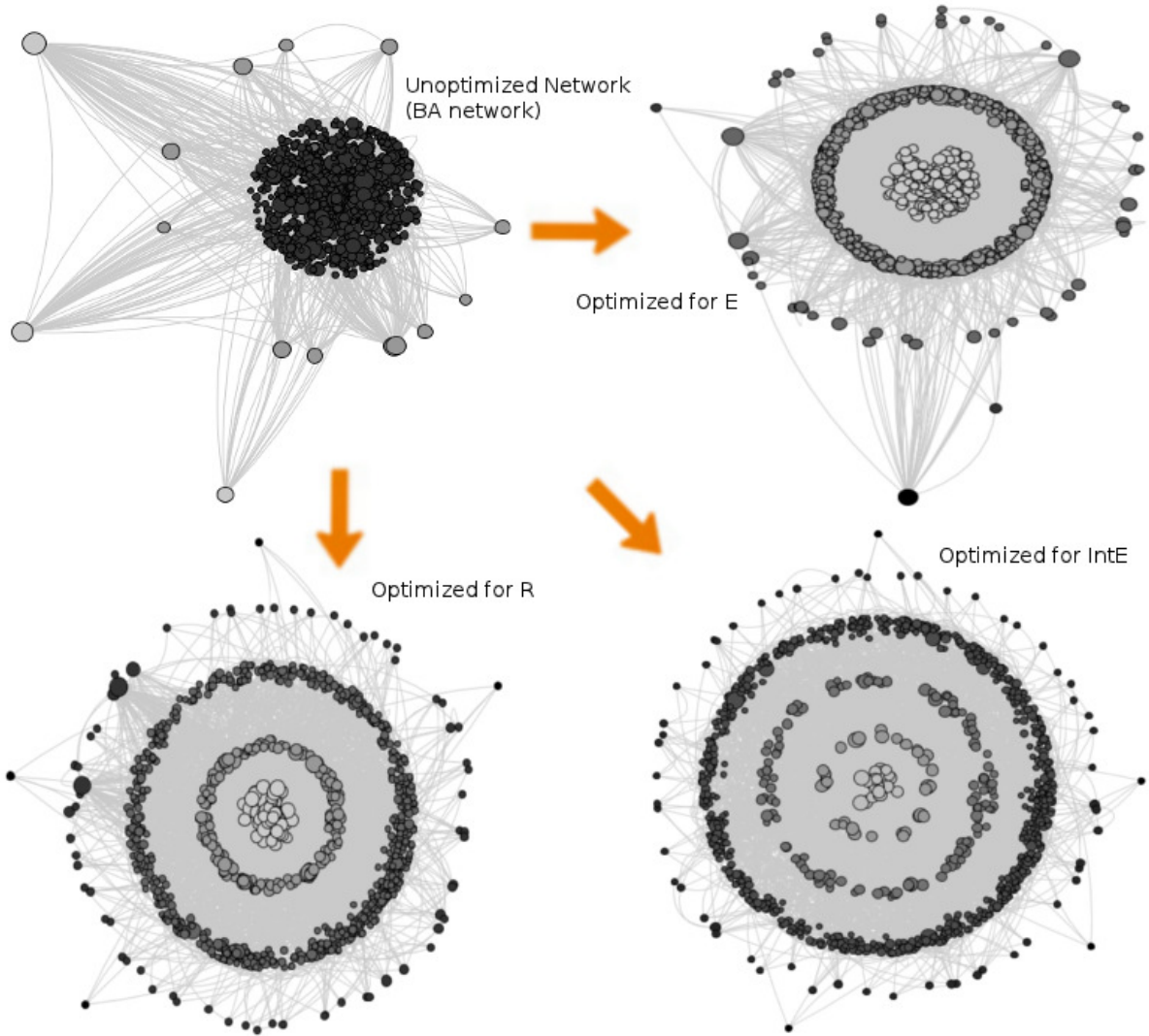
Figure 2.2 – Examples of networks belonging to each set. Networks are drawn using the k-core decomposition, represented by the different intensities of gray.

τ of link swaps, by following the equation: $T(\tau) = 0.0001 \times 0.8^{\tau}$. Variations to this function have shown little effect on the results. The search is stopped when a predefined amount of link swaps is reached.

2.3 Results

The procedure outlined in Sec. 2.2.4 is applied to the cost functions: R (Robustness as described in Sec. 2.2.1), E (Efficiency as described in Sec. 2.2.2), and $IntE$ (Integral Efficiency as described in Sec. 2.2.3), starting from the same set of randomly generated of BA networks. Hence, we created three

Table 2.1 – Average values of the cost functions, standard deviation in subscripts. Each set comprises 100 networks with $n = 1000$ nodes. $\langle k \rangle$ = average degree, $\langle cc \rangle$ = average of clustering coefficient, $\langle a \rangle$ = average assortativity coefficient, $\langle E \rangle$ = average efficiency, $\langle R \rangle$ = average robustness, $\langle IntE \rangle$ = average integral efficiency.

Set	$\langle k \rangle$	$\langle cc \rangle$	$\langle a \rangle$	$\langle E \rangle$	$\langle R \rangle$	$\langle IntE \rangle$
Unopt.	5.95	0.0242 ± 0.0033	-0.085 ± 0.015	$\mathbf{0.1486 \pm 0.0012}$	$\mathbf{0.1837 \pm 0.0053}$	$\mathbf{0.0308 \pm 0.0011}$
E	5.95	0.0053 ± 0.0014	-0.076 ± 0.011	$\mathbf{0.1539 \pm 0.0015}$	0.1826 ± 0.0056	0.0310 ± 0.0012
R	5.95	0.0200 ± 0.0027	0.038 ± 0.024	0.1459 ± 0.0013	$\mathbf{0.2266 \pm 0.0055}$	0.0372 ± 0.0012
IntE	5.95	0.0195 ± 0.0029	0.055 ± 0.026	0.1456 ± 0.0013	0.2268 ± 0.0052	$\mathbf{0.0391 \pm 0.0012}$

sets of networks: *Robustness set*, *Efficiency set*, and *Integral Efficiency set*. As a control, we compare to the original set of BA networks, from now on called the *Unoptimized set*.

The Unoptimized set is composed of 100 networks of $n = 1000$ nodes and average degree $\langle k \rangle = 5.95$. The size of the networks was chosen based on a trade-off between the appearance of topological features such as the scale-free phenomenon, only present in large networks, and computational cost, as the $IntE$ cost function requires $O(n^3)$ operations to be calculated. The amount of link swaps, 10.000, was chosen so that for each optimized set its cost function is already statistically different from the Unoptimized set. It is possible to see that this goal was achieved by comparing the values in bold for columns $\langle E \rangle$, $\langle R \rangle$, and $\langle IntE \rangle$ in Table 2.1. To provide a visualization of the network structure created, some examples of each set are drawn in Fig. 2.2.

To analyze the robustness of each set, a plot of $S(Q/N)$ versus Q is shown in Fig. 2.3, in which the area below each curve represents R for each set. As expected, the Robustness set shows a bigger area (23% of increase), keeping a considerable size of the LCC after several attacks. Indeed, Schneider et al. [58] obtained an improvement of almost 75% for this cost function, but by using a much more exhaustive approach: their search stops after 10.000 link-swaps without increase in R. Therefore, our results show that it is possible to increase network robustness using less computational effort. The plot also shows that E, a cost function that does not consider attacks in its formulation, has a bad performance in this scenario. We conclude that, though more efficient, networks optimized exclusively for E might not be appropriated in a realistic context, in contrast to $IntE$, which considers both effects. Moreover, it is interesting to note also that the curves for R and the Integral Efficiency set have comparable areas, considering the standard deviation of

the measurements as detailed in Table 2.1.

In Fig. 2.4, the cost function $IntE$ is analyzed through the plot of $E(Q/N)$ versus Q, showing that, as expected, the Integral Efficiency set has the better performance, i.e. the area under the corresponding curve is bigger. Interestingly, the curve referring to the set of networks obtained by optimizing for E alone shows that both have about the same performance as the unoptimized ones for this cost function (data on Column $\langle IntE \rangle$ of Table 2.1).

Another interesting aspect of the work of Schneider et al. [58] is the topology obtained by this optimization: a so-called onion-like structure. In this topology, each layer is composed of nodes connected with nodes of the same degree, with few connections between layers. A direct procedure to generate this topology can be found in the work of Wu et al. [63].

To investigate the presence of an onion-like structure on our optimized sets, three quantities were analyzed. In Fig. 2.5, we show the *k-core* decomposition [64] for several k, showing that the Robustness and Integral Efficiency sets have several k-core's or layers, thus confirming a hierarchical structure of the network. The Efficiency set does not present this clear hierarchy, but has more layers than the Unoptimized set. In the inset of Fig. 2.5 we show that the Integral Efficiency set and the Robustness set of networks have the greater assortativity through the plot of Newman's a coefficient [24]; the Efficiency set is as dissortative as the Unoptimized set.

Finally, we check network layers by analyzing the sub-graph of each network composed of N_k nodes with degree smaller of equal to k. In this sub-graph, S_k represents the size of its largest cluster. In Fig. 2.6, we plot S_k/N_k for several values of k. This plot shows that the Robustness and the Integral Efficiency sets present practically the same increase in robustness with respect to the Unoptimized set. In contrast, the Efficiency set does not show any improvement with respect to the original scale-free unoptimized networks.

Given the several layers showed by the k-core decomposition, its dissortative nature, and the increase in robustness of each layer, we conclude that the Integral Efficiency set also has an onion-like structure similar to the Robustness set.

2.4   Discussion

We outline here a procedure that optimizes a specific characteristic in any type of network and create three sets of BA networks with distinguishable
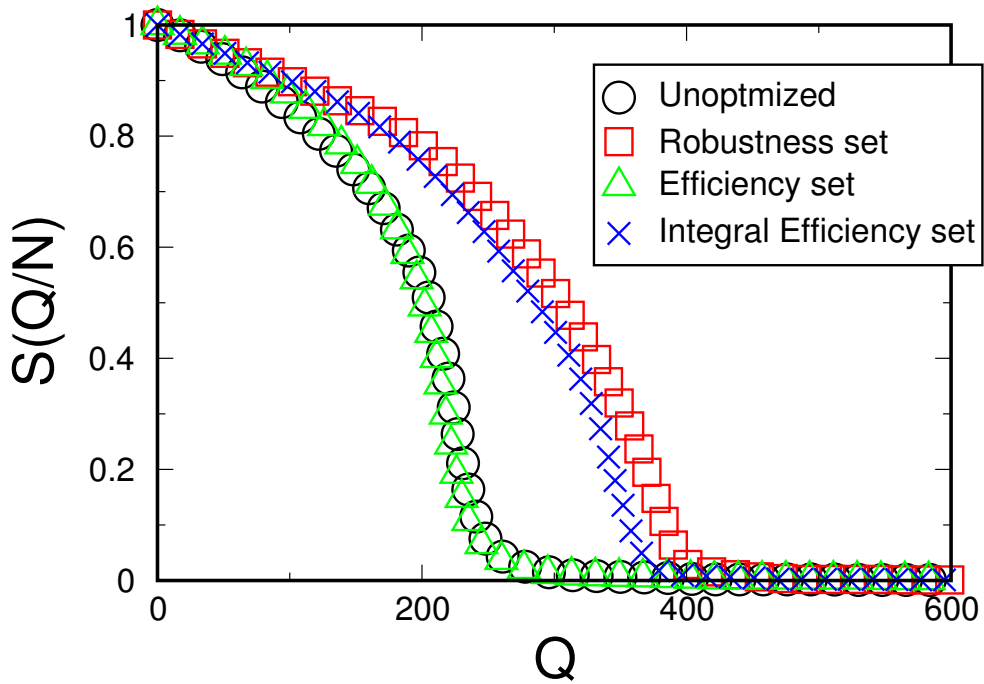
Figure 2.3 – Largest component size after the removal of Q nodes. The area bellow each curve is the cost function R. Symbols represent sets optimized for different cost functions and are larger than the standard deviation.
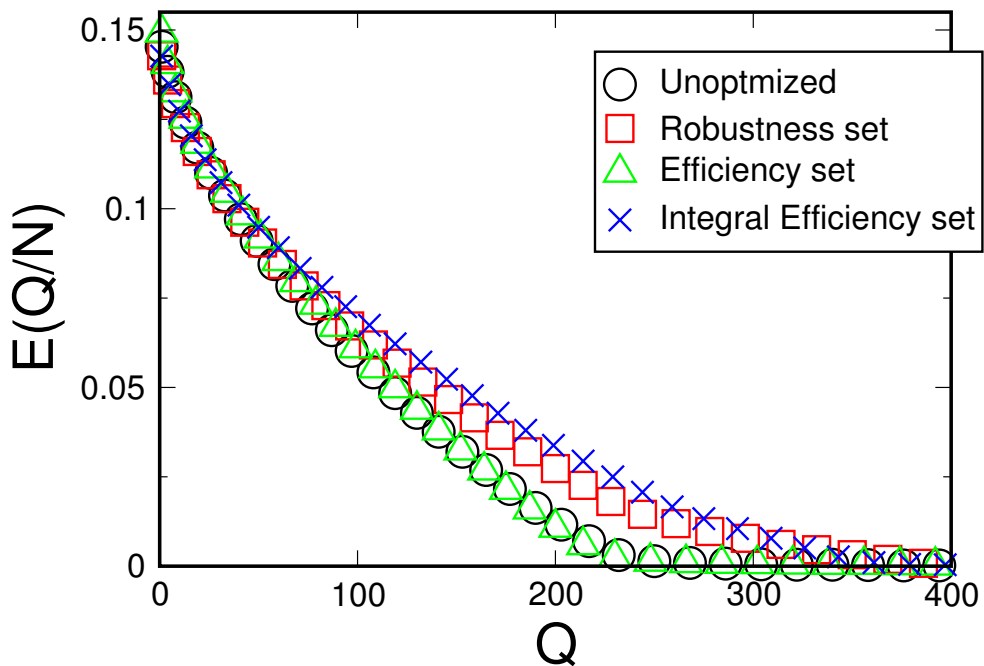
Figure 2.4 – Network efficiency $E(Q/N)$ after the removal of Q nodes. The area bellow each curve is the cost function $IntE$. Symbols represent sets optimized for different cost functions are larger than the standard deviation.
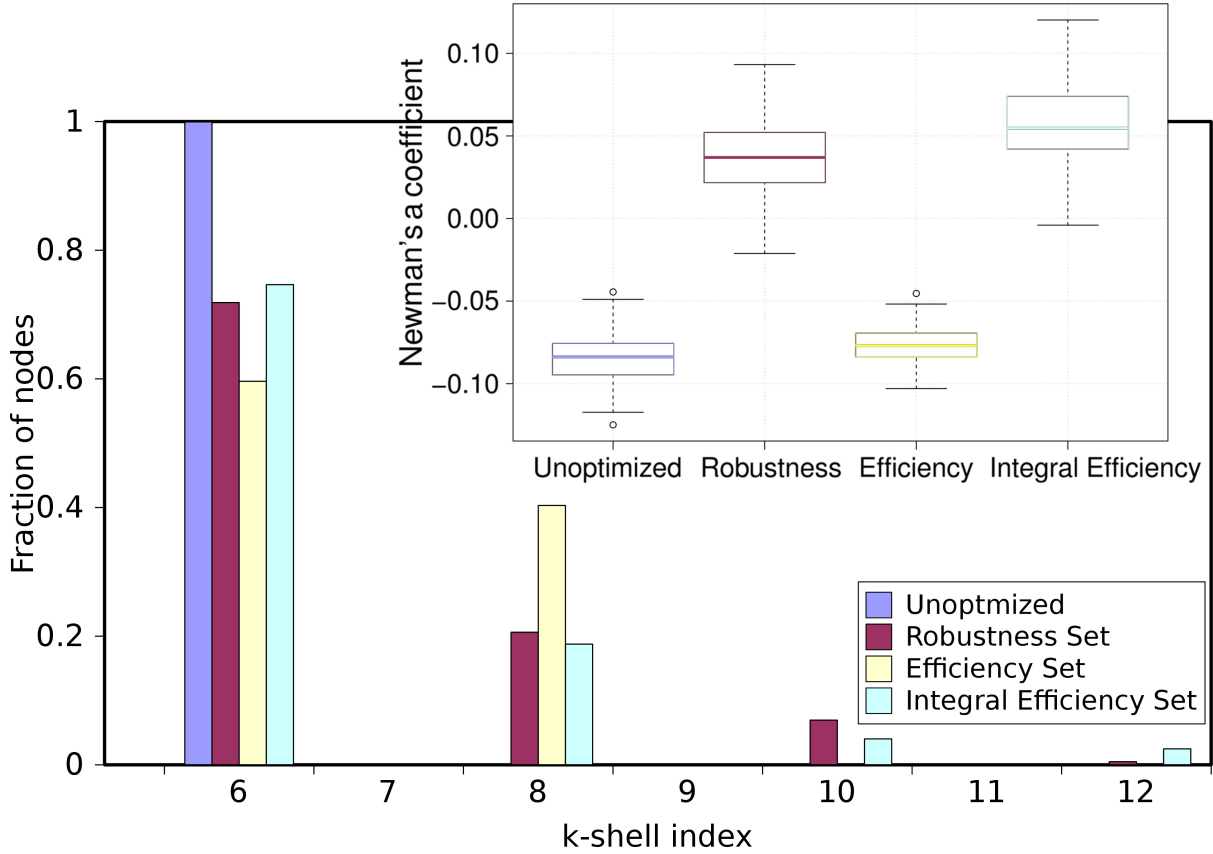
Figure 2.5 – Main plot shows the K-core decomposition for several values of k. It can be seen that the same network optimized for $IntE$ presents more layers than the network resulted after the optimization for R. Inset shows Box-and-whiskers plot of the degree assortativity through Newman's a coefficient. Thick lines depict the median value; lower and higher hinges gives the 0.25 and 0.75 quantiles, respectively; the whiskers extend to 1.5 times this inter-quantile range. Values outside this range are considered outliers and appear as circle dots in the plot.

features. Though BA networks are known to be resilient to random removals of nodes and present other interesting properties [21], we show here a method that creates networks with a certain specific characteristic enhanced, which might be useful in some realistic scenarios.

Firstly, our results show that the Integral Efficiency set substantially improved efficiency after attacks, compared to the Robustness, Efficiency, and Unoptimized sets. Moreover, this set also sustains a large connected cluster after attacks. Therefore, this cost-function could be used to generate highly robust and efficient networks.

Another important result of our work is that networks optimized for $IntE$ also present an onion-like structure. This result suggests that this struc-
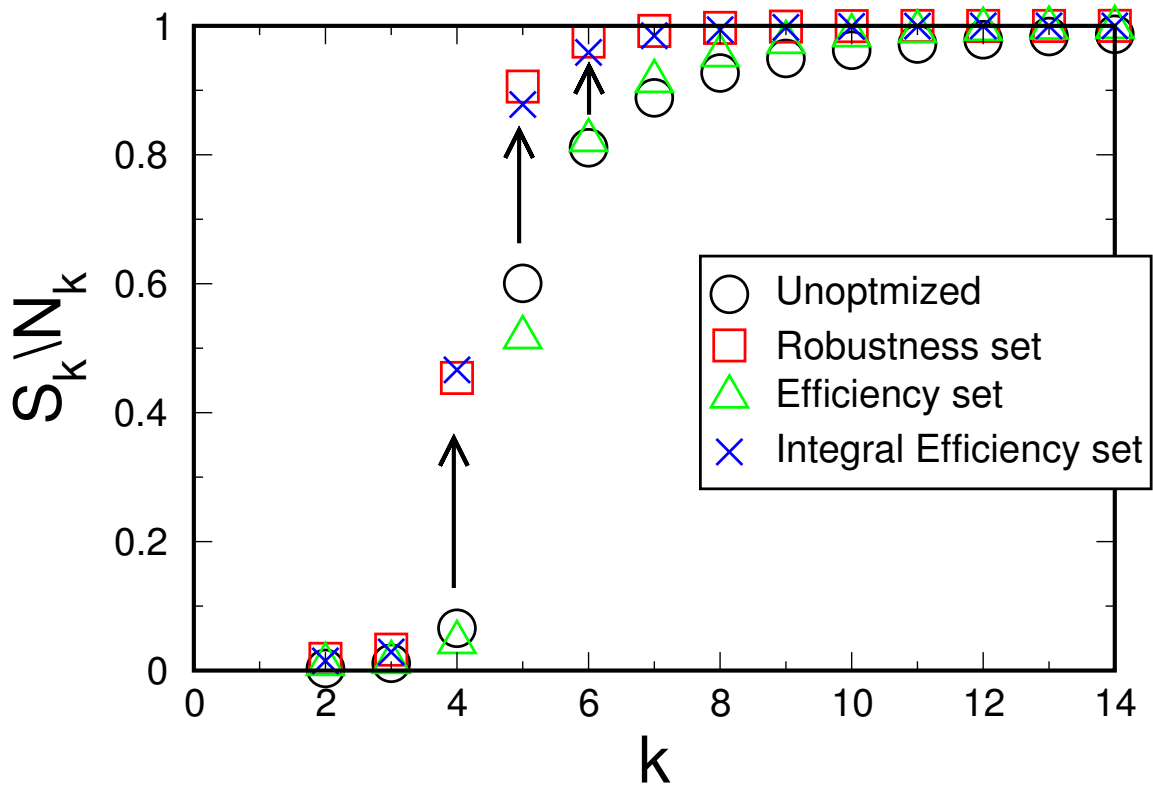
Figure 2.6 – Relative size of the largest component in networks composed of nodes of degree less than k. Symbols represent sets optimized for different cost functions are larger than the standard deviation.

ture is generically the optimal scale-free net independently of the chosen cost function. It also helps the design of networks from scratch, as it is possible to construct scale-free networks which present this structure.

It is also interesting to note that the Integral Efficiency set maintains several similarities with the Robustness set, such as: high assortativity, size of the largest cluster after attacks, efficiency after attacks, size of the largest cluster for each degree layer, and a hierarchical structure regarding the k-core decomposition. In fact, the Integral Efficiency set has a slightly better performance on assortativity and efficiency after attacks, while the Robustness set has a better performance on the others.

Future works might focus on the structures of the three generated sets. The Efficiency set does not present an onion-like structure, remaining unclear if this optimization could lead to a different structure. The Integral Efficiency set might have a hidden feature that differentiates it from the Robustness set. By finding a typical structure of optimized networks, new net-

works could be designed from scratch with a desired feature.

Chapter 3

Robustness Risk of Complex Networks

> *Sometimes the only thing more dangerous than a question is an answer.*
>
> — FERENGUI RULE OF AQUISITION 208.

3.1 Introduction

The construction of a robust infrastructure network represents a great challenge to our society. In order to guarantee a broad and efficient coverage of basic services such as water, electricity, and telecommunications, decision makers need to take into account the effects of a great number of threats to the correct functioning of the system [21, 65]. Targeted terrorist attacks or random extreme weather conditions impose a systemic risk of catastrophic failure that has to be mitigated. In this way, tools provided by network science have offered interesting insights on common features of robust networks or methods and strategies to protect infrastructures [66–71].

Consider the construction of an air-transportation network as an example, a challenge currently faced by many developing nations [72, 73]. The localization of the airports should be decided given a tight supply and demand rule in order to ensure their efficiency, but other factors should also be included in the planning, such as security measures or noise reduction [74]. Besides that, the overall system robustness should be taken into account, as the transportation of goods and people cannot be entirely halted in case that some airports close.

When designing a new network from scratch, decision makers have an excellent opportunity to warrant its future robustness against failures [75]. However, most of the current infrastructure has been built in a non-supervised

fashion, mostly through a preferential attachment mechanism, where highly connected nodes (e.g. airports, Internet Service Providers) have a higher probability of receiving a new link (e.g. flights, transmission cables) [26]. Inspired by this situation, we propose in this chapter a strategy to improve the robustness of a given network by a small number of interventions, which makes the method useful for real-time actions under budget constrains.

Simple modifications of the network topology, the connection pattern of nodes through links, have been shown to be an effective way to increase the robustness under node or link attacks [76–80]. In particular, Schneider et al. [58] showed that successive random rewirings (link swaps) create a robust network through the formation of an onion-like structure in which high-degree nodes compose a core with further interconnected layers of radially decreasing degrees.

In this chapter we propose a *smarter* rewiring that lowers by several orders of magnitude the computational effort necessary to improve robustness. Our method is consistently better than the random rewiring for a small number of swaps and yields the same level of robustness in the long term. An onion-like structure is also created, although a higher modularity and degree correlation is observed in comparison to networks created by random swaps. We apply our rewiring strategy to the World Air-transportation network and we show that an improvement of 30% in its overall robustness can be achieved through smart swaps of around 9% of its links.

3.2   Model

We describe here a generic approach to improve network robustness and consider only the simple case of networks where all links have the same importance (unweighted) and no orientation (undirected). For illustration purposes, we explain our model and related concepts in the framework of the World Air-transportation network, a system of paramount importance to our globalized world. Complex Networks have been used to study airflight networks, with simple abstractions of flights and airports used to characterize its robustness [81], study its structural properties [34, 82–89] and evolution [90].

An Air-transportation network is defined here as *robust* when it allows a passenger to travel between most of the airports even considering the disruption of the service in the major connection hubs, i.e., the airports with largest number of flights. This feature is directly associated to the size of the largest
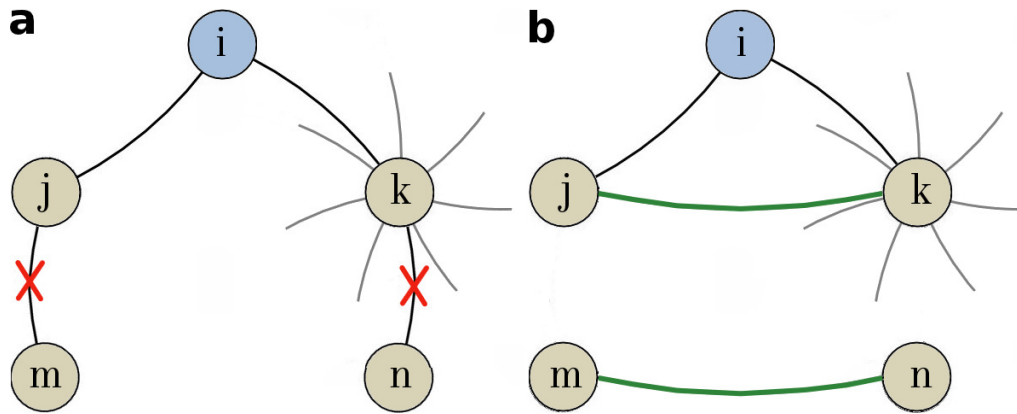
Figure 3.1 – **Smart rewiring for robustness improvement.** Diagrammatic representation of the smart rewiring. **a**, First steps of the smart rewiring: For a randomly selected node (i, blue), its lowest degree neighbor (j, brown) and highest degree neighbor (k, brown) are selected. In sequence, two neighbors of j and k are randomly selected (m and n, both brown), and links to them (e_{jm} and e_{kn}) are removed (red X). **b**, Last step of the smart rewiring in which links e_{jk} and e_{mn} (green) are added.

connected component (LCC) of a network, and we define robustness R as in Sec. 2.2.1.

To focus on targeted attacks, the node removal starts first with the highly connected nodes, the network hubs, which intuitively have the largest impact on the size of the LCC. After removing the more connected node we update the degrees (number of connections) of every node, and remove the next largest network hub. This process is further repeated until the network completely collapses.

To improve robustness, one could simply add more flights between airports. In the limit, the network becomes fully connected: all airports have connections to each other and the disruption of one does not affect other destinations. But improving an airport flight capacity by adding redundancy might prove very impractical in the short term. In fact, numerous examples of infrastructure networks present this capacity constraint, such as adding new transmission lines to a power station or new traffic cables to an Internet Service Provider. Therefore, a rewiring strategy where links are only swapped, keeping the nodes' degree fixed, is more appropriate: we reroute flights from airports and create new connection possibilities, without considerably changing the airports' load.

Here we propose a novel rewiring strategy that improves network robustness by creating alternative connections between parts of the network that would otherwise be split upon the failure of a hub. As robustness is always
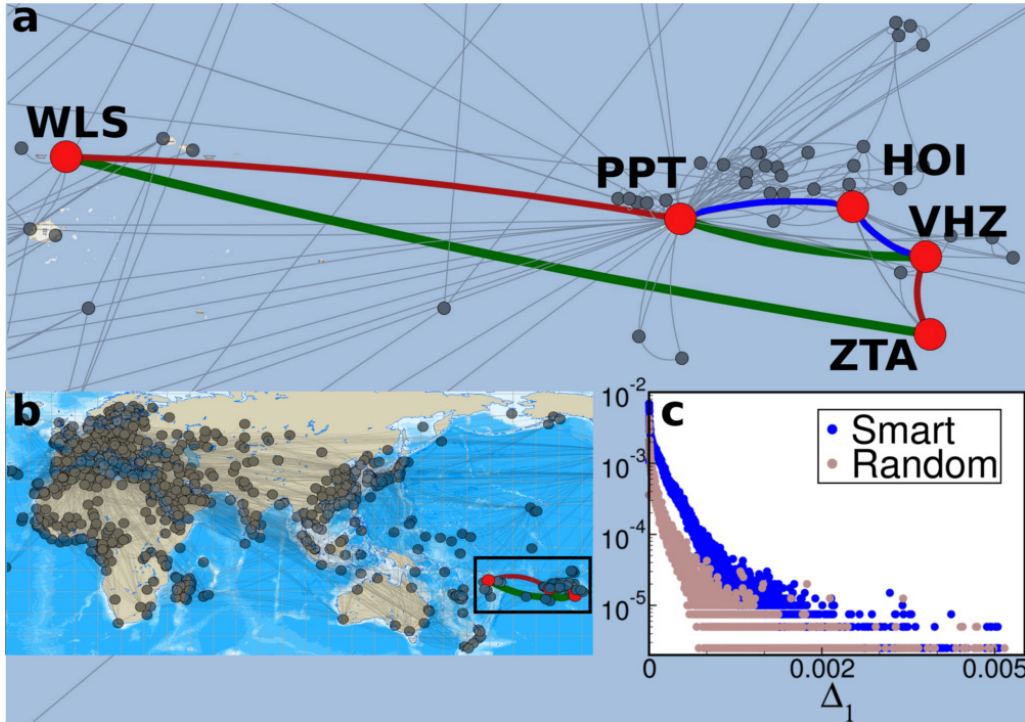
Figure 3.2 – **Proposed rerouting of flights for some airports in Oceania. a**, Example of the smart rewiring applied to the Hao Island Airport (HOI node), connected (in blue) to Faaa Airport (PPT), a regional hub, and to Vahitahi Airport (VHZ), a small airport. Connections Wallis Island (WLS) to Tureira Airport (ZTA) and PPT to VHZ are added (in green), while previous links from WLS to PPT and VHZ to ZTA are removed (in red). This simple swap increases the robustness of the World Air-transportation unweighted network by 1.85%. **b**, Section of the World Air-transportation network showing the region in which airports in **a** are located. **c**, Effects of a single swap following the random and smart strategies on the overall robustness of a set of randomly generated Barabási-Albert networks.

relative to a type of attack strategy, in our targeted attack scenario we implicitly admit that the attacker perfectly knows the network degree sequence and would attack first the current most connected node, which intuitively can cause great damage. In the same way, we assume that the "defender" knows that the attacker has this information and thus acts upon it through a smart rewiring defined as follows:

1. Select a node i randomly with at least two neighbors with degree larger than one;

2. Select the lowest degree neighbor of i, the node j, and its highest degree neighbor, the node k;

3. Select randomly a neighbor m of node j and a neighbor n of node k;

4. Repeat steps 1-3 until all nodes concerned are different from each other;

5. Remove links e_{jm} and e_{kn};

6. Create links e_{jk} and e_{mn}.

where e_{ij} represents an undirected link between nodes i and j. An illustration of this strategy is provided in Fig. 3.1. Swaps can provide positive or negative change in the robustness. In Chapter 2 we propose different swap acceptance mechanism in order to increase robustness faster. To focus on the comparison of the random and smart strategies, we perform a simple greedy choice: at every step we compare the robustness before and after the swap, and consider it a successful step if the robustness has improved. If unsuccessful, the swap is reverted and another rewiring is considered. In what follows, we define R_0 as robustness of the network before any swap is executed, R_1 as robustness after one successful swap, and R as its value after some steps are executed.

3.2.1 Onionlikeness

The onion-like structure was first proposed by Schneider et al. [58] as an emerging structure resulting from the random swap robustness optimization. To quantify this feature, we start by plotting the maximal number of nodes S_k with degree k that are connected through nodes with a degree smaller or equal to k. The onion-like structure presents more often paths between nodes of equal degree, which are not passing through nodes with higher degree, so a vertical positive shift in the S_k curve is observed in comparison to a randomly generated BA network. Hence, a possible way to quantify this structure is through an *onionlikeness* parameter c, the area below the S_k curve,

$$c = \frac{1}{k^*} \sum_{k=1}^{k^*} \frac{S_k}{N_k}, \tag{3.1}$$

where k^* is the maximum degree among the nodes and N_k is the number of nodes with degree k. In this formulation $1/k^* \leq c < 1$. At the lower bound, $c = 1/k^*$, no special relation between a node degree and its neighbors' degree is present. A regular lattice, for instance, where all nodes have the same degree, has $c = 1/k^*$. The value of c is close to the upper bound for networks with prominent onion structures, such as scale-free networks optimized for robustness.
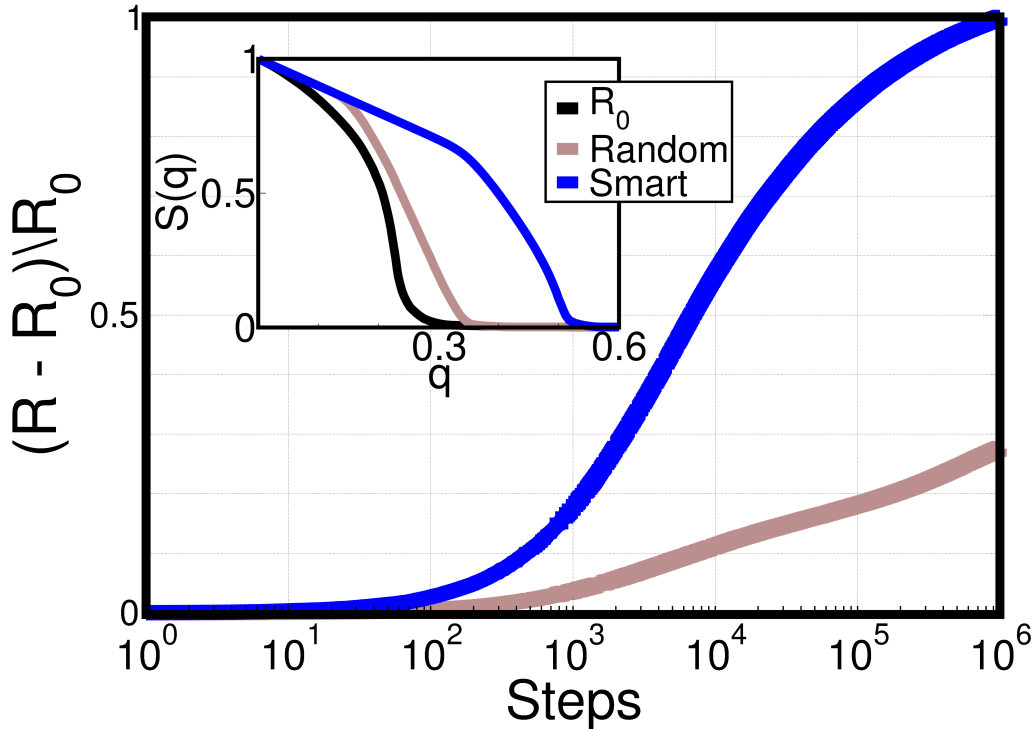
Figure 3.3 – **Fast improvement of network robustness for the smart rewiring strategy.** The smart rewiring allows a much faster improvement of R in comparison to the random strategy. For 10^6 steps, the inset shows the LCC during a sequence of targeted attacks.

3.3 Results

A swap keeps the number of links and nodes' degree unchanged, and is capable of changing the network robustness. A simple example is presented in Fig. 3.2a-b for an unweighted representation of the World Air-transportation network. In this example, a single smart rewiring applied to an airport in Oceania is capable of improving the overall robustness by 1.85%. If a swap is randomly executed, however, there is no guarantee that an improvement occurs, or that the magnitude of the improvement is satisfactory. Smart rewiring diminishes this problem as it presents a bias toward improvement. In a set of Barabási-Albert (BA) networks, the distribution of the robustness improvement after one swap, $\Delta_1 = R_1 - R_0$, shows that significant changes of robustness are more common with our strategy (Fig. 3.2c). Details regarding this and all other simulations are in Appendix A.

If positive swaps are executed in sequence, a systematic increase in the network robustness is achieved. Schneider et al. [58] showed an improvement of roughly 100% in R for a network of $N = 1000$ after an extremely large num-
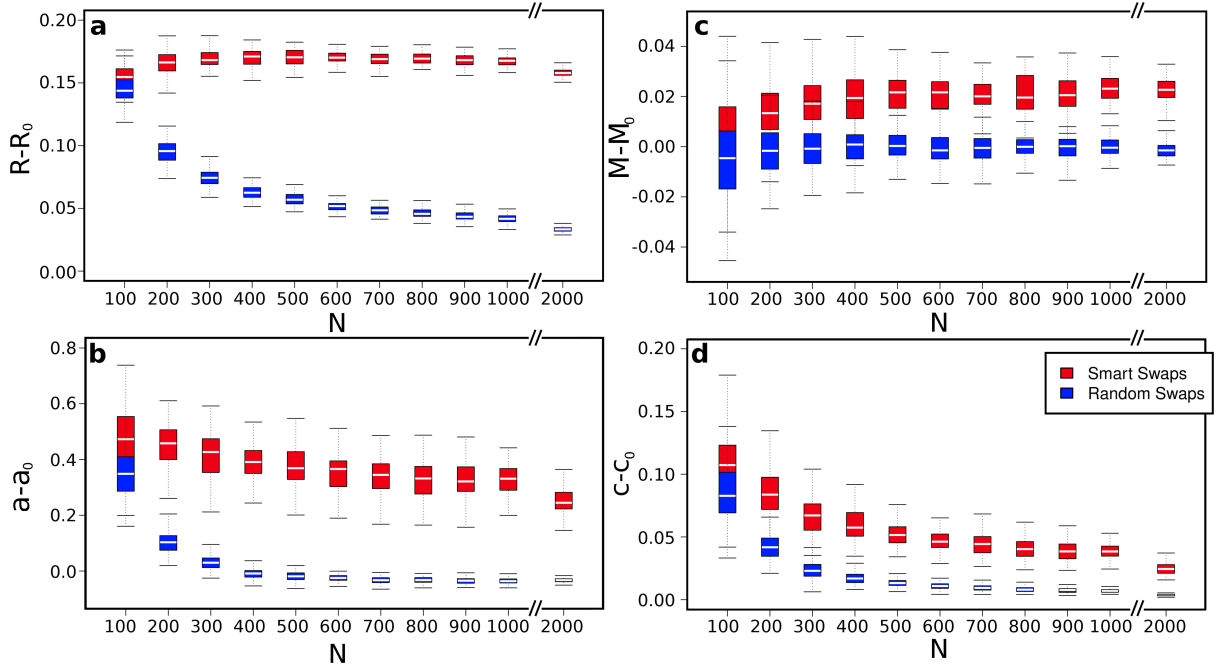
Figure 3.4 – **Smart and random rewiring for networks of different sizes**. **a**, Robustness. **b**, modularity. **c**, assortativity. **d**, onionlikeness. Each plot shows the difference between the quantity after 10^5 steps (R, M, a, and c) and its initial value (R_0, Q_0, r_0, and c_0).

ber of swaps. Successive applications of the smart rewiring are much more efficient. We compare the evolution of R in both methods starting from a set of BA networks in Fig. 3.3, considering only the execution of successful swaps for both cases. While the smart rewiring doubles R after roughly 10^6 steps, random swaps are still at the level of 20% improvement. The collapse of the LCC happens after a removal of 52% of the nodes, a 50% improvement over the random rewiring strategy (inset of Fig. 3.3). Tests for different network sizes show that the performance difference increases with network size (see Fig. 3.4a). In the limit of a large amount of swaps, random swaps can yield close to optimal robustness [58]. Smart rewiring approaches the optimal robustness much faster and, consequently, both methods converge to the same level of robustness (see Fig. 3.5). Successive swaps in the World Air-transportation network improve its robustness by 4.82% with as few as 50 swaps, 0.32% of the total of links, as shown in Fig. 3.6a. In this network, for a fixed level of robustness improvement (30%), smart swaps affect only 9.24% ± 0.53% of the total of links, while random swaps have to change 15.19% ± 0.90% links (Fig. 3.6b).

Successive applications of the smart rewiring change drastically other characteristics of the network as well. Fig. 3.6c shows the evolution during
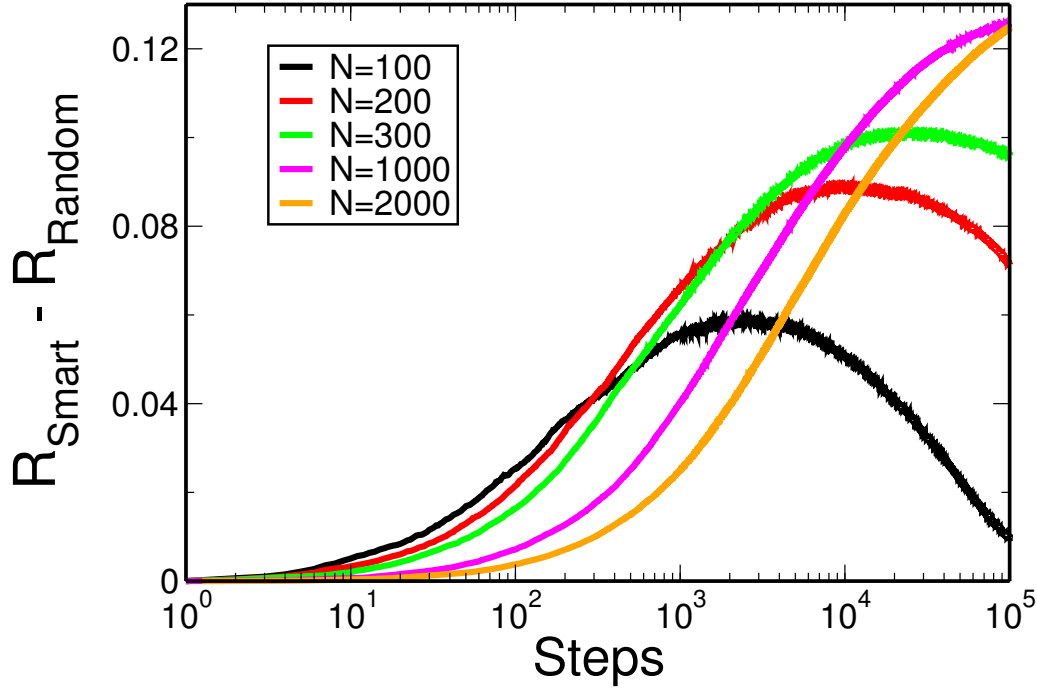
Figure 3.5 – **Evolution of the difference between robustness for smart and random rewirings.** Comparing the difference between both methods, it is clear that for small networks a large number of swaps, either random or smart, lead to the same level of robustness. Each curve represents a system size.

rewiring steps of modularity (M). The smart rewiring makes networks consistently more modular than random rewiring. This difference is a consequence of the intervention performed in the local connectivity by the smart rewiring, as our strategy deliberately creates triangles of connections. This structure reduces the importance of the hubs, which are now connected to leaves (nodes of low degree), and their removal does not have huge impact on global connectivity. These results are valid for different system sizes (See Fig. 3.4c).

Despite the creation of connections between hubs and leaves, network assortativity [24] *increases*, as the evolution of Newman's a coefficient shows in Fig. 3.6d. This result can be qualitatively understood considering the edges swapped. Before the rewiring, two edges contribute in a negative way to assortativity: e_{jm} connects a leaf to an average degree node and e_{kn} connects a hub to an average node. After the rewiring, one edge contributes negatively (e_{jk} connects leaf to hub) and the other contributes positively (e_{mn} connects average to average nodes). This effect is also persistent for different system sizes (See Fig. 3.4b) and considering assortativity through neighbor connec-
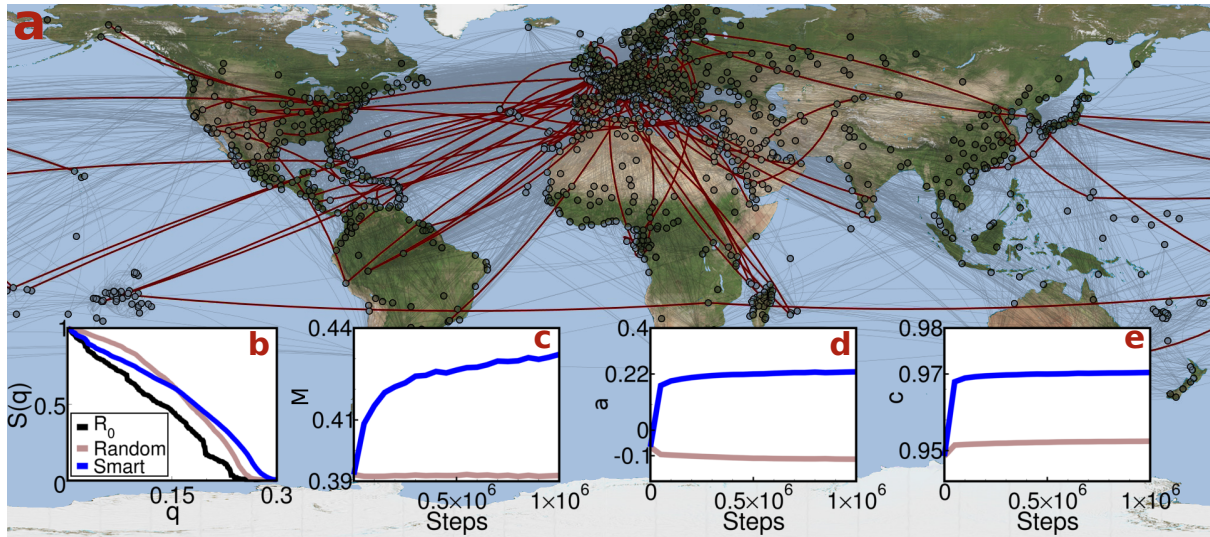
Figure 3.6 – **Robust Air transportation network**. **a**, The World Air-transportation network has its robustness improved by 4.82% with swaps of 50 links (red) following the smart rewiring strategy. **b**, Size of the largest cluster for the World Air-transportation network through a sequence of targeted attacks before and after the application of the smart and random rewiring strategies. In this case, both strategies reach the same level of robustness (30% of improvement), but while random rewiring changes 15.19% ± 0.90% of network links, smart rewiring changes only 9.24% ± 0.53%. **c-e**, modularity (M), assortativity (a), and onionlikeness (c) during the application of the random and smart rewiring strategies.

tivity [25] (See Fig. 3.7). In comparison, both the original BA networks and networks optimized through random swaps are dissortative.

Higher modularity and assortativity produced by the smart rewiring do not interfere with the formation of the onion-like structure, where layers of nodes of increasing degree hold the network robustness. Both strategies produce the onion-like structure but, by yielding a larger robustness, the onion structure is more prominent in the case of the smart rewiring (Fig. 3.6e). Onionlikeness also remains larger for smart rewiring for different system sizes (See Fig. 3.4d).

3.4   Discussion

Through a simple rewiring strategy we present here a method that improves drastically the network robustness while consuming little computational time. The proposed smart rewiring quickly increases robustness in comparison to a random choice of links. The high efficiency, together with the fact that only local knowledge of the two first neighbors of a given node is necessary, makes
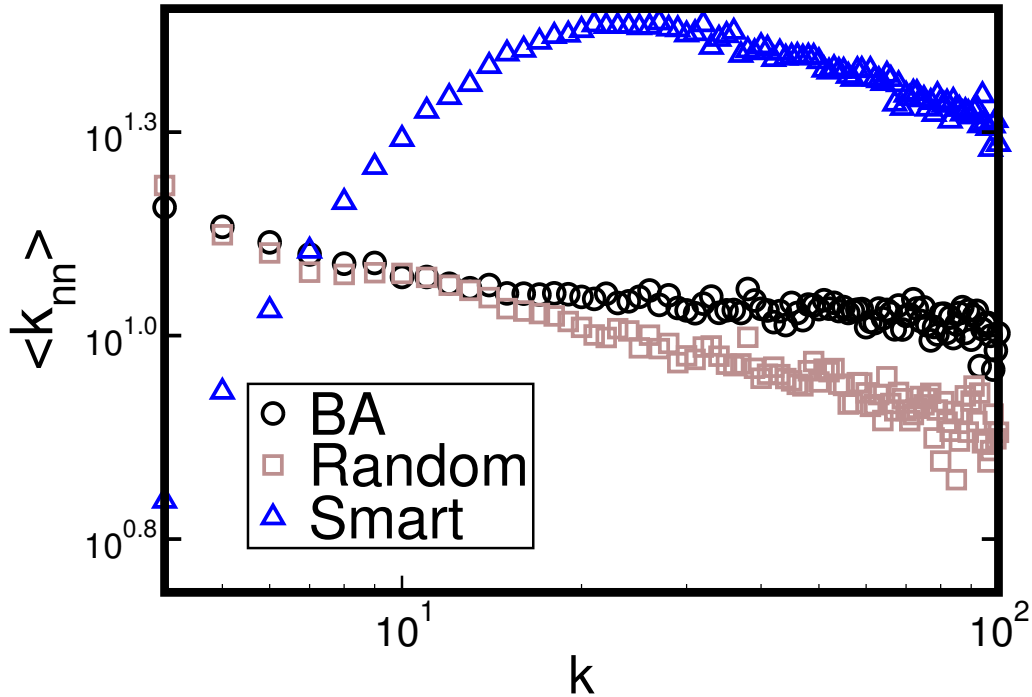
Figure 3.7 – **Assortativity for different swap strategies**. Assortativity through neighbor connectivity [25] for networks optimized using different strategies, and for BA networks in comparison. For each degree, $< k_{nn} >$ represents the average degree of the neighbors of nodes of degree k. The scattered values for large k are due to statistical fluctuations.

this strategy a potential tool for network designers and policy makers having the task of protecting our already built infrastructure against targeted attacks. As an example, simple interventions on the World Air-transportation network have been able to considerably improve its robustness. Our main analysis is performed on a set of randomly generated BA networks, which suggests that the same findings would apply to all real networks with a broad degree distribution since the smart swap is general and not limited to a particular network class.

Besides its simplicity, the smart strategy counter-intuitively improves the maintenance of the largest cluster through a local division of the network: at each step five nodes previously connected are transformed into a triangle and a pair of nodes. This apparent division does not fully fragment the network, it only reduces the importance of the network hubs in keeping the global connectivity through the addition of links between nodes of average degree. These rewired links might eventually bridge different parts of the network after the hub failure. Moreover, smart rewiring creates also a highly modular and assortative topology while forming an onion-like structure.

As modularity and assortativity differ radically from networks modified through random swaps, we define the structure of networks generated through successive applications of the smart rewiring as a *modular onion* structure. This new topology gives rise to the question if further changes in the swap mechanism could create different structures. Following this, swap mechanisms could be designed to improve a certain desired feature, in the same way as the smart rewiring enhances modularity, while improving network robustness. As a method based on a simplified framework, another possible application of the current study is to adapt the strategy to real-time circumstances of an infrastructure network, such as flight capacity and climate conditions in the air transportation problem.

It is noteworthy that our model does not account for weights in the links, which would represent the number of passengers traveling between airports in a certain period of time. A rewiring method that takes advantage of this information, together with adaptations of the robustness concept, could have direct applications in the optimization of a real technical system.

Chapter 4

Robustness Risk of Spatial Networks

The best that most of us can hope to achieve in physics is simply to misunderstand at a deeper level.

— WOLFGANG PAULI.

4.1 Introduction

The construction of a new terminal at the Schenzen airport, Southeast China, has been used to question the current strategies of infrastructure growth in developing countries [91, 92]. Schenzen is a large city, but its airport is directly connected by an eight kilometer ferry to the Hong Kong airport, which can handle twice as many passengers. Is it reasonable to invest more than one billion dollars increasing the capacity of such a large infrastructure with another one nearby? Opponents to this investment classify it as a white elephant and as one example of the misbegotten infrastructure growth in developing countries. The ones in favor, argue that not only the costs of investing in Schenzen are lower than in Hong Kong but also global connectivity can profit from cooperation between stakeholders of air-transportation systems in the region. Here we address, from a network science perspective, how such proximity and cooperation between local actors is key to the robustness of spatial networks.

The simplified representation of complex systems as a network of nodes and links has provided important insights into the design of a variety of systems. In many cases, nodes are spatially embedded according to the geographical coordinates of the elements. This simplification allows us to focus on the topological aspects of the system and to easily extend our results to many applications. We characterize the robustness of a network as its capacity to

maintain global connectivity under a sequence of node removals and describe a strategy based on local cooperation to improve robustness under possibly realistic constraints. We discover a continuum transition when changing the distance for which nodes are allowed to swap links, a cooperation range. We calculate the critical exponents of this transition and show that the key factor controlling the value of the critical exponents is the exponent of the algebraic decay of the connection probability with the node distance.

As an ubiquitous infrastructure system, we explain our method in the context of the worldwide air-transportation network (WAN), though our results impact the whole class of spatially embedded networks. It is paramount that the WAN works in an extremely reliable and efficient fashion, as any temporary airspace closure, such as the one caused by the eruption of the volcano Eyjafjallajökull in 2010, may cause huge losses worldwide [93, 94].

4.2   Model

In this chapter, we go one step further of Chapter 3 and model the WAN with greater detail. We summarize data provided by OpenFlights in the year 2011 as a single static network with 3237 airports (nodes, modeled as points distributed across the surface of a sphere with distance calculated according to the Haversine formula) and around eighteen thousand links [95]. Links are undirectional, assuming that each flight should return to its origin, and weighted according to the number of possible flights between two airports. Airports are weighted by the number of passengers transported.

As a self-organized system, in which preferential attachment is expected to play a pivotal role, the WAN is quite fragile to targeted attacks, i.e., intentional removal of the most connected nodes causing the collapse of the giant connected component [89]. The aim of our optimization strategy is to create a robust yet economically feasible WAN. Since robustness can be defined in different ways, we consider that a robust WAN should be capable of transporting passengers even in face of a targeted attack, in contrast with Chapter 3 and 2, and previous works as well, where only the size of the largest connected component is considered [57, 58, 63, 78]. We simulate a sequence of airport closures (node removal) and quantify robustness r as:

$$r = \frac{1}{\Pi(0)} \sum_{n=1}^{N} \Pi\left(\frac{n}{N}\right) , \qquad (4.1)$$
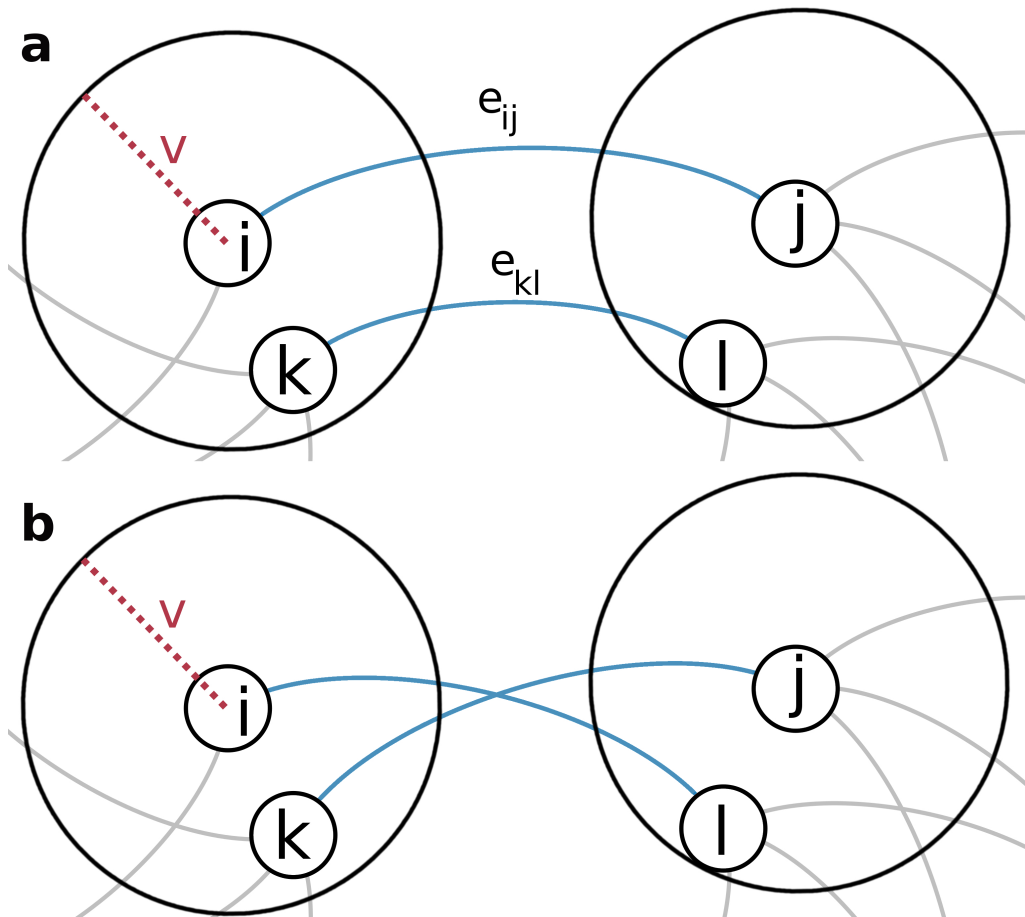
Figure 4.1 – **Geo swap: a cooperation range rewiring.** Diagrammatic representation of a rewiring procedure based on a cooperation range. For a randomly selected node i, a node k at distance $d(i,k) \leq v$ is selected (Panel **a**). If nodes j, neighbor of i, and l, neighbor of k, also have $d(j,l) \leq v$ then links e_{ij} and e_{kl}, in blue, are swapped (Panel **b**).

where N is the total number of nodes, n is the number of nodes removed from the network, and $\Pi(q)$ is the number of passengers in the largest component after a fraction $q = n/N$ of nodes were removed. Closures are executed from the most to the least connected node.

The location of airports are mostly determined by economical forces, such as to cater to local demands. In many cases, airports are located within a short distance from each other, sometimes only a few kilometers away as, e.g., airports in the Schenzen-Hong Kong area, or a few hundred kilometers but still easily reachable, such as the airports in the northeast of the United States. We assume that a flight rerouted to an airport within a cooperation range v of the original destination has a similar attractiveness. If need be, a passenger landing at a different airport could easily take another means of transportation, such as the local train network or a shuttle bus, to go to the desired
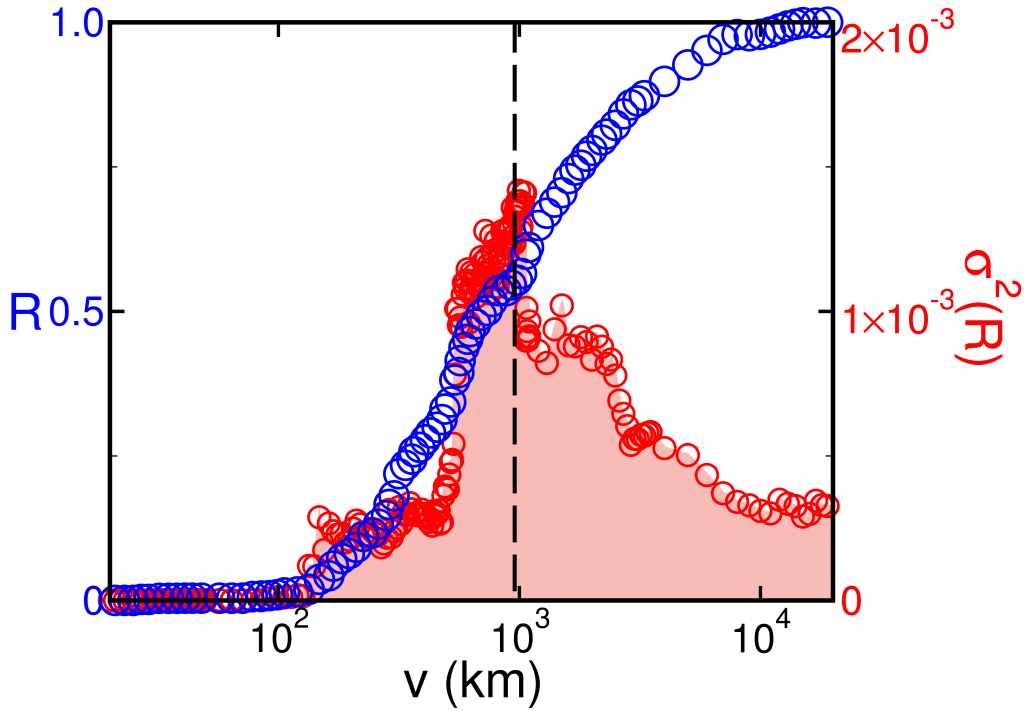
Figure 4.2 – **Robustness increase of the WAN under the geo swap.** Dependence of the optimized robustness on the cooperation range (blue) and variance over samples (red) with a maximum at 910 ± 90 km, in which the standard deviation reaches the maximum.

destination. For transportation networks, the cooperation range is defined as the geographical distance between nodes, but other spatial networks might require other metrics, such as travel time or cost.

We increase network robustness through link swaps. Instead of adding or deleting connections, rerouting does not change the transportation capacity of the system: no airport would have to be expanded as the number of routes does not change. Moreover, a connection is only rerouted to an airport within the cooperation range of the original destination. As an example, flights could be distributed between Hong Kong and Schenzen or among the airports surrounding London. Lastly, the probability to swap a route is inversely proportional to the weight of a link e_{ij} between airports i and j, so that important connections are affected with less priority.

Table 4.1 – **Characteristics of the WAN and its continents.** Continental networks contain flights in which both end-points are in the same continent. Australia includes all islands in the Pacific ocean. For simplification, Russia is entirely part of Europe, and Turkey is entirely in Asia.

Name	Nodes	Links	Passengers (daily)	Flights (daily)	Average Degree	Passengers per Airport (daily)	Flights per Airport (daily)	Distance btw Airports (km)	Route Length (km)
Africa	269	642	220,481	3,023	4.77 ± 0.43	819.63 ± 129.59	2.35 ± 0.10	3,759.92 ± 10.52	1,139.23 ± 44.35
Asia	773	3,911	2,409,160	23,406	10.12 ± 0.64	3,116.64 ± 281.14	2.99 ± 0.07	4,089.57 ± 4.16	1,338.13 ± 19.76
Australia	288	567	178,447	2,499	3.94 ± 0.39	619.61 ± 132.87	2.20 ± 0.11	3,450.12 ± 10.14	810.18 ± 39.03
Europe	602	5,188	1,907,980	25,587	17.24 ± 1.07	3,169.40 ± 391.04	2.47 ± 0.07	2,410.24 ± 4.05	1,250.84 ± 12.11
North America	1,006	4,289	2,344,470	20,593	8.53 ± 0.62	2,330.48 ± 245.49	2.40 ± 0.08	3,386.44 ± 2.66	1,150.44 ± 15.67
South America	299	762	380,348	3,984	5.10 ± 0.44	1,272.07 ± 154.33	2.61 ± 0.10	2,719.93 ± 6.84	793.98 ± 27.81
World	3,237	18,125	7,440,880	94,644	11.20 ± 0.42	2,298.70 ± 127.80	2.61 ± 0.04	8,678.58 ± 1.92	1,734.64 ± 14.58

Given a cooperation range v and a metric $d(i,j)$, which calculates the distance between nodes i and j, the following swap strategy is performed:

1. Select a node i randomly having at least one neighbor;

2. Select a neighbor j of node i with probability inversely proportional to the weight of e_{ij};

3. Select a pair of connected nodes k and l so that $d(i,k) \leq v$ and $d(j,l) \leq v$ with probability inversely proportional to the weight of e_{kl};

4. Remove links e_{ij} and e_{kl} and create links e_{il} and e_{jk}.

This strategy is illustrated in Fig. 4.1. Swaps change the network robustness r but we only perform swaps that increase r. From this point on, we call such a swap, a *geo swap*. A fixed number of geo swaps of the order of the number of links is executed. To compare networks of different sizes and populations, we normalize the robustness as $R = (r - r_{\min})/(r_{\max} - r_{\min})$, in which $r_{\min}$ is the value of r for $v = 50$ km, the minimum value for which a geo swap
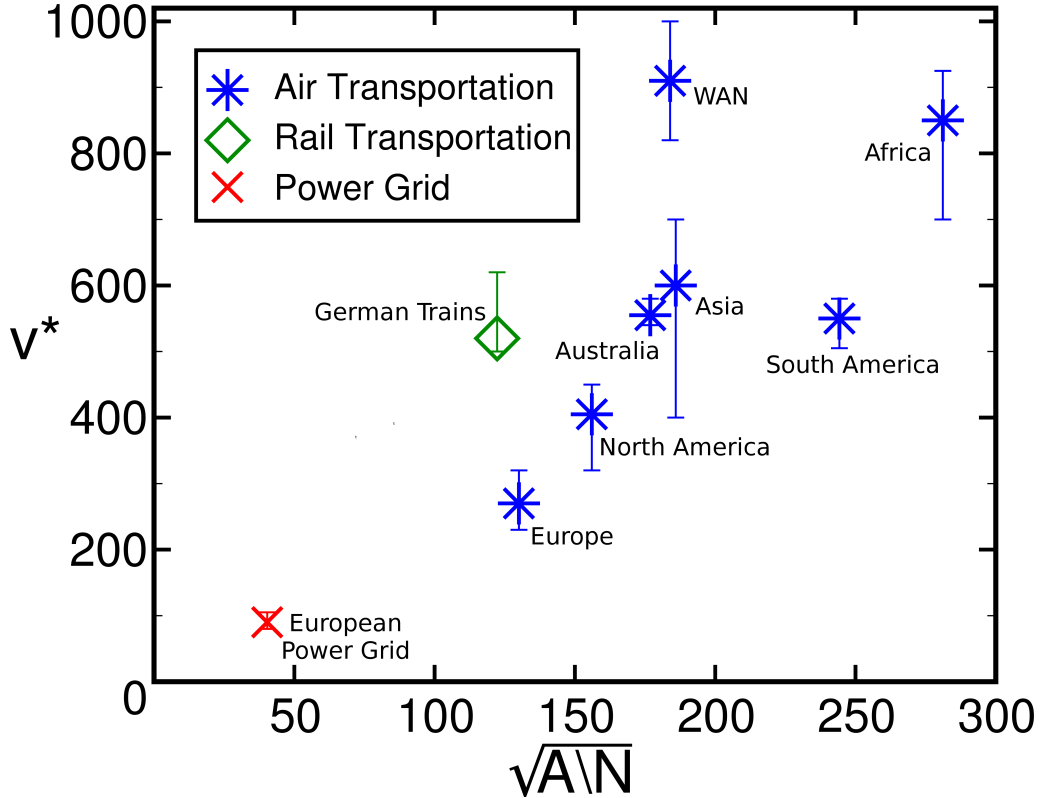
Figure 4.3 – **Critical cooperation range as a function of the nodes' coverage.** The critical cooperation v^* is positively correlated with $\sqrt{A/N}$, where A is the total area in which N nodes are embedded. The three different symbols represent the types of infrastructure networks in which the geo swap is applied.

will be considered in the WAN, and the maximum robustness r_{max} obtained for $v = 18 \times 10^3$ km, which is approximately half of the planet perimeter. This strategy builds on top of our previous approaches based on different acceptance mechanisms (Sec. 2.2.4) or topological characteristics (Sec. 3.2), but differs significantly by focusing on geographic limitations and low-weight links.

4.3 Results

The cooperation range v limits the area of possible swaps to guarantee that a geographically acceptable change is performed. A too small value of v does not provide sufficient room for robustness improvement. If v is too large we recover the properties of networks optimized with random swaps [58], such as the presence of an onion-like structure (Sec. 3.2.1), but we end up swapping connections to impractically far away airports. By tuning the values of v, we
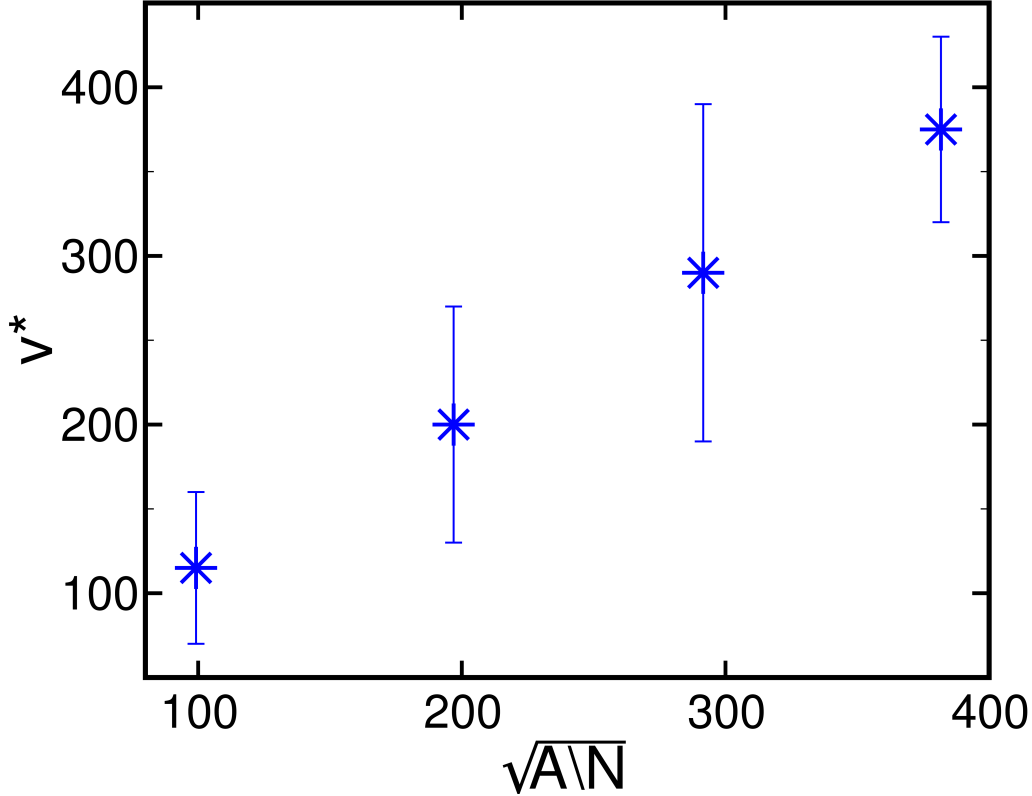
Figure 4.4 – **The critical cooperation v^* correlated with** $\sqrt{A/N}$, where A is the total area in which N nodes are embedded, in ER networks.

observe a critical value of the cooperation range $v^* = 910 \pm 90$ km at which a significant improvement in the WAN is first registered. This range in fact yields the highest variance of robustness increase among all possibilities, as shown in Fig. 4.2. Details regarding this and all other simulations are in Appendix B.

By considering continental airflight networks - constructed from the division of the WAN into continents (details in Table 4.1) - together with other spatially embedded networks (the European Power Grid and the European Rail network), we observe that v^* is positively correlated with $\sqrt{A/N}$ (Spearman's correlation coefficient $\rho = 0.78$), where A is the total area in which the N nodes are embedded (Fig. 4.3). Being the combination of local and intercontinental flights, the WAN lies slightly off the trend, but in general we can conclude that the typical radius served by an airport is correlated to the minimum distance at which swaps become effective. Artificially generated random networks also confirm this relationship (Fig. 4.4). Other topological characteristics of the optimized networks are detailed in Fig. 4.5.
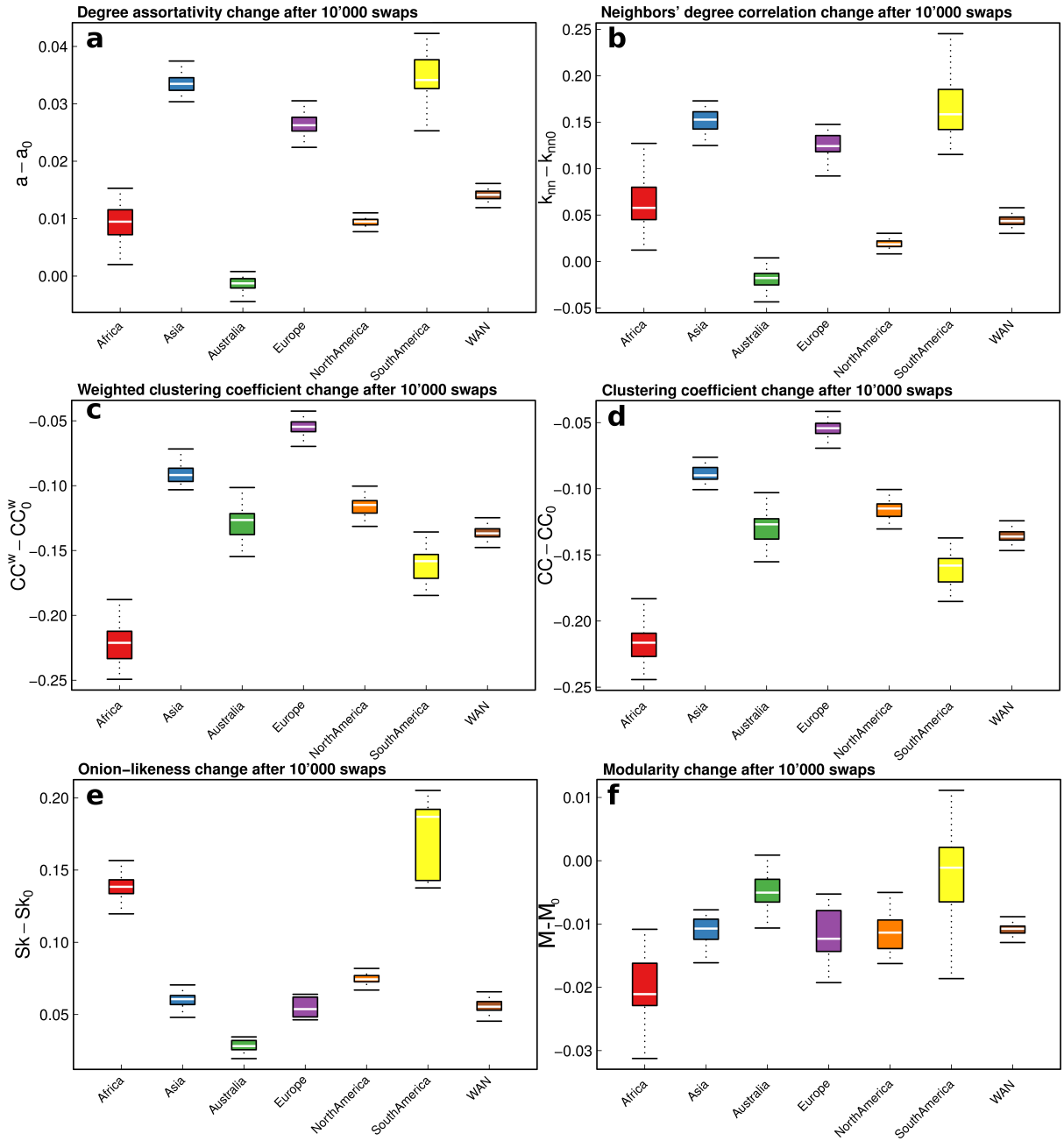
Figure 4.5 – **Changes on networks characteristics after successive geo swaps with** $v = v^*$. The strategy makes the networks more assortative, more onion-like, but also more random, as clustering coefficient and modularity decrease. Plots show the change of several features of the airport networks after 10^4 tentative geo swaps. **a,** Degree assortativity (a) [96]. **b,** Neighbors' degree correlation (k_{nn}) [25]. **c,** Weighted clustering coefficient (CC^w) [97], weighted by the number of passengers per airport. **d,** Clustering coefficient (CC). **e,** Onionlikeness (Sk) (Sec. 3.2.1). **f,** Modularity (M) [98]. The subscript 0 represents the value of the feature without any optimization.

Close to the critical cooperation range, the evolution of R scales with $v - v^*$ for the continental networks. Applying the finite-size scaling,

$$R = N^{-\frac{\beta}{\nu}} \mathcal{F} \left[(v - v^*) N^{\frac{1}{\nu}} \right], \qquad (4.2)$$

where ν and β are critical exponents and $\mathcal{F}[x]$ is a scaling function, we collapse the data for different system sizes. For $v = v^*$, as shown in the inset of Fig. 4.6, R scales with $N^{-\frac{\beta}{\nu}}$, with $\beta/\nu = 0.08 \pm 0.01$, as expected for a continuous transition. This allows us to calculate the exponents in the main panel of Fig. 4.6 as $\beta = 0.20 \pm 0.02$ and $1/\nu = 0.40 \pm 0.03$. The data suggest that the construction of airports and the creation of connections follow a similar mechanism in all continents, though the limited system size of each continent and obvious geographic differences prevent strong conclusions. However, data for Australia significantly differs from the others. Because a great number of islands in Oceania have many small airports, sometimes being the only feasible connection between remote areas, we assume that airports and flights in this continent were established following a different mechanism.

Spatial networks are mainly defined by three properties: nodes' position, degree distribution, and connection pattern. A simplified model - where nodes are assigned random positions, the degree distribution is a Poisson distribution, and connections are randomly assigned without any spatial/degree bias - displays different critical exponents (Fig. 4.7). However, if the probability $P(i, j)$ that nodes i and j are connected decays algebraically with the distance between i and j,

$$P(i, j) \propto \frac{1}{d(i, j)^\alpha}, \qquad (4.3)$$

where $\alpha \in \mathbb{R}$ is the decay exponent, we obtain exponents that are numerically consistent with the ones in Fig. 4.6. Based on a simplification of the gravity model, used to describe connections between geographically distributed nodes [29, 99–101], we call Eq. 4.3 a *distance-decay* model as it does not take into account the degree/weight of the nodes to calculate $P(i, j)$.

To test Eq. 4.3, we plot a new data-collapse in Fig. 4.8 based on networks generated as follows. Node positions are uniformly distributed across an Earth spherical cap of area A and in order to keep $\sqrt{A/N} \approx 195$, the same value of the WAN, network size is calculated accordingly. Node degree follows a Poisson distribution of average degree 12. Node weights are chosen according to the equation $W(i) = 102.6 k_i^{1.1}$, where k_i is the degree of
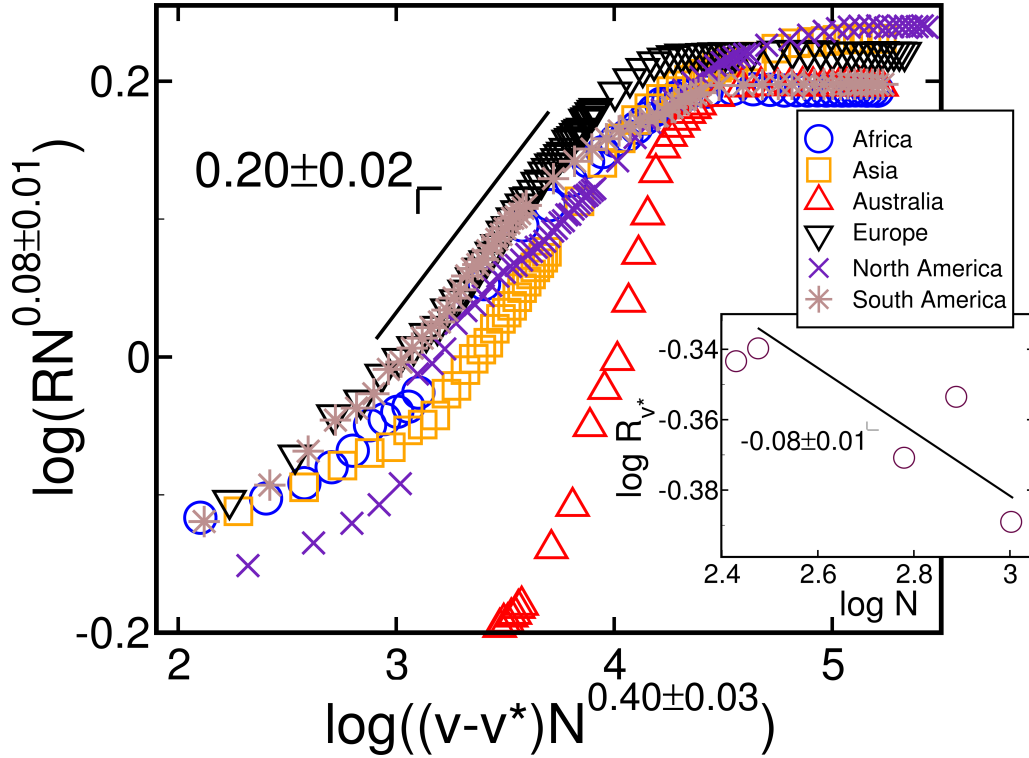
Figure 4.6 – **Continuous transition of robustness.** Data collapse of the robustness evolution for $v - v^* > 0$ after successive applications of the geo swap. Curves in the main panel represent each continent. A total of 10^4 tentative geo swaps are executed for several cooperation range values. The value of v^* is selected as the highest variance point over 100 samples. Data is scaled using $1/\nu = 0.40$ and $\beta/\nu = 0.08$. The inset shows size dependence of R at $v = v^*$, scaling as $R \sim N^{-\frac{\beta}{\nu}}$, with $\beta/\nu = -0.08 \pm 0.01$, where N is the total number of nodes. Symbols are larger than the standard deviation.

node i, which is a fit of the relationship between node weights and degree of the WAN. Link weights are randomly distributed from $[1, 14]$, in which 14 is the maximum link weight on the WAN. We observe that changes in the value of α affect consistently the slope in the data-collapse (Fig. 4.8b). We find a value of β similar to the one of the continents, without Australia, for $\alpha \in [1.8, 2.0]$. For $\alpha = 2.0$, the finite-size scaling in Fig. 4.8c allows us to estimate: $\beta = 0.23 \pm 0.02$ and $\beta/\nu = 0.08 \pm 0.01$ (Fig. 4.8a and Fig. 4.8c). Further analysis also show that when $\alpha \approx 2$ the ratio between the average length of routes and the average distance between two airports is similar to that found for the continents (Fig. 4.9). Interestingly, the empirical probability distribution of link lengths in the WAN is a power law of exponent $\alpha = 2.2 \pm 0.2$ (Fig. 4.10) with some studies linking this value to intrinsic characteristics of the underlying metric space [102, 103]. This suggests that
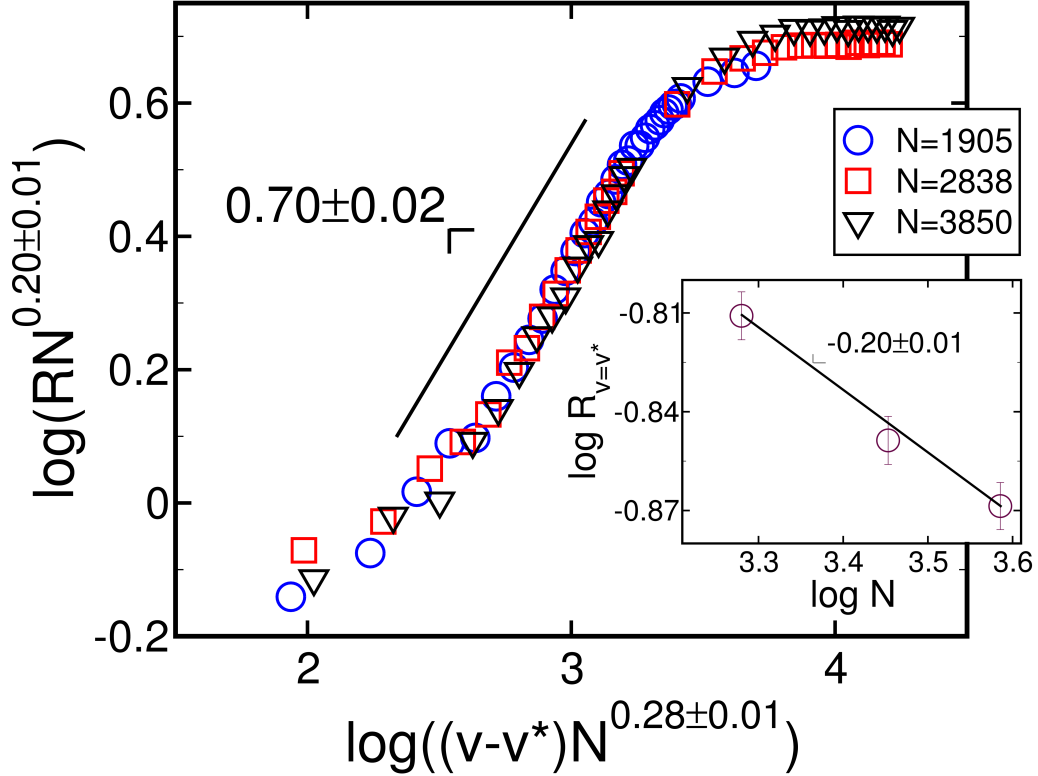
Figure 4.7 – **Data collapse of the robustness evolution for** $v - v^* > 0$ **after successive applications of the geo swap in random networks**. Curves in the main panel represent each continent scaled with $1/\nu = 0.28$ and $\beta/\nu = 0.20$. The inset shows the size dependence of R at $v = v^*$, scaling as $R \sim N^{-\frac{\beta}{\nu}}$, with $\beta/\nu = -0.20 \pm 0.01$, where N is the total number of nodes. Data is based on artificially generated random networks but with links randomly assigned without any bias.

correlations as the ones developed in the distance-decay model are consistent with the ones found for the WAN and characteristic for the universality class.

4.4   Discussion

In order to provide applicable insights, any network modification strategy should take into account realistic constraints naturally imposed by the problem. The geo swap contains a simple set of rules specifically designed to improve the robustness of spatial networks. It is important to note however that a probabilistic approach is more a guidance than a closed optimization recipe. We expect that future procedures built on top of our strategy should be carefully tailored to the underlying system.

In an infrastructure perspective, the geo swap, which makes flights land in different airports, has two crucial implications. Firstly, a second transporta-
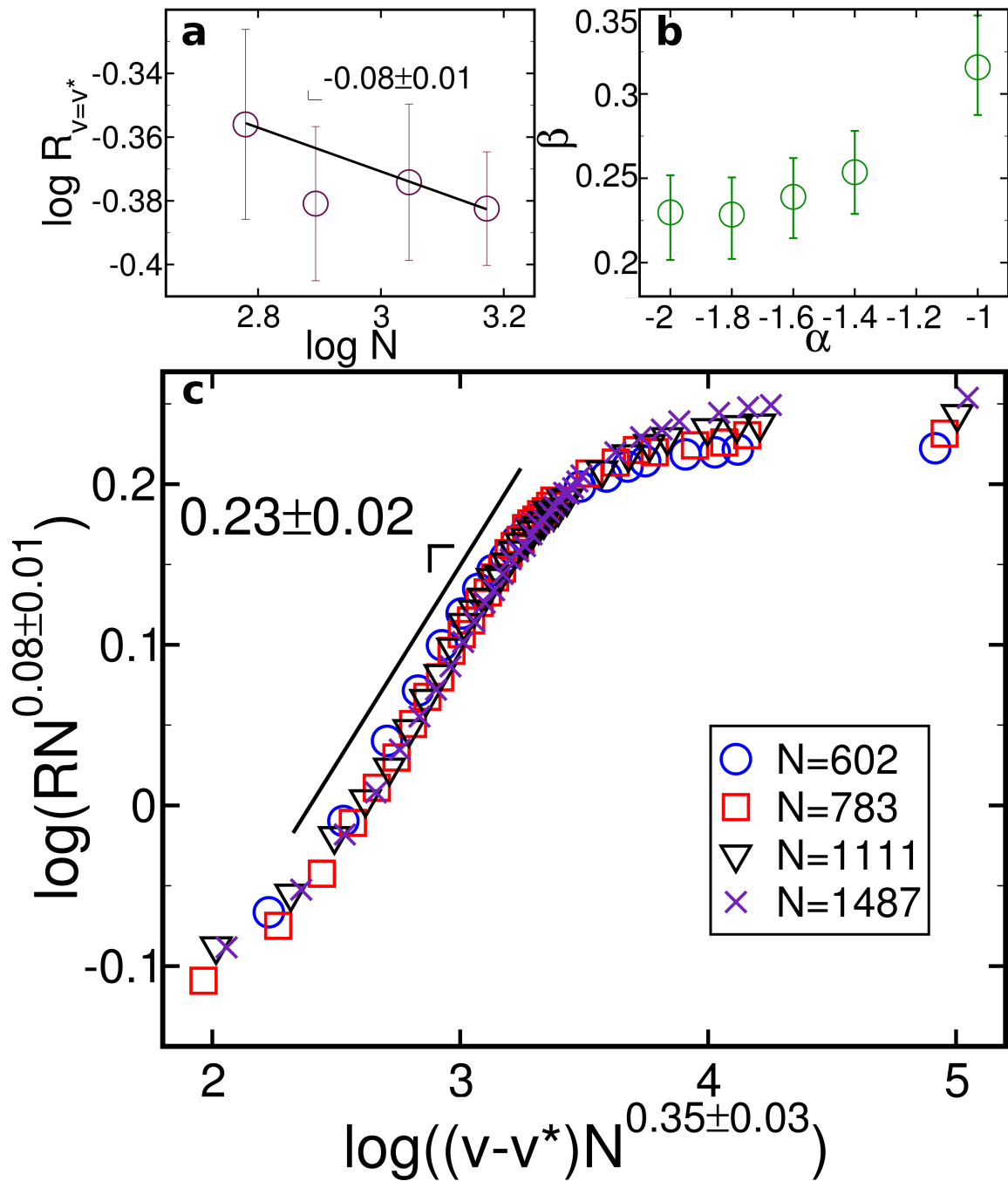
Figure 4.8 – **Distance-decay model reproduces the same critical exponents of the WAN.** Data-collapse of the robustness evolution for $v - v^* > 0$ after successive applications of the geo swap on random networks generated through the distance-decay model with $\sqrt{A/N} \approx 195$. **a,** value of R at $v = v^*$ with $\alpha = 2.0$ scaling with the number of nodes (N) as $R \sim N^{-\frac{\beta}{\nu}}$, with $\beta/\nu = -0.08 \pm 0.01$. **b,** impact on β for the distance-decay model with different values of α. **c,** curves for different system sizes with $\alpha = 2.0$, scaled using $1/\nu = 0.35$ and $\beta/\nu = 0.08$.

tion system should be used to connect nearby airports, in line with recent works dealing with the coupling of infrastructure networks [104]. By taking into account the critical cooperation range these couplings could be designed or improved for distances close to v^*. Secondly, a local level of cooperation is necessary between airports. Flights in Schenzen and Hong Kong could be rerouted to attend different yet nearby airports worldwide, further increasing the reliability of the local service and the overall WAN robustness.

Our rewiring strategy is also able to show that the continents, with one exception, follow the same universality class regarding robustness improvements, as the probability that two airports are connected decays quadratically with their distance. Being a continent with its own geographical idiosyncrasies, Australia does not fit our analysis, for which further studies are necessary. In summary, our results show that, for any spatial network, the universality class of the robustness improvement strongly depends on the spatial correlation of connected nodes.
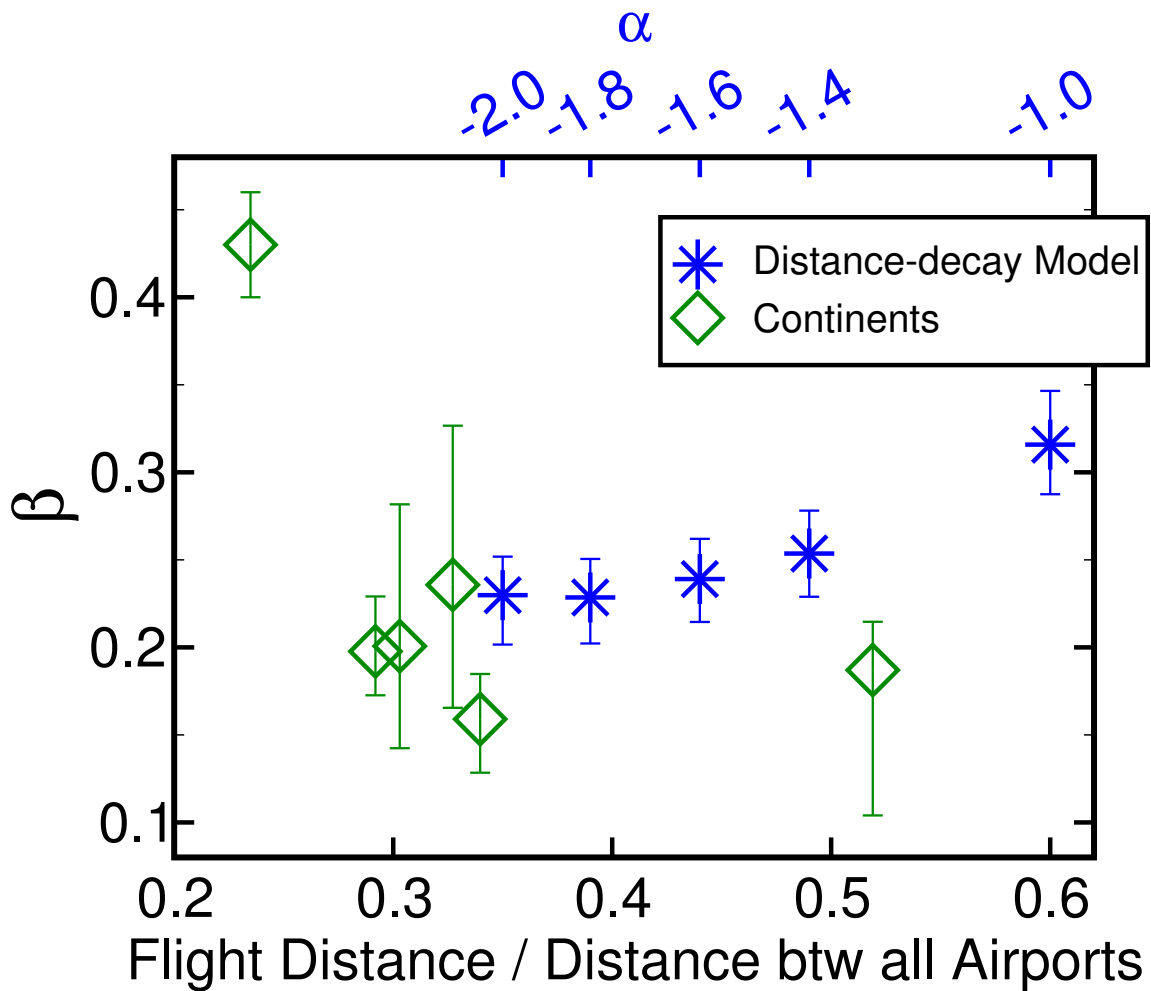
Figure 4.9 – **Distance-decay model reproduces the same β for different ratios between the average distance traveled by the flights (route length) and the average geographical distance between two airports of the WAN.** Plot shows the impact on β for the distance-decay model with different values of α (blue) in comparison with data for the continents (green).
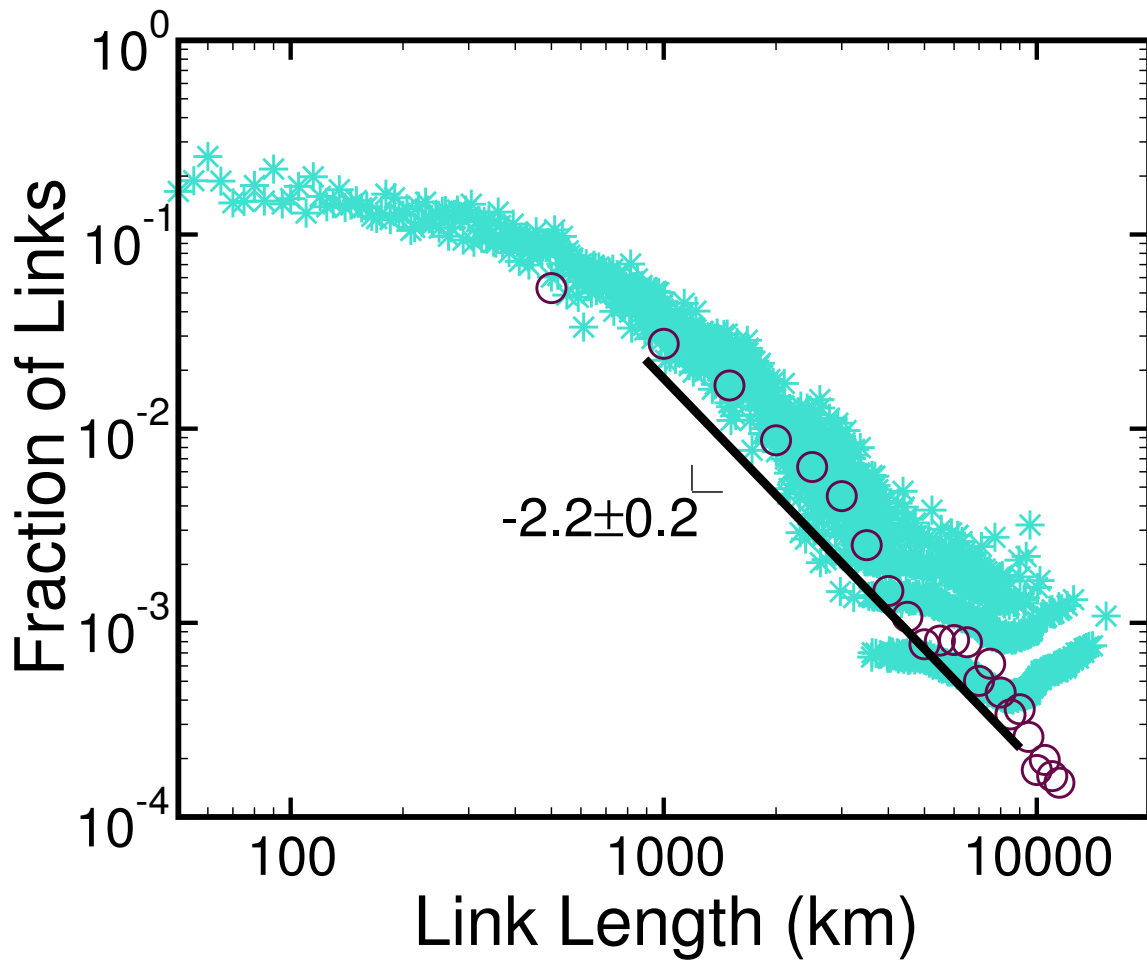
Figure 4.10 – **Flight distance distribution (route length) of the WAN**. The empirical distribution of flight length shows a power law decay with exponent -2.2 ± 0.2. Both raw (turquoise) and binned (purple) data are shown in the plot. For simplicity, an exponential cutoff is not considered.

Chapter 5

Synchronization Risk of Complex Networks

It's a poor sort of memory that only works backwards.

— Lewis Carroll.

5.1   Introduction

In the year 2000, Londoners were presented with the Millennium Bridge, a futuristic footbridge that became the center of attention on the inauguration day. The elbowing of the crowd, eager to be the first to cross it, forced the synchronization of walkers causing a lateral swing of the structure [105]. Once on this wobbly structure, how could one avoid such uncomfortable situation? The risk of synchronization, here defined as the possibility that agents behave in a synchronized fashion with further dreadful consequences, is a real threat in many situations.

In fact, the risk of synchronization has been observed in many other circumstances. Abnormal synchronization is also the origin of neurological diseases such as epilepsy and Parkinson [106]. Brain pacemakers have been developed and implanted in the patient to discharge an electrical signal into the brain tissue and restore the normal activity [107–109]. But imagine a, still to develop, device able to interact with individual neurons. What would be the best strategy to break the synchronization? A third source of inspiration can be found in the Internet, where several interconnected routers receive and redistribute the information packages in the network. When multiple routers synchronize their delivering events, the network collapses, a dysfunction known as TCP global synchronization. To avoid it, several algorithms

have been developed and implemented in some routers [110]. What is the fraction of such proactive routers required to avoid global synchronization? In social context, avoiding synchronization might represent a political tool to fight a charismatic leader. Consider a speech that inflames a crowd. Initially every individual claps at his/her own rhythm but rapidly a coherent clap emerges [111]. If a set of political adversaries (contrarians) try to destroy the harmony, what would be the best strategy, the proper amount of contrarians, and their spatial distribution in the hall?

The Kuramoto model has extensively been used as the paradigm to study synchronization [19, 111–122]. In a first attempt to address the questions raised above, we generalize this well-established model to include contrarians which try to suppress the emergence of global synchronization. We present a systematic study of how the synchronizability depends on the fraction of contrarian oscillators for two different strategies and analyze the influence of the topology in the mitigation process. To illustrate our results, contrarian oscillators have been studied *in silico* for two real networks, namely, the routers that compose the Internet [123] and the network of neurons of the organism *C. elegans* [124, 125]. Our results suggest that local contrarians can be used as a powerful way to control synchronization, avoiding the necessity of monitoring the global state. Moreover, spreading contrarians as hubs is also much more effective.

5.2   Model

The described examples are characterized by a set of N oscillators (walkers, neurons, routers, or spectators), mutually interacting. Hereafter we take the example of the walkers but the model can be straightforwardly extended to all other cases. The stepping of each walker i is characterized by the phase $\theta_i(t)$ and its natural frequency ω_i, corresponding to the stepping frequency when isolated. When the crowd moves, all walkers initially step at their natural frequency but herding (under strong coupling) rapidly leads to coherent walking [105]. In the Kuramoto model, the motion of each oscillator is described by a phasor $e^{i\theta_i(t)}$, where $\theta_i(t)$ is the phase, and the coupling between walkers is such that the dynamics of each is governed by,

$$\dot{\theta}_i = \omega_i + \lambda \sum_{j=1}^{N} A_{ij} \sin\left(\theta_j - \theta_i\right), \qquad (5.1)$$

where the sum is over all other walkers ($i \neq j$), λ is the coupling strength, ω_i is the walker's natural frequency, and $\mathbf{A}$ is the connectivity matrix such that $A_{ij} = 1$ if walker i is influenced by walker j or zero otherwise. The collective walking can be characterized by the complex order parameter defined as,

$$r(t)e^{i\Psi(t)} = \frac{1}{N} \sum_j^N e^{i\theta_j(t)}, \qquad (5.2)$$

where the sum is over all walkers, the amplitude $0 \leq |r(t)| \leq 1$ measures the global coherence, and $\Psi(t)$ is the average phase (geometric mean).

To account for contrarians we introduce a second population of N_c walkers also coupled with the others but following a different dynamics. A contrarian k is also characterized by the phase $\theta_k(t)$ and its natural frequency ω_k. We consider two types of coupling: a mean-field (Model A) and a pairwise (Model B). In the mean-field coupling the dynamics of contrarians is governed by,

$$\dot{\theta}_k = \omega_k + \lambda \sin\left(\Psi - \theta_k - \delta\right), \qquad (5.3)$$

where $\Psi(t)$ is the average phase and δ is a phase shift. In the pairwise coupling the dynamics of contrarians is governed by,

$$\dot{\theta}_k = \omega_k + \lambda \sum_{j=1}^{N_T} A_{kj} \sin\left(\theta_j - \theta_k - \delta\right), \qquad (5.4)$$

where the sum is over all the N_T walkers ($N_T = N + N_c$). Hereafter, we take $\delta = \pi$ in both cases. Such phase shift between two walkers (k and j) would correspond to a walking such that when k steps with the left foot j steps with the right. It is noteworthy that these two models yield different types of frustration. While in Model A frustration between regular and contrarian walkers is mediated by the average phase, in Model B the frustration results from a pairwise interaction between regular and contrarian walkers where the former attempts to mutually synchronize while the latter tries to dephase.

Two models accounting for frustration in the mean-field Kuramoto model have recently been discussed in the context of a mixture of positive and negative couplings. Zannette [126] considered a pairwise coupling where the strength and sign of the interaction between two oscillators is symmetric. This model, in the limit $\omega_k = 0$, is equivalent to a magnetic XY model with a distribution of couplings. Hong and Strogatz proposed a different scheme, where regular walkers are also solely coupled with the average phase $\Psi(t)$ and the spatial distribution of regular walkers is not considered [127, 128]. This
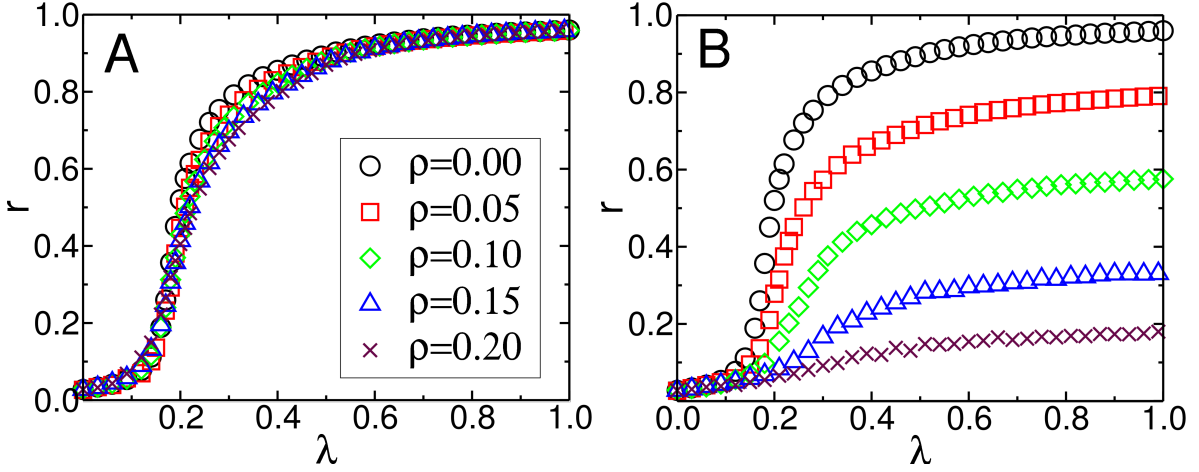
Figure 5.1 – **Comparison between mean-field and pairwise coupling.** Dependence of the order parameter r on the coupling strength λ, for the mean-field (A) and the pairwise (B) couplings. Different curves stand for different fractions of contrarians ρ randomly distributed in a random graph with average degree equal to four.

model is similar to the mean-field limit of Model A discussed here. In contrast to the model discussed here, synchronization cannot be suppressed in any of these previous models. Wang and Slotine [129] use contraction theory to derive results when the interaction between two oscillators are of a contrarian nature. While failing to consider the minimal amount of contrarian oscillators to achieve any practical interference, nor the influence of a spatial distribution of contrarians, they recognize that the application of such types of oscillators in possible brain pacemakers or network communication are promising.

5.3 Results

In the absence of contrarians, the classical Kuramoto model is characterized by the emergence of synchronization at a critical coupling λ_c which depends on the distribution of natural frequencies (ω) and on the degree. While under weak coupling ($\lambda < \lambda_c$) the motion is incoherent ($r = 0$), above the critical coupling a coherent motion emerges ($r > 0$). In the limit of very strong coupling ($\lambda \gg \lambda_c$) all oscillators participate in the coherent motion.

The presence of contrarians can affect the coherent motion. In Figure 5.1, different fractions $\rho = N_c/N$ of contrarian oscillators are considered in the mean-field (A) and pairwise (B) models. While mean-field contrarians are not able to reduce the value of r, a fraction as small as 5% of pairwise contrarians
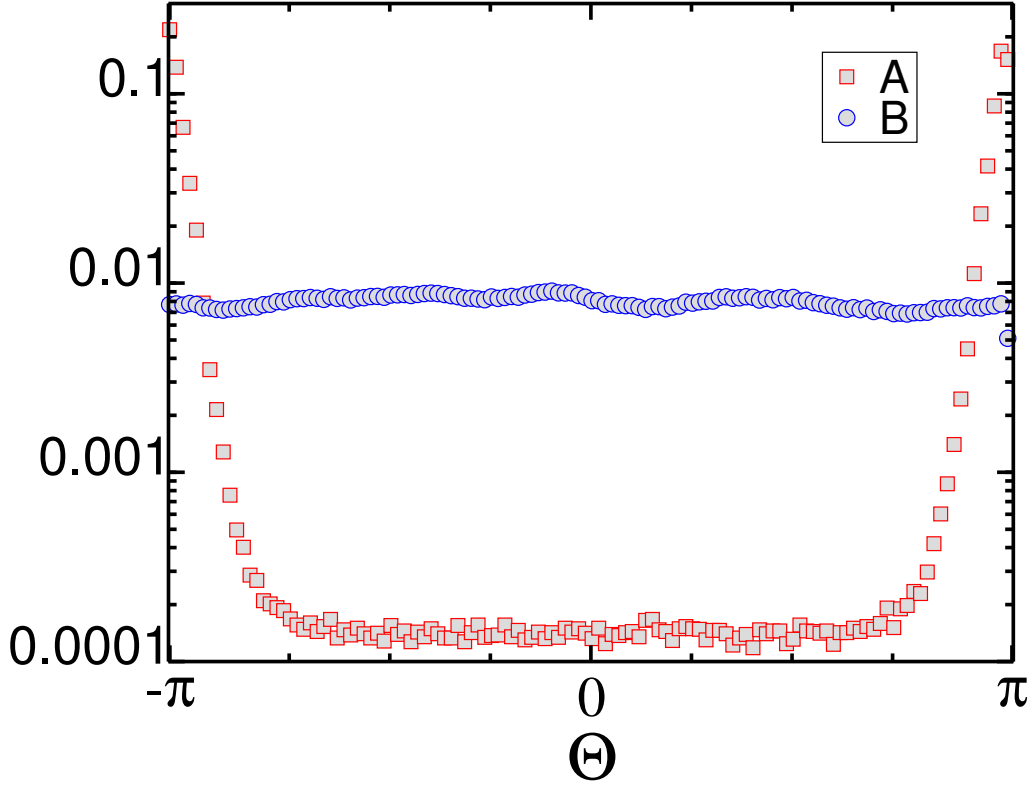
Figure 5.2 – **Distribution of oscillator phases**. Histogram of the phase of oscillators for $t = 100$. Curves represent oscillators according to the mean-field (A) and pairwise (B) models, both with 10% of contrarians and $\lambda = 1.0$. While mean-field contrarians are frozen in $-\pi$ and π, pairwise contrarians are uniformly distributed through all phases.

is enough to significantly reduce the synchronizability. Further investigation shows that, although contrarians enable the system to desynchronize, mean-field contrarians drive the system to a polarized state, where oscillators are concentrated around two phases: $-\pi$ and π. It is possible to understand this splitting through the analysis of the stable point (given by $\dot{\theta}_k = 0$) for contrarians in the mean-field model, yielding

$$\lambda \sin(\Phi - \theta_k - \pi) = -\omega_k. \tag{5.5}$$

Assuming that ω_k is symmetrically distributed around zero, this equation shows that the difference between the phase of contrarians and the average phase must be equal to π. Thus, contrarians have a tendency towards the extremes of the possible phases, dragging their conformist neighbors in the process. Hence, mean-field contrarians introduce differences in the dynamic behavior of oscillators by polarizing them in two distinct phases (see Fig. 5.2). Details regarding this and all other simulations are in Appendix C.
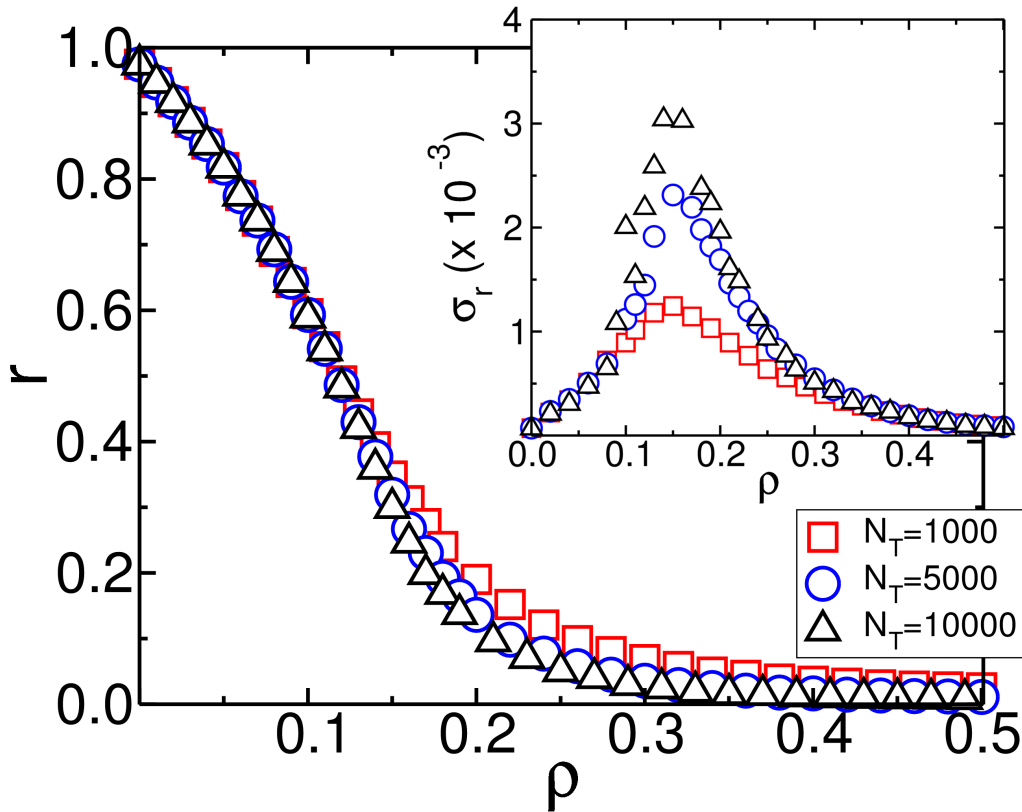
Figure 5.3 – **Impact of pairwise contrarians on the synchronization.** Order parameter r dependence on the fraction of contrarians ρ showing suppression of synchronization. Different curves stand for different network sizes. The inset contains a plot of the standard deviation of r among samples showing a transition around $\rho = 0.15$. A coupling strength of $\lambda = 2.0$ has been used.

For the pairwise (B) contrarians, the emergence of a coherent state is suppressed above a certain fraction of contrarians (Figure 5.3). We notice that synchronization is suppressed for values of $\rho > 0.15$, as shown by the peak in the standard-deviation of r in the inset of Figure 5.3. The peak increases with the network size. For small values of ρ synchronization is maintained, $r > 0$, as conformists synchronize their phases with each other and the small fraction of contrarians dephase from their neighbors without destroying global synchronization. In this situation, the average phase of contrarians and conformists create a periodic alternating wave over time, an interesting mechanism that resembles, for instance, the oscillation of populations of predators and preys which characterizes the classical Lotka-Volterra model [130]. Figure 5.4 shows an example where contrarians (the central layer of the networks in the upper part) are in opposition to their first neighbors conformists, which in turn try to synchronize with them. The sequence of networks
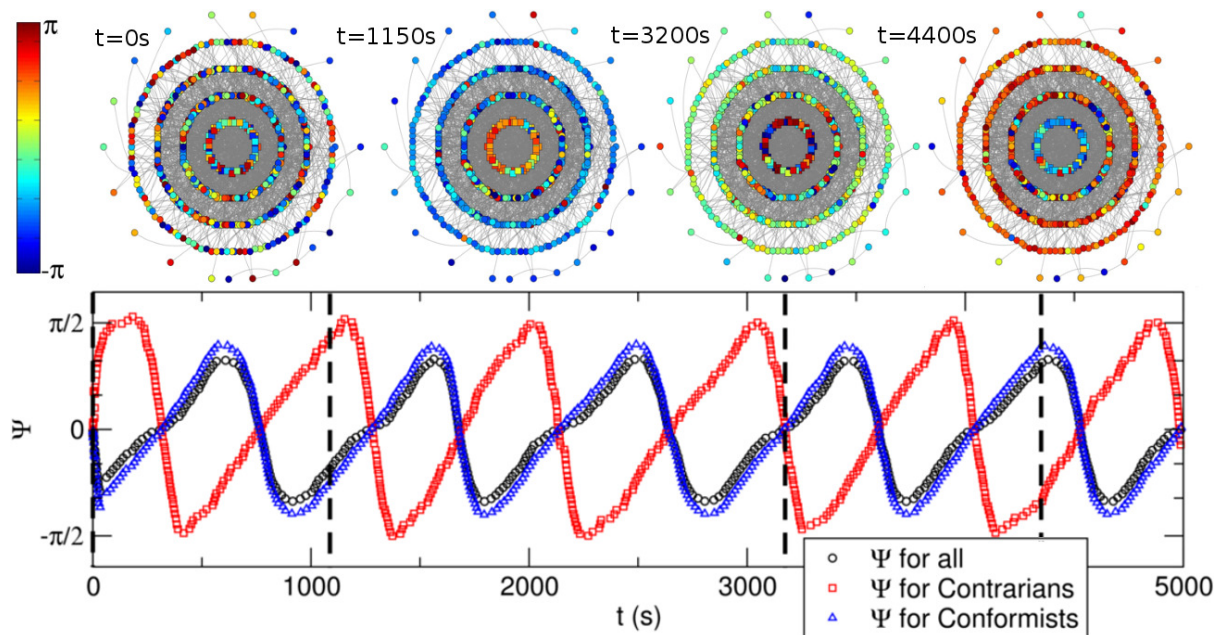
Figure 5.4 – **Time dependence of the phase. Upper part**: Snapshot of a network of 200 oscillators at 4 different time steps (vertical dashed lines in the lower part). A total of 20 pairwise contrarians are displayed in the central layer. Each concentric layer i, from inside to outside, contains the ith neighbors of the contrarians. The color of each node represents its phase. **Lower part**: Time dependence of the average phase of contrarians (red squares), conformists (blue triangles), and the whole set of oscillators (black circles) showing a periodic oscillation over time.

in the figure are snapshots of the oscillators and their phase over time. Before all conformists could match their phases with contrarians, the latter already have an opposite phase. The periodic wave that conformists and contrarians create is clear in the lower part of Figure 5.4 which shows the average phase of different types of oscillators.

As the fraction of contrarians overcomes a certain threshold, the effect of contrarians spreads over the entire network completely suppressing global synchronization. This suppression is a consequence of an increasing fraction of contrarian/contrarian interactions, which naturally tend to be dephased, reinforcing their impact. For $\rho > 0.15$, neither synchronization ($r = 0$) nor a periodic wave is observed (see Fig. 5.5).

5.3.1 Contrarians as Hubs

The phenomenon of synchronization is known to result from the interplay between the network topology and the dynamics of oscillators [131, 132]. In
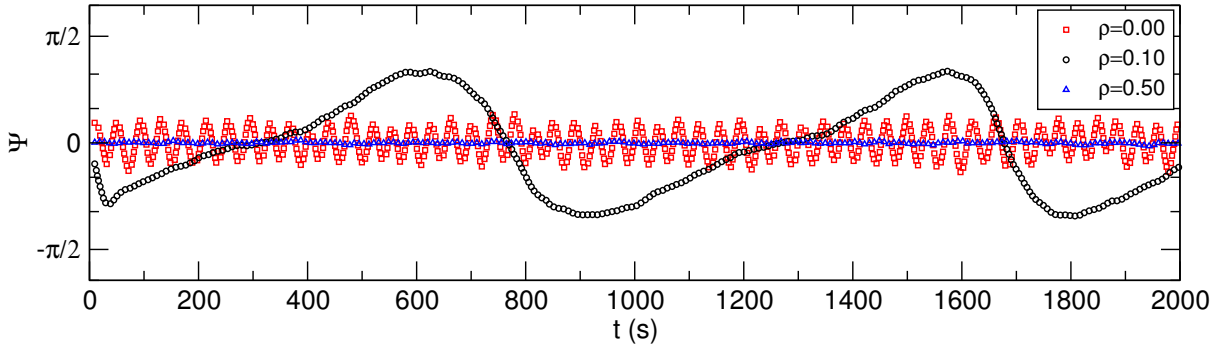
Figure 5.5 – **Average phase of oscillators with different fractions of pairwise ρ contrarians**. Time dependence of the average phase of oscillators for different fractions of randomly assigned contrarians. The amplitude of the wave goes to zero with the fraction of contrarians.

this section, we discuss the improvement in the desynchronization efficiency by distributing the contrarians among the oscillators (nodes) with higher degree and compare this strategy with the random distribution case discussed above.

We start considering the case of a random graph (Erdős-Rényi (ER) network), characterized by a Poisson distribution of degree. As shown in the Fig. 5.6, in spite of the narrow degree distribution, the fraction of contrarians necessary to reduce synchronization is reduced to one third ($\rho = 0.05$) when contrarians sit at the nodes with higher degree. In this case, the disturbing effect of contrarians occurs even for smaller fractions ρ and synchronization is efficiently suppressed. In scale-free networks, where the degree distribution follows a power-law and highly connected nodes are more frequent, the assignment of hubs as contrarians is even more effective (see Fig. 5.7).

5.3.2   Contrarians in Real Networks

The presence of communities and other features, such as assortativity and clustering, also play a role in synchronization [133, 134]. Here we consider two real networks and show that the same behavior holds (see Figure 5.8). The first one is the network of routers in the Internet. This network is believed to have grown through the mechanism of preferential attachment, being characterized by a scale-free degree distribution of exponent $\gamma = 3.00$ [135]. Moreover, it has been shown to have a hub dominant structure, where many hubs share low degree neighbors [136]. In this case, similarly to scale-free networks, hubs play a major role in the synchro-
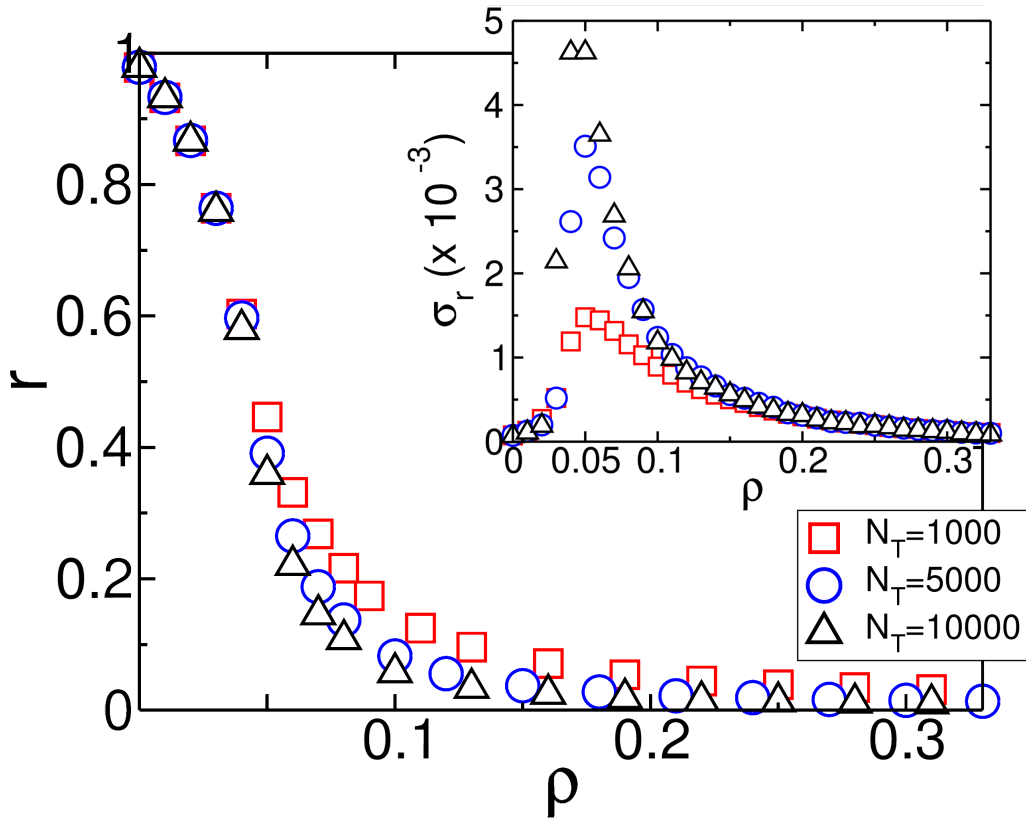
Figure 5.6 – **Impact of pairwise contrarians assigned to the nodes of highest degrees on the synchronization of ER networks of average degree four.** Order parameter r dependence on the fraction of contrarians ρ for different network sizes showing a suppression of synchronization after the introduction of pairwise contrarians. The inset is the standard-deviation of r showing a transition around $\rho = 0.05$, much smaller than randomly assigned contrarians.
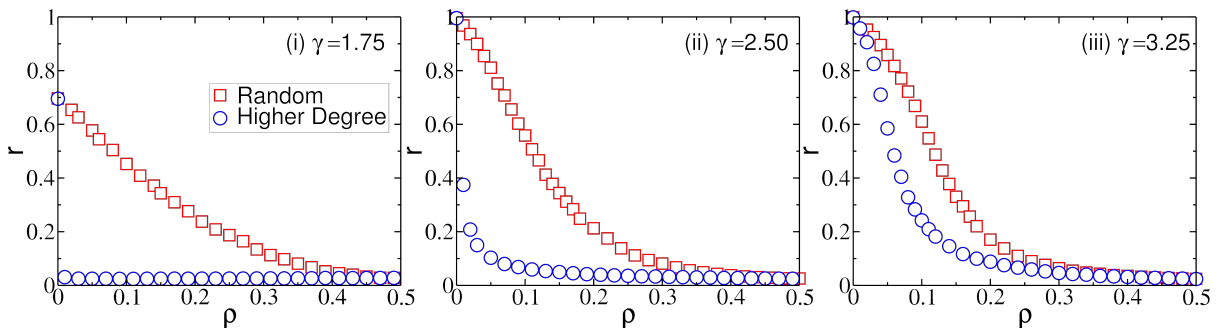
Figure 5.7 – **Scale-free networks with contrarians.** Fraction of pairwise contrarian oscillators assigned randomly and based on their degree to scale-free networks of different degree exponent γ, namely, 1.75, 2.5, and 3.25.
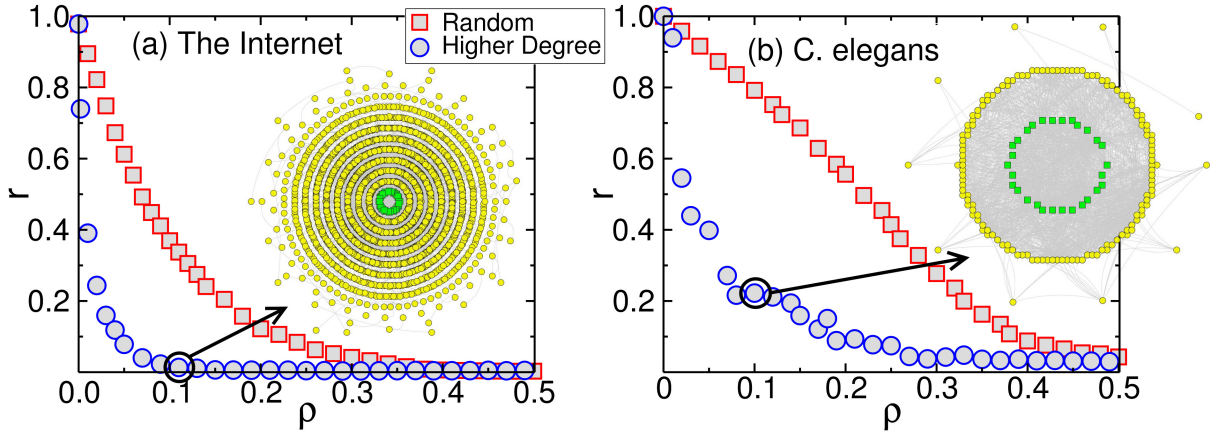
Figure 5.8 – **Pairwise contrarians on real networks.** Fraction of contrarian oscillators randomly assigned and based on the degree for different networks: **(a)** the routers of the Internet, **(b)** neurons on *C. elegans*. The insets are snapshots of the referred networks where each concentric layer i, from inside to outside, contains the ith neighbors of the contrarians. The color of each node represents its type: contrarians (green) and conformists (yellow). A coupling strength of $\lambda = 4.0$ has been used.

nization, and only 10% of them are necessary to suppress synchronization. Highly connected contrarians have a disordering effect on a great number of conformists and a few hubs control the phase of the entire set of oscillators. The second one is the neuronal network of the organism *C. elegans*, a Small-World network and the largest network of neurons that has been totally mapped [20]. There, random or degree-based distribution of contrarians suppress synchronization, although the network seems to be more resilient to such control than ER networks. The presence of functional communities of neurons that are highly connected within themselves might be the cause of this resistance [137]. It is interesting to note that this biological system, evolved under evolutionary pressure, has converged to a resilient structure regarding synchronization.

5.4   Discussion

The best way to use agents to control the dynamics of a network is still an open debate [138, 139]. We have shown that global synchronization can be suppressed with local agents (contrarians) which systematically dephase from their nearest neighbors. We show that solely local information is required to efficiently avoid a coherent oscillatory state. If instead, global information is considered, the set of oscillators splits into two oscillatory states with differ-

ent phases and a global coherent state is still possible. Analyzing the impact of the network topology in desynchronization we concluded that, when contrarians sit at the nodes of higher degree, the process is more efficient than in the random case. Even with random graphs, characterized by a narrow degree distribution, the degree strategy reduces to one third the amount of required contrarians to suppress synchronization. We also show that the synchronization of real networks that present underlying features such as communities and dominant hubs is also suppressed with the use of contrarians.

The present work is the first attempt to understand the interplay between the desynchronization dynamics and the topology when considered to mimic real systems. The Kuramoto model provides a standard framework to study synchronization, however it entails several approximations when discussing real networks. For example, social systems are composed of adaptive agents that might change their strategy over time and avoid being trapped in a locked state. Developments build up on top of this work should account for further details on the coupling scheme and on the contrarian dynamics. For instance, here we have focused on the distribution of contrarians, but recent works have shown that rewiring interventions, such as swapping, adding, or removing edges, have a crucial role in the collective dynamics [140, 141]. Nevertheless, general conclusions can be drawn shedding light on the problems discussed in the introduction. For instance, as referred, some routers on the Internet have a special algorithm implemented to avoid synchronization. We have shown that placing contrarian routers as hubs on the network could optimize the fraction of proactive routers necessary to prevent global synchronization. Also, modifying the coupling mechanism between two routers and the contrarian strategy implemented, it becomes possible to extend our work to define the best location of contrarians on the Internet.

Regarding the development of brain pacemakers, our study suggests that a set of small size devices spread throughout the brain, and solely tracking the phase of neighboring neurons, would be more effective to prevent a seizure than monitoring the global state. After the mapping of a neural network [142], and the characterization of the coupling dynamics between neurons, our work also gives helpful hints about the minimum amount and the optimal spatial distribution of these active devices.

Interesting applications could also be found in social dynamics. Whenever a "social synchronization" is achieved, such as clapping after a speech, a small amount of influential agents can be trained to prevent this synchronization.

Political opponents could be spread in the crowd to avoid a proper salutation simply by "dephasing" their claps with their close neighbors. The same method might be used to prevent a synchronized walk on a bridge where instructed actors could walk dephased from others. Evidently crowd behavior control is a very hard task [143], but here we show that it could theoretically be achieved.

Chapter 6

Synchronization Fragility of Coupled Networks

If you cannot control yourself, you cannot command others.
— KLINGON HONOR GUARD MANUAL.

6.1 Introduction

Technology has furnished us with global connectivity changing the functioning of cooperative work, international business, and interpersonal relationships. However, despite the ever faster Internet connections, there will always be a physical limit speed to information transport, thereby imposing a time delay in communication. As we discuss here, this time delay affects the synchronization risk of oscillators.

Understanding the consequences of a communication lag is of major concern in different fields [65, 144, 145]. In what follows, we discuss the synchronization fragility of two networks connected through a communication delay, but our study might have impact on several biological and techno-social systems as, for example, the human brain. Being a highly modular structure, its coherent operation must rely on the independence of different brain modules, which are functionally specialized, as well as on their efficient connection to ensure proper information transmission and processing. In a recent study [146], it was shown that the optimal integration of these modules, which can be interpreted as complex networks made of intra-network couplings, is achieved through the addition of long-range inter-network ties, therefore behaving globally as a small-world system.

Recent geometrical studies of coupled networks with intra- and inter-network links have revealed novel features never observed for isolated networks [147]. In particular, it has been shown that the overall robustness is reduced [148,149] and the collapse of the system occurs through large cascades of failures [150,151]. Dynamic properties of coupled networks have also been studied [152–159], but the impact of a time delay on their synchronization is still an open issue, which we address here. Typically, the intra- and inter-network couplings have different time scales. For simplicity, we consider the case where intra-network interactions can be considered instantaneous and the inter-network ones have a communication lag that depends on the distance between networks. In particular, we show that, when isolated, the two networks would naturally move in unison. However, when interacting the oscillators in the same network split into two groups, synchronized with different frequencies, leading to breathing synchronization.

6.2 Model

We consider two populations (Γ and Θ) of n Kuramoto oscillators each (Sec. 5.2) interacting through inter and intra-network connections. Each network is a random graph of average degree four. For simplicity, we assume the same frequency $\omega_i \equiv \omega_0$ for all oscillators. We couple each $j \in \Gamma$ with one, and only one, corresponding partner $i \in \Theta$, forming the inter-network couplings. The inter-network coupling is subjected to a time delay τ, corresponding to the time required for information to travel between networks [160]. Previous studies introduced time delay among oscillators of the same population [161, 162]. Here we consider the competition between an *instantaneous* intra-network and a *delayed* inter-network coupling. In a nutshell, the dynamics of oscillators is described by,

$$
\begin{cases}
\dot{\theta}_i = \omega_0 + \sigma_{\text{EX}} \sin\left(\gamma_{j(i)}^{t-\tau} - \theta_i\right) + \sigma_{\text{IN}} \sum_{k=1}^{N} A_{ik}^{\Theta} \sin\left(\theta_k - \theta_i\right) \\
\dot{\gamma}_j = \omega_0 + \sigma_{\text{EX}} \sin\left(\theta_{i(j)}^{t-\tau} - \gamma_j\right) + \sigma_{\text{IN}} \sum_{k=1}^{N} A_{ik}^{\Gamma} \sin\left(\gamma_k - \gamma_j\right)
\end{cases},
$$

$$(6.1)$$

where the superscript $t - \tau$ indicates the instant when the phases are calculated, θ_i and γ_i are the phase of oscillators at the two networks, and σ_{EX} and σ_{IN} are the inter and intra-network couplings, respectively.
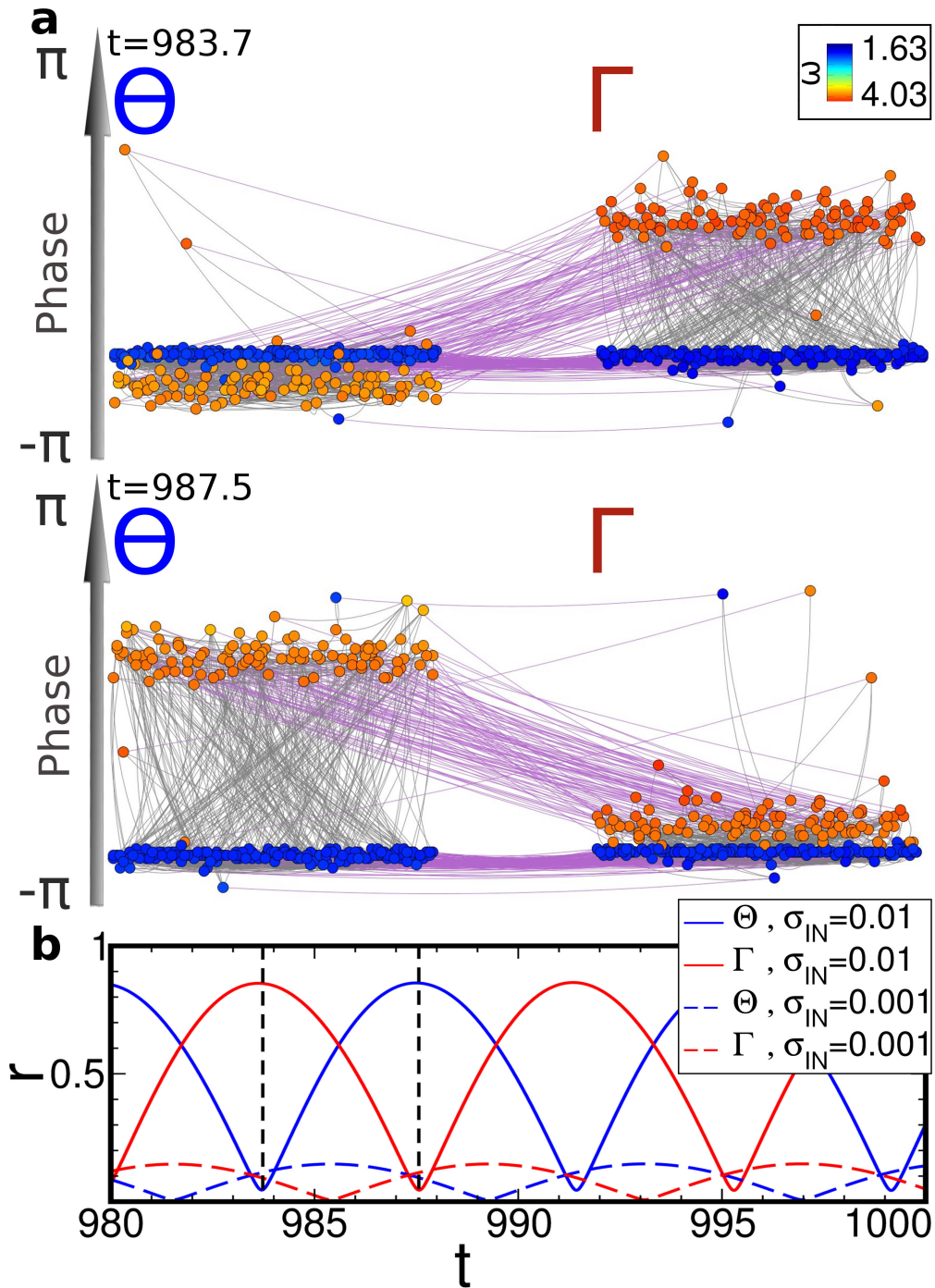
Figure 6.1 – **The interactions between a strongly delayed inter-network coupling and a weak intra-network coupling create two communities of different frequencies in steady state. a,** Snapshot of populations at two different time steps (black dashed vertical lines in b) near the steady state, for $\omega_0 = 1.0$, $\tau = 1.53$, $\sigma_{IN} = 0.01$, and $\sigma_{EX} = 0.5$. The vertical position of each oscillator represents its phase, from $-\pi$ to π, and the color represents the frequencies achieved with oscillators mostly presenting values near the theoretical frequencies (1.63 and 4.63) of the steady state. Superposition of these two communities leads to breathing synchronization. **b,** Time evolution of the order-parameter of populations Θ (blue) and Γ (red) composed of $n = 305$ oscillators each with $\omega_0 = 1.0$, $\tau = 1.53$, and $\sigma_{EX} = 0.5$. Two scenarios of weak intra-network coupling are represented: $\sigma_{IN} = 0.01$ (continuous lines) and $\sigma_{IN} = 0.001$ (dashed lines).

6.3 Results

We observe that two frequency communities emerge within the same network, each synchronized with its mirror in a breathing mode, if two networks are connected with time delay, weak intra-network coupling, and random initial distribution of phases (Fig. 6.1a). In the figure, the color describes the frequency and the vertical position the phase. The frequency synchronization within groups occurs with phase locking. Interestingly, inter-network coupled pairs of nodes oscillate with the same frequency (same color) but might be either in phase or anti-phase (phase shift of π). Consequently, the presence of these two frequency groups affects the perception of the new global oscillatory state, which we call breathing synchronization. Figure 6.1b shows the time evolution of the order parameters r_Θ and r_Γ for each population, quantifying this breathing behavior. For each curve, the maximum corresponds to the instant at which both groups of frequencies are in phase, while the minimum to an anti-phase between groups in the same network. Additionally, since for one frequency there is a phase shift of π between inter-network pairs of nodes, the minimum in one network corresponds, necessarily, to the maximum in the other. Cohesion within each community affects the amplitude of the breathing, as indicated by the order parameters for different values of σ_{IN} in Fig. 6.1b. The weaker the intra-network coupling, the smaller is this amplitude.

The observed breathing behavior is in deep contrast with what is expected for an isolated network ($\sigma_{EX} = 0$). For isolated networks, the classical Kuramoto model is recovered, with frequency and phase synchronization emerging at a critical coupling $\sigma_{IN} = \sigma_{IN}^*$. Above this threshold, a macroscopic fraction of oscillators is synchronized, all with the same frequency and phase. The value of σ_{IN}^* increases with the variance of the natural frequency distribution. Since here we consider the same natural frequency for all oscillators ($\omega_i \equiv \omega_0$), $\sigma_{IN}^* \to 0$. The group of synchronized oscillators has frequency $\omega = \omega_0$ and the order parameter $r_\Theta(t)$ (or $r_\Gamma(t)$) saturates in time at a non-zero steady-state value [19], which is a monotonically increasing function of ($\sigma_{IN} - \sigma_{IN}^*$). Interestingly, in the case of coupled networks, and for sufficient inter-network couplings, none of the two frequencies is ω_0.

To better understand the breathing synchronization, and in particular the emergence of frequency groups, let us consider the case of two coupled oscillators with time delay. The analytic solution obtained by Schuster and
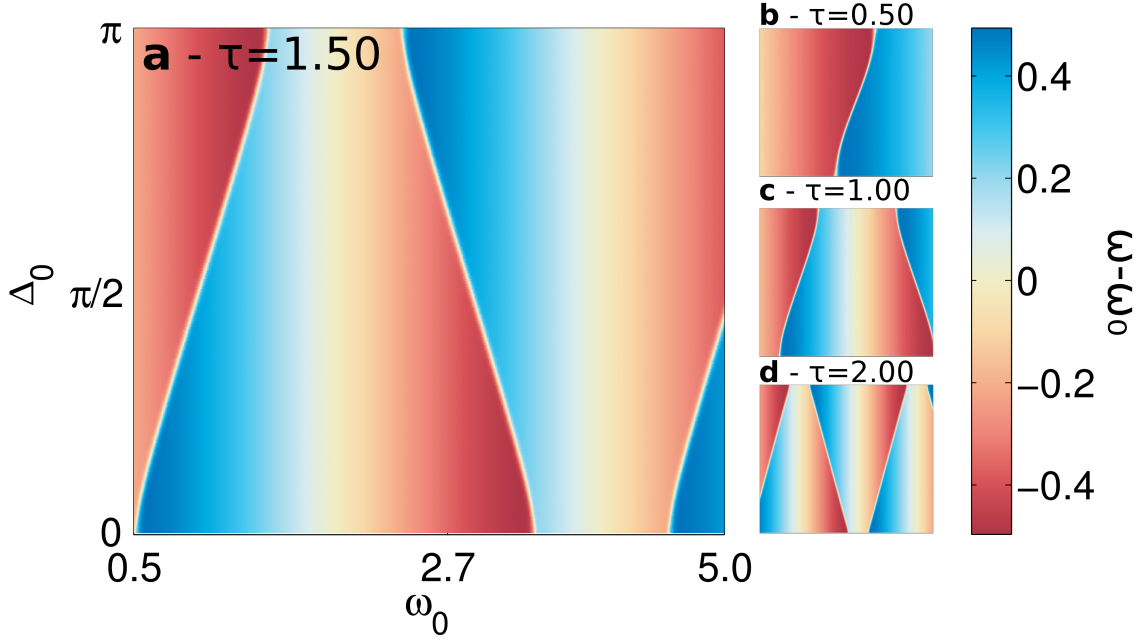
Figure 6.2 – **Steady state frequency achieved for varying initial conditions.** For a combination of Δ_0, the initial phase displacement between inter-network oscillators, and ω_0, we map the final frequency ω achieved in the case of a weak intra-network coupling ($\sigma_{\text{IN}} = 0.01$ and $\sigma_{\text{EX}} = 0.50$). The color scale represents the variable $\omega - \omega_0$. As for our simulations phases are initially randomly distributed, blue and red areas can be seen as the size of the basin of attraction of different frequency solutions. Panels **a-d** show different time delays.

Wagner [160] for this problem indicates that, depending on the initial phase difference between oscillators, the pair can synchronize with different frequencies ω (see Fig. 6.2a-d), which are solutions of,

$$\omega = \omega_0 - \sigma_{\text{EX}} \sin (\omega \tau) . \tag{6.2}$$

In spite of oscillating with the same frequency in the stationary state, the two oscillators might either be in phase, if $\cos(\omega \tau) > 0$, or anti-phase, otherwise. In the case of inter-connected networks, in the limit $\sigma_{\text{IN}} = 0$, the stationary state is expected to include all possible solutions of Eq. 6.2. Surprisingly, our results with a weak σ_{IN} reveal instead two frequency groups with phase locking. Nevertheless, the observed frequencies are consistent with the solution of Eq. 6.2 and are unique with respect to ω_0 and τ. The final frequency of a pair of oscillators only depends of their relative initial displacement.

As we show next, when the internal coupling (σ_{IN}) is further increased, breathing synchronization is no longer stable and each network is synchronized, in one of two other synchronization regimes. In simulations with $\sigma_{\text{EX}} = 1.5$, $\omega_0 = 2.75$ and $\tau = 1.53$, when $\sigma_{\text{IN}} = 0.4$ interactions among os-

Figure 6.3 – **Scatter plot for the matrix of frequency pairs of intra-network neighboring oscillators,** for 500 different re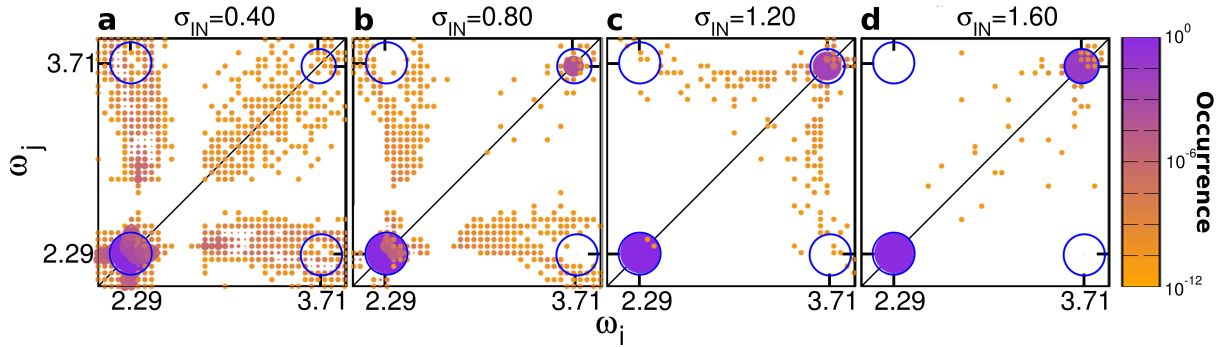alizations of random coupled networks of $n = 750$, with $\omega_0 = 2.75$, $\tau = 1.53$, $\sigma_{EX} = 1.5$, and various σ_{IN}, namely, 0.4 (**a**), 0.8 (**b**), 1.2 (**c**), and 1.6 (**d**). Empty and filled circles are centered on the frequency pairs (ω_i, ω_j) for each (i, j) neighboring nodes within a network, calculated with a 2D binning of size 0.05. The filled circles color, according to a purple-yellow scale, corresponds to their relative occurrence in the dataset: purple circles are the predominant frequencies registered, while yellow circles are less common. For comparison, blue empty circles correspond to results for $\sigma_{IN} = 0$. The size of the symbols is also used for the relative occurrence of each pair.

cillators in the same network become more relevant than the inter-network delayed coupling, and the larger frequency group, in terms of population size, dominates over the smaller one. This competition results in all oscillators synchronizing at the same frequency and the order parameter of each network saturates in time. To systematically study the dependence on σ_{IN}, we analyze the frequency correlation among intra-network neighbors i and j. Figure 6.3 shows the scatter plots of the pair (ω_i, ω_j) for different values of intra-network coupling strengths. The limit $\sigma_{IN} = 0$ is represented by the blue empty circles in all panels and the radius corresponds to the relative population of pairs when considering several samples. In this limit, the oscillators have all one of two possible frequencies, with four possible combinations of frequency pairs. From the relative size of the circles, we observe that the lowest frequency ($\omega \approx 2.3$ for $\omega_0 = 2.75$ and $\tau = 1.53$) is the most populated one. As shown in Fig. 6.3a, for $\sigma_{IN} = 0.4$ most nodes are synchronized with the lowest frequency and therefore a large percentage of the pairs are in the left-bottom corner. Similarly to the Kuramoto model, in this *competing* state, oscillators synchronize at a unique stable frequency ($\omega \approx 2.3$), which is a solution of Eq. 6.2. As σ_{IN} is further increased (Fig. 6.3b-d), due to the strength of the intra-network coupling, each network tends to behave like a *supernode* and, depending on the initial conditions, one of two frequencies is
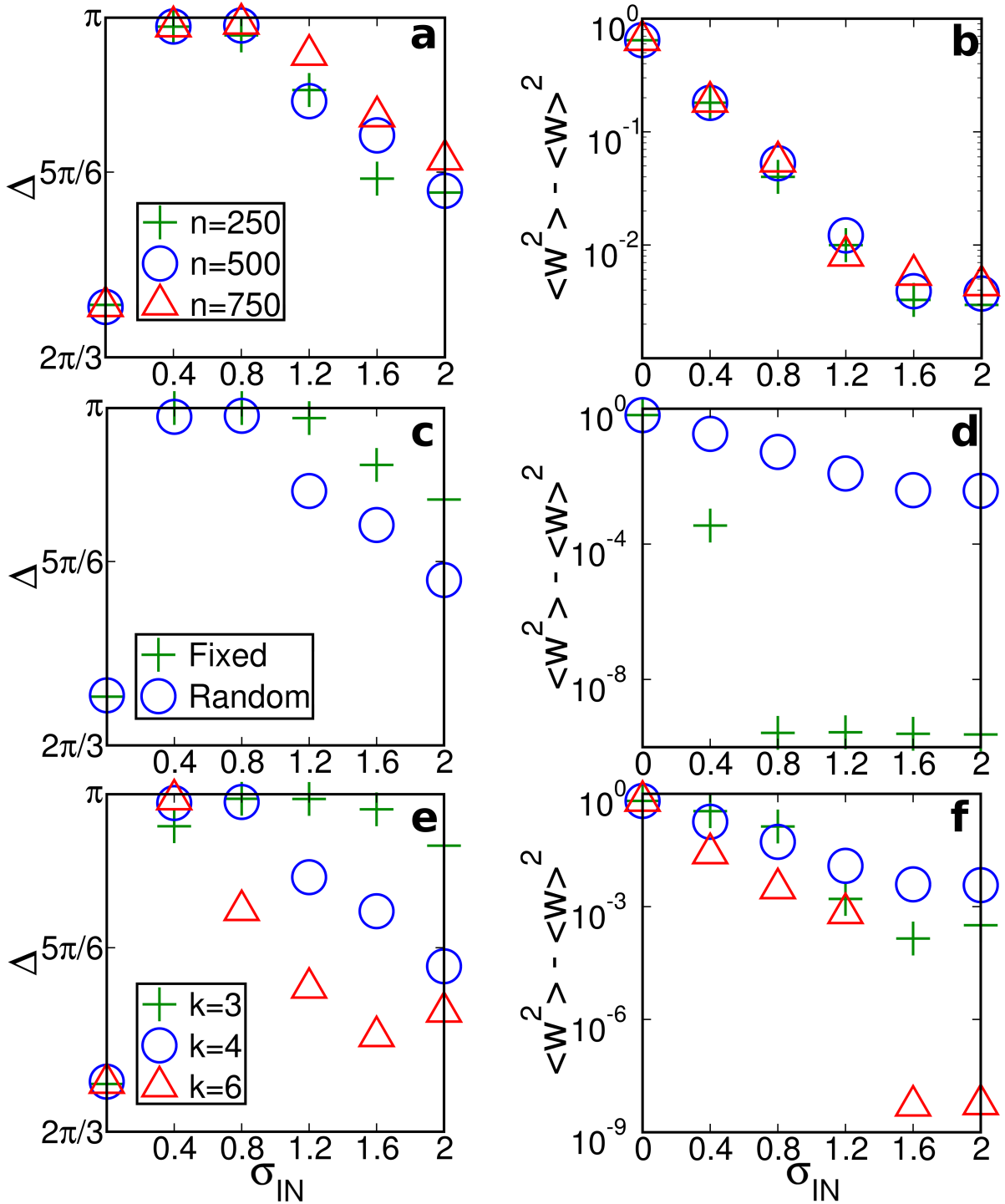
Figure 6.4 – **Dependence of the phase difference and frequency variance on the strength of the intra-network coupling.** Panels on the left column represent the phase difference Δ between pairs of inter-network neighboring oscillators. Panels on the right column represent the average phase variance of the frequency of oscillators in the same network. **a** and **b**, results for networks with different sizes and average degree of four. **c** and **d**, results for networks with node degree fixed at four in comparison with networks with randomly distributed degree of average four. **e** and **f**, results for networks with different average degrees. Each point in all plots represents an average over 500 samples with $\omega_0 = 2.75$, $\tau = 1.53$, and $\sigma_{EX} = 1.5$. Panels **c-f** represent results for networks with 500 nodes. The standard deviations in all cases are smaller than the symbols.
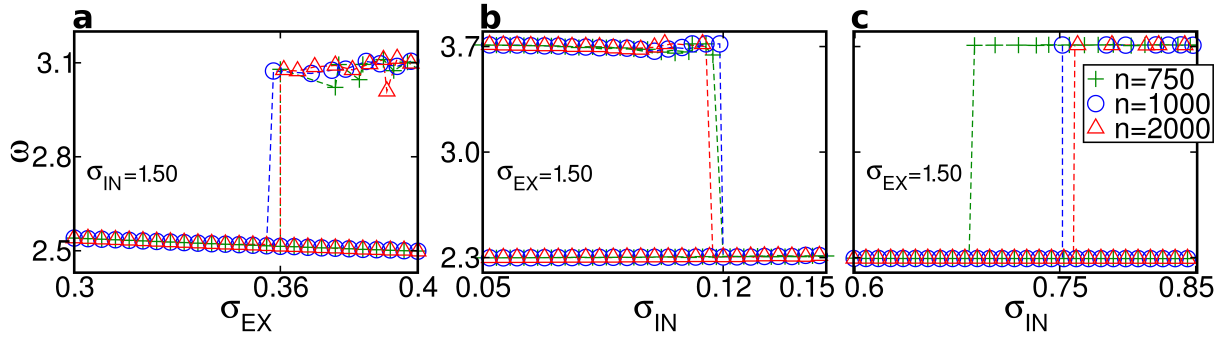
Figure 6.5 – **Frequency communities in transition regions.** For certain combinations of coupling strengths, one can observe abrupt transitions in which global synchronization is lost (Panels **a** and **c**) or recovered (Panel **b**). Points are averages over oscillators in each frequency community. Simulations were performed with 300 samples with $\tau = 1.53$ and $\omega_0 = 2.75$. In Panel **a**, we show results for $\sigma_{IN} = 1.5$, while Panels **b** and **c** are for $\sigma_{EX} = 1.5$.

obtained, which is again a solution of Eq. 6.2. Further analysis across samples (See Fig. 6.4) also shows that the average phase displacement between pairs of oscillators in different networks reaches $\Delta = \pi$ for intermediary values of σ_{IN}, and decreases again once the supernodes are formed (See Fig. 6.4a). For large σ_{IN}, the supernodes can be either in phase or anti-phase and, therefore, the average variance within a network has a value between zero and π (See Fig. 6.4b). Results are qualitatively similar for networks with fixed node degree (See Fig. 6.4c-d) or with different average degree (See Fig. 6.4e-f).

We further analyze the transitions between synchronization regimes. The transitions between regions of one and two stable frequencies are not smooth (See Fig. 6.5). We investigate three regions of the parameter space where transitions between states are expected. All are consistently abrupt, i.e., a small difference in the coupling strength triggers a bifurcation in the possible stable frequencies. Differences in the transition point can be explained in the context of finite size effects. A certain combination of coupling strengths and time delays leads to synchronization at a single stable frequency, but a small difference in any of the parameters can give rise to two stable frequencies, with the possibility of breathing synchronization, and a strong dependence of the final state on the initial conditions.

To summarize the effect of several combinations of parameters, we plot in Fig. 6.6a the phase diagram in the space of the two coupling strengths (σ_{IN} and σ_{EX}). To identify each regime, we compute the amount of oscillators with steady frequency below and above the mean value of possible frequencies (see Appendix D), A_1 and A_2, respectively, over different samples (see

Fig. 6.6b). The color map of the main plot of Fig. 6.6 shows the ratio of these quantities. While the blue area represents the domain of σ_{IN} and σ_{EX} combinations that leads to the smaller frequency, the shades in red represent the two regions where two frequencies can be achieved. Note that the nature of the two synchronization regimes in red is different. The one in the left (lower σ_{IN}) is characterized by the breathing behavior due to the presence of two frequency groups within each network. By contrast, in the supernode regime all nodes within a network are in phase locking, with the same frequency and, therefore, the order parameter is constant in time in the steady state. In Fig. 6.6c, we show the phase boundaries for different time delays. From this, one can also see that the transition between regimes changes substantially for different time delays. Since delay and natural frequency are not multiples, harmonic interactions are considered negligible. Table 6.1 contains a brief summary of all states reported in Fig. 6.6.

6.4 Discussion

The presence of a time delay between two coupled networks of oscillators poses a new challenge to the synchronization risk of the system. We have shown that the interplay between coupling and delay leads to states of either a unique or two possible synchronized frequencies. We have found that, even with a weak intra-network coupling, oscillators within the same network split into two frequency groups. Each group has a mirror one in the other network oscillating at the same frequency. However, depending on their frequency, a group can be either in phase or anti-phase with its mirror in the other network, resulting in breathing synchronization. Also, we show that an arbitrary increase of the intra-network coupling is not an option to achieve phase and frequency synchronization regardless of its initial conditions. In a certain region of the parameter space, the intra-network coupling promotes the formation of two supernodes (one per network), and two frequencies become stable. We have numerically identified the transition regions between regimes. Future works should consider recent advances on group synchronization to analytically study these transitions through linear stability analysis using the master stability function [163, 164].

It is possible to prepare controlled experiments to evaluate the existence of these different regimes in biological systems. For example, the plasmodium *Physarum polycephalum*, an amoeba-like organism consisting of a network of
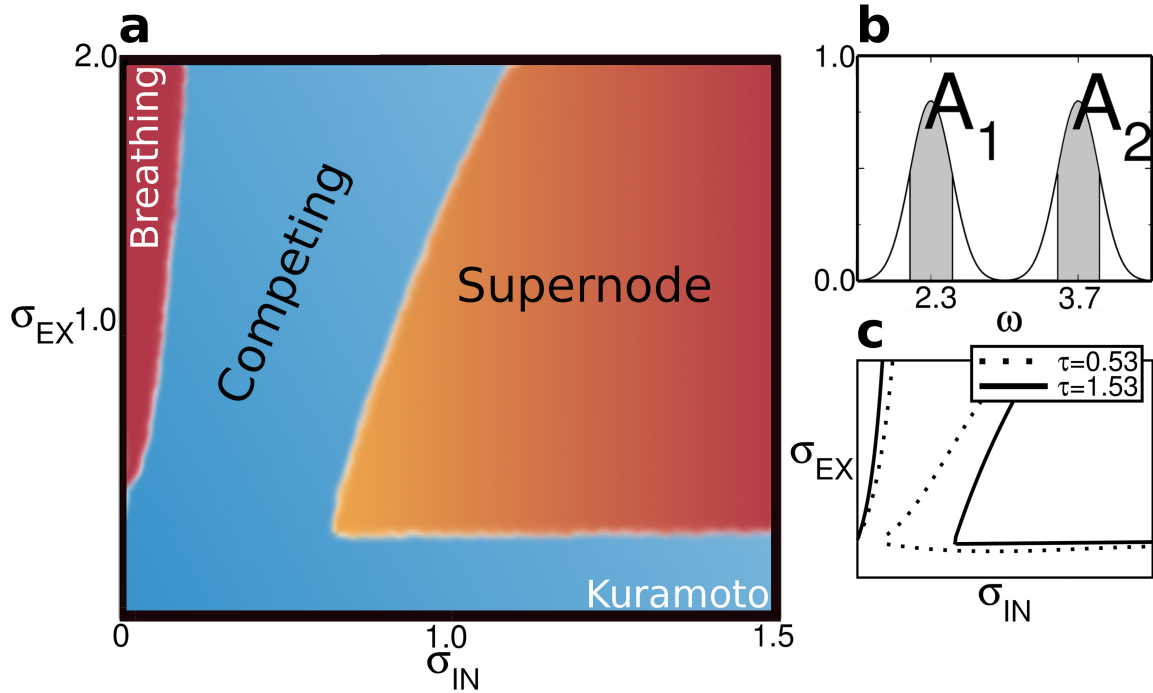
Figure 6.6 – **Phase diagram for delayed coupled networks**. Parameter space of two coupling strengths σ_{EX} and σ_{IN} showing that the prevalence of one frequency over the other changes according to the coupling strengths. **a**, parameter space in which the color of each region represents the occurrence of the two theoretical frequencies: red if two frequencies ($\omega = 2.3$ and $\omega = 3.7$) and blue if only one ($\omega = 2.3$) is observed. Shaded regions mark the boundaries between states. The dominant mechanisms of each region are labeled accordingly: Breathing, Kuramoto [19], Competing, and Supernode states. **b**, example of the histogram used to calculate Panel **a**: areas around the theoretical frequencies are defined (A_1 and A_2) and their ratio used to define the prevalence of only one or two of them. **c**, state boundaries for different time delays. Regions are defined based on simulations over 300 different realizations of random coupled networks of $n = 500$, with $\omega_0 = 2.75$ and $\tau = 1.53$.

.

tubular structures for protoplasm flow, naturally shows periodic variations in its thickness, a necessary feature for its survival. A controlled setup has been prepared by Takamatsu *et al.* where two regions of the same organism have been physically separated by a certain distance with the possibility of fine tuning the communication between them [165, 166]. Depending on the coupling strength and time delay, the two regions have been shown to present phase and anti-phase synchronization of the oscillatory thickness. This is precisely what we find in the regime of strong intra-network coupling. In the experimental study, the focus was only on the regime where the intra-region interaction is much stronger than the inter-region one. Using the same methodology, it is possible to control the intra-region interaction and study

Table 6.1 – **Summary of different synchronization regimes.** A brief description of the properties of all states encountered for $\omega_0 = 2.75$ and $\tau = 1.53$.

State	Frequency groups	Phase shift
Breathing	Two groups: $\omega = 2.29$ (low freq.) and $\omega = 3.71$ (high freq.)	π for low freq. and 0 for high freq.
Competing	One group: $\omega = 2.29$	π
Supernode	One group: $\omega = 2.29$ or $\omega = 3.71$	π if low freq. or 0 if high freq.

the different regimes described here. In particular, it would be of interest to observe oscillations with two different frequencies within the same region due to the communication lag with the other region, resulting in breathing synchronization.

Chapter 7

Conclusion

If one considers the abundance of data, and techniques to handle them, that exists in our technological society, it is rather surprising that studies based on the simplification and abstraction of a system receive so much attention. One could argue that abstractions can be modeled and simulated much faster, or that beauty lies in simplicity. Here however, we defend that a simplification let us focus on the most important mechanisms of the underlying system, avoiding complications that an excessive number of dimensions might bring, and argue that this approach can actually give some contribution to the solution of a problem. More specifically, we show that network theory can give meaningful insights to the risk analysis of real systems. Our findings are mainly divided in two frameworks: static and dynamic models, though we focus, whenever possible, on the interplay between them.

For static networks, we present in Chapter 2 a simple technique that generates robust and efficient networks. Though based on random link swaps and simulated annealing, this method is quite inefficient for larger networks and, in Chapter 3, we present a new rewiring method to modify the network topology, improving its robustness, based on the evolution of the network's largest component during a sequence of targeted attacks. In comparison with previous strategies, our method lowers by several orders of magnitude the computational effort necessary to improve robustness. Our rewiring also drives the formation of layers of nodes with similar degree while keeping a highly modular structure. This "modular onion-like structure" is a particular class of the onion-like structure previously described in the literature. We

66

apply our rewiring strategy to an unweighted representation of the World Air-transportation network (WAN) and show that an improvement of 30% in its overall robustness can be achieved through smart swaps of around 9% of its links.

In Chapter 4 we go one step further into modeling the WAN by adding information about number of passengers, flights, and airports' location. We address how WAN's robustness can profit from local cooperation between airports. For this, we reroute a series of flights among airports within a certain distance, a cooperation range, and describe the improvement of WAN's robustness with distance as a continuum transition. We calculate the critical exponents and identify a critical cooperation range below which improvement is negligible. We propose a network model that falls into the same universality class in which the probability to connect two nodes decays algebraically with their distance. As a by-product of our high level of abstraction, our results impact the whole class of spatially embedded networks.

By using the Kuramoto model of synchronization, we have made relevant contributions to the study of the synchronization risk of networks as well. In Chapter 5 we propose the use of contrarians to suppress undesired synchronization. We perform a comparative study of different strategies, either requiring local or total knowledge, and show that the most efficient one solely requires local information. Our results also reveal that, even when the distribution of neighboring interactions is narrow, significant improvement is observed when contrarians sit at the highly connected nodes.

Extending the problem to the synchronization fragility of interconnected networks, we study in Chapter 6 the synchronization properties of oscillators with a time delay between networks and analyze the dynamics as a function of the couplings and communication lag. We discover a new breathing synchronization regime, where two groups appear in each network synchronized at different frequencies. Each group has a counterpart in the opposite network, one group is in phase and the other in anti-phase with their counterpart. For strong couplings, instead, networks are internally synchronized but a phase shift between them might occur.

Through a handful of examples, our thesis shows that network theory provides a nice foundation on which the risk of several systems can be debunked. Instead of developing over-specialized network models, we use a common vocabulary in our approach and, when possible, common concepts and risk measures (robustness of the largest connected component and the

synchronization order parameter). We show here that it is possible to start a comprehensive risk analysis of distinct systems, from airports to the slime mold, if they are simplified with the help of complex network models. We expect that future works built upon our models study more and diverse systems until the similarities are stronger than the specificities. This will be the first step towards a unified risk analysis theory.

Appendix A

Methods and Parameters of Chapter 3

The World Air-transportation network was retrieved from Amiel et. al [167]. It contains data regarding only international airports and flights. The number of nodes/airports is 1326, with 16001 links, and average degree of 24.13. Artificial networks considered in this work are all BA networks of average degree six.

In Fig. 3.2, Panels **a** and **b** represent sections of the World Air-transportation. In particular, airports in Panel **a** are labeled according to their IATA code. Panel **c** is an average over 100 BA networks of 1000 nodes, the standard deviation of the points being smaller than the symbols.

In Fig. 3.3, the main plot is an average over 100 BA networks of 2005 nodes, which is the same data used for Fig. 3.7. The inset is an average of 100 BA networks of 1000 nodes subjected to 10^5 steps of rewiring (smart or random) in comparison to the original network. In both plots the thickness of the lines is bigger than the standard deviation.

In Fig. 3.4, box plots are used to represent the quantities computed for 100 BA networks, according to: lower whisker for the lowest observation still within 1.5 IQR of the lower quartile, bottom of the box for the lower quartile, white trace for the median, top of the box for the upper quartile, and upper whisker for the highest value still within 1.5 IQR of the upper quartile.

In Fig. 3.5, data is an average of 100 BA networks, with standard deviations smaller than curve thickness.

The main plot of Fig. 3.6 contains the entire World Air-transportation network with rewired links in red and thicker. The location of some airports are slightly altered due to map projection distortions. Inset **b** contains data regarding the Air-transportation network before and after 10^5 smart swaps, for which the smart rewiring curve is an average over 100 different sequences

of random swaps. Insets **c-e** are averages over 100 BA networks of 2005 nodes. In all insets the thickness of the lines is bigger than the standard deviation.

Appendix B

Methods and Parameters of Chapter 4

Figure 4.2 results from the application of 10^4 tentative geo swaps for each value of v in the WAN. Each blue circle is the average over 250 samples while red circles stand for the variance over samples.

In Fig. 4.3, data for the European Power Grid (red) is retrieved from Ref. [168] and the Rail transportation network was manually assembled using public data. The power grid network has 1254 nodes and 1812 links, and the rail network has 39 nodes and 70 links. For continents, the power grid, and the rail network, a total of 10^4 tentative geo swaps are executed for several cooperation range values. The value of v^* is selected as the highest variance point over 100 samples, with error bars representing the values where variance is equal to $0.75\sigma^2(v^*)$. The same data for the continents is used to construct Fig. 4.6, in which symbols are larger than the standard deviation.

In Fig. 4.4, data is based on artificially generated random networks, similar to the ones used for the distance-decay model in Fig. 4.8, but with links randomly assigned without any bias. Each point represent the average over 100 randomly generated networks of 500 nodes. A total of 10^4 tentative geo swaps are executed for several cooperation range values. The value of v^* is selected as the point with highest variance, with error bars representing the values where the variance is equal to $0.75\sigma^2(v^*)$.

In Fig. 4.5, box plots are used to represent the quantities computed for 100 networks, according to: lower whisker (horizontal trace below and on top of the box) for the lowest observation still within 1.5 IQR of the lower quartile (25% percentile of the distribution), bottom of the box for the lower quartile, white trace for the median, top of the box for the upper quartile, and upper whisker for the highest value still within 1.5 IQR of the upper quartile.

In Fig. 4.7, a total of 10^4 tentative geo swaps are executed for several cooperation range values. Each point represents the average over 200 samples,

with symbols being larger than standard deviation in the main panel. The critical cooperation range is defined as $v^* = 240 \pm 10$.

For all panels in Fig. 4.8, a maximum of 10^4 tentative geo swaps are executed for several cooperation ranges. Each point represents the average over 100 samples, with symbols being larger than standard deviation in Panel **c**. The critical cooperation range is defined as $v^* = 240 \pm 10$ km. In Fig. 4.9 the data used is the same from Fig. 4.6 and Fig. 4.8b.

Appendix C

Methods and Parameters of Chapter 5

Equations 5.1, 5.3, and 5.4 have been numerically solved using a fourth order Runge-Kutta method with discrete time steps $\delta t = 0.001$. The complex order parameter was computed in the interval $t \in [90, 100]$ using the average value of Eq. 5.2. For all considered cases, natural frequencies of oscillators have been uniformly distributed between -0.5 and 0.5 and initial phases have also been uniformly distributed between $-\pi$ and π. A coupling strength of $\lambda = 2.0$ has been used. For the Internet and the *C. elegans*, natural frequencies and initial phases have been distributed uniformly between -0.1 and 0.1, and between $-\frac{\pi}{2}$ and $\frac{\pi}{2}$, respectively, and a coupling strength of $\lambda = 4.0$ has been used.

Networks of oscillators have been constructed as undirected ER networks of average degree four, unless otherwise stated. The network of Internet Routers has been analyzed through data retrieved from the Opte Project that represents all the communication among 40028 routers on January 15th of 2005 [123]. Each node of this network is a Router with an associated IP address and the links (edges) are established between two IP address which have communicated at least once. The network of neurons was constructed through data obtained on the WormWeb website [125] and is mostly based on the work by Chen *et al.* [124]. In this network, links have been established whenever an interaction between neurons has been registered, regardless of their type or direction. Other measures regarding these networks are available in Table C.1.

All results have been averaged over several samples. The error bars were omitted in all figures, being smaller than the symbols. For the Internet and the *C. elegans* only the natural frequencies and initial phases change among samples. Panels in Figure 5.1 are constructed using the average value over 100 networks of size $N = 1000$. In Figure 5.2, results are averages over 1000

Network	Nodes	Average Degree	Max Degree
The Internet	40028	2.36	259
C. elegans	283	17.39	115

Table C.1 – Number of nodes, average degree, and maximum degree for network of routers in the Internet and the neural network of the *C. elegans*.

networks of size $N = 1000$, where $\rho = 0.1$ and $\lambda = 1.0$. Figures 5.3 and 5.6 show averages of 5000 networks of size $N = 1000$, 1000 networks of size $N = 5000$, and 600 networks of size $N = 10000$. In Figure 5.4 and 5.5, we represent a single network of $N = 200$ with $\lambda = 1.0$. Figure 5.7 is an average over 1000 networks of size $N = 1000$. For Figure 5.8, Panel **a** is an average over 200 initial distributions of phases and frequencies, and Panel **b** is an average over 10.

Appendix D

Methods and Parameters of Chapter 6

Eq. 6.1 has been numerically solved using a fourth order Runge-Kutta method with discrete time steps $\delta t = 0.003$. The stable frequencies were computed at $t_{max} = 100$, using the difference between phases after one δt step. The natural frequency has been chosen as $\omega_0 = 1.00$ in Fig. 6.1 and $\omega_0 = 2.75$ for Figs. 6.3-6.6. Initial phases of oscillators in all simulations have been sampled from a random uniform distribution between $-\pi$ and π. Different values of ω_0 do not affect qualitatively the results. The same values of δt and t_{max} were adopted for all simulations in this study.

In Fig. 6.1, Panels **a** and **b** are based on one pair of undirected random networks of average degree four and 305 nodes in each. Oscillators in this figure have been simulated for $\tau = 1.53$, $\sigma_{EX} = 1.5$. Panel **a** is based on $\sigma_{IN} = 0.01$.

In Fig. 6.2, Panels **a-d** are an average over 500 samples of $n = 576$ oscillators simulated with $\sigma_{IN} = 0.01$ and $\sigma_{EX} = 0.50$.

In Fig. 6.3, Panels **a-d** contain the simultaneous representation of 500 pairs of random networks of 750 nodes. Color and size of each point represents the relative occurrence in all data. Oscillators in this figure have been simulated for $\tau = 1.53$ and $\sigma_{EX} = 1.5$.

In Fig. 6.5, Panels **a-c** are averages over 300 pairs of random networks of 1000 nodes, 300 pairs of 1500 nodes, and 300 pairs of 1950 nodes. The standard deviation in all cases are smaller than the symbols. To reduce noise, we consider only frequencies with a relative occurrence of more than 10% to calculate averages.

Figure 6.6 is a schematic representation based on the average over 300 pairs of undirected random networks of average degree four and 500 nodes in each. Panel **b** is a graphical representation of the histogram of all stable frequencies. Panel **c** contains the same study for different delays, also averaged

over 300 pairs of undirected random networks of average degree 4 and 500 nodes in each. A cutoff of $\omega = 3.00$, the midpoint of the stable frequencies for $\sigma_{\mathrm{IN}} = 0$, was used to determine the areas A_1 and A_2. Colors in Panel **a** are defined according to the ratio of A_1 and A_2: blue if $log(A_1/A_2) < 4$ and red if $log(A_1/A_2) > 4$, with shades of these colors used to represent the transition regions. To avoid the effect of oscillators that did not reach a stable state by the end of the simulation, we consider only frequencies with a relative occurrence of more than 10%. Oscillators in this figure have been simulated with $\tau = 1.53$ in Panel **a** and $tau = 0.53$ in Panel **c**.

Bibliography

[1] J. M. Ford. *The Final Reflection*. Pocket Books, 1984.

[2] V. H. P. Louzada, N. A. M. Araújo, J. S. Andrade Jr, and H. J. Herrmann. How to suppress undesired synchronization. *Scientific Reports*, 2:658, 2012.

[3] V. H. P. Louzada, F. Daolio, H. J. Herrmann, and M. Tomassini. Smart rewiring for network robustness. *J Comp Netw*, 1:150–159, 2013.

[4] V. H. P. Louzada, N. A. M. Araújo, J. S. Andrade Jr, and H. J. Herrmann. Breathing synchronization in interconnected networks. *Scientific Reports*, 3:3289, 2013.

[5] V. H. P. Louzada, N. A. M. Araújo, T. Verma, Daolio F., H. J. Herrmann, and M. Tomassini. Critical Cooperation Range to Improve Spatial Network Robustness. *Plos ONE*, 10:e0118635, 2015.

[6] V. H. P. Louzada, F. Daolio, H. J. Herrmann, and M. Tomassini. Generating robust and efficient networks under targeted attacks. In Dariusz Król, Damien Fay, and Bogdan Gabryś, editors, *Propagation Phenomena in Real World Networks*, volume 85 of *Intelligent Systems Reference Library*, pages 215–224. Springer, 2015.

[7] N. A. M. Araújo, V. H. P. Louzada, J. S. Andrade Jr, and H. J. Herrmann. Controlling Synchronization in Complex Networks. In *International workshop on Phase Transition, Critical Phenomena and Related Topics in Complex Networks*, page 2. Topologica, vol. 3, 2014.

[8] V. H. P. Louzada, F. M. Lopes, and R. F. Hashimoto. A Monte Carlo Approach to Measure the Robustness of Boolean Networks. In *BCB '12 Proceedings of the ACM Conference on Bioinformatics, Computational Biology and Biomedicine*, pages 696–699, 2012.

[9] Y. Malevergn and D. Sornette. *Extreme financial risks: From dependence to risk management.* Springer Berlin Heidelberg, Berlin, 2006.

[10] T. Maillart and D. Sornette. Heavy-tailed distribution of cyber-risks. *Eur Phys J B*, 75:357–364, 2010.

[11] FOC. *forecasting financial crises, http://www.focproject.eu/.* 2012.

[12] D. Helbing. Globally networked risks and how to respond. *Nature*, 497:51–9, 2013.

[13] P. Erdős and A. Rényi. On the evolution of random graph. *Publ Math Inst Hung Acad Sci*, 5:17–60, 1960.

[14] *A Guide to the Project Management Body of Knowledge (PMBOK Guide).* Project Management Institute, 2013.

[15] *BEA (Bureau Enquetes-Accidents) Accident on 25 July 2000 at La Patte d'Oie in Gonesse (95) to the Concorde registered F-BTSC operated by Air France.* 2000.

[16] D. Sornette. *Critical phenomena in natural sciences: chaos, fractals, self-organization and disorder: concepts and tools.* Springer, Berlin, 2006.

[17] N. A. M. Araújo and H. J. Herrmann. Explosive Percolation via Control of the Largest Cluster. *Phys Rev Lett*, 105:035701, 2010.

[18] S. Vitali, J. B. Glattfelder, and S. Battiston. The network of global corporate control. *Plos ONE*, 6:e25995, 2011.

[19] Y. Kuramoto and I. Nishikawa. Statistical Macrodynamics of Large Dynamical Systems. Case of a Phase Transition in Oscillator Communities. *J Stat Phys*, 49:569–605, 1987.

[20] D. J. Watts. *Small Worlds: The Dynamics of Networks Between Order and Randomness.* Princeton Univ Press, Princeton, 1999.

[21] R. Albert, H. Jeong, and A. Barabasi. Error and attack tolerance of complex networks. *Nature*, 406:378–382, 2000.

[22] D. J. Watts and S. H. Strogatz. Collective dynamics of 'small-world' networks. *Nature*, 393:440–442, 1998.

[23] V. D. Blondel, J. Guillaume, R. Lambiotte, and E. Lefebvre. Fast unfolding of communities in large networks. *J Stat Mech*, P10008, 2008.

[24] M. E. J. Newman. Assortative Mixing in Networks. *Phys Rev Lett*, 89:208701, 2002.

[25] R. Pastor-Satorras, A. Vasquez, and A. Vespignani. Dynamical and correlation properties of the Internet. *Phys Rev Lett*, 87:258701, 2001.

[26] A. Barabási and R. Albert. Emergence of Scaling in Random Networks. *Science*, 286:509–512, 1999.

[27] R. Albert, I. Albert, and G. Nakarado. Structural vulnerability of the North American power grid. *Phys Rev E*, 69:025103, 2004.

[28] A. E. Motter, S. A. Myers, M. Anghel, and T. Nishikawa. Spontaneous synchrony in power-grid networks. *Nat Phys*, 9:1–7, 2013.

[29] P. Kaluza, A. Kölzsch, M. T. Gastner, and B. Blasius. The complex network of global cargo ship movements. *J R Soc Interface*, 7:1093–1103, 2010.

[30] R. Cohen, K. Erez, D. Ben-Avraham, and S. Havlin. Breakdown of the Internet under Intentional Attack. *Phys Rev Lett*, 86:3682, 2001.

[31] J. C. Doyle, D. L. Alderson, L. Li, S. Low, M. Roughan, S. Shalunov, R. Tanaka, and W. Willinger. The "robust yet fragile" nature of the Internet. *P Natl Acad Sci USA*, 102:14497–502, 2005.

[32] P. Mátray, P. Hága, S. Laki, G. Vattay, and I. Csabai. On the spatial properties of internet routes. *Comput Netw*, 56:2237–2248, 2012.

[33] G. L. Mamede, N. A. M. Araújo, C. M. Schneider, J. C. Araújo, and H. J. Herrmann. Overspill avalanching in a dense reservoir network. *P Natl Acad Sci USA*, 109:7191–7195, 2012.

[34] R. Guimerà, S. Mossa, A. Turtschi, and L. A. N. Amaral. The worldwide air transportation network: Anomalous centrality, community structure, and cities' global roles. *P Natl Acad Sci USA*, 102:7794–7799, 2005.

[35] E. Strano, V. Nicosia, V. Latora, S. Porta, and M. Barthélemy. Elementary processes governing the evolution of road networks. *Scientific Reports*, 2:296, 2012.

[36] D. Sornette, F. Deschâtres, T. Gilbert, and Y. Ageon. Endogenous Versus Exogenous Shocks in Complex Networks: An Empirical Test Using Book Sale Rankings. *Phys Rev Lett*, 93:228701, 2004.

[37] F. Schweitzer, G. Fagiolo, D. Sornette, F. Vega-Redondo, A. Vespignani, and D. R. White. Economic networks: the new challenges. *Science*, 325:422–425, 2009.

[38] S. Maslov and K. Sneppen. Specificity and stability in topology of protein networks. *Science*, 296:910–913, 2002.

[39] S. A. Kauffman. Metabolic stability and epigenesis in randomly constructed genetic nets. *J Theor Biol*, 22:437–467, 1969.

[40] C. H. A. Higa, V. H. P. Louzada, T. P. Andrade, and R. F. Hashimoto. Constraint-based analysis of gene interactions using restricted boolean networks and time-series data. *BMC proceedings*, 5(Suppl 2):S5, 2011.

[41] K. Takemoto. Does Habitat Variability Really Promote Metabolic Network Modularity? *Plos ONE*, 8:e61348, 2013.

[42] M. Dhamala, V. Jirsa, and M. Ding. Enhancement of Neural Synchrony by Time Delay. *Phys Rev Lett*, 92:074104, 2004.

[43] F. Lombardi, H. J. Herrmann, C. Perrone-Capano, D. Plenz, and L. De Arcangelis. Balance between excitation and inhibition controls the temporal organization of neuronal avalanches. *Phys Rev Lett*, 108:228703, 2012.

[44] F. Abdelnour, H. U. Voss, and A. Raj. Network diffusion accurately models the relationship between structural and functional brain connectivity networks. *NeuroImage*, 90:335–47, 2014.

[45] N. B. Mota, N. A. P. Vasconcelos, N. Lemos, A. C. Pieretti, O. Kinouchi, G. A. Cecchi, M. Copelli, and S. Ribeiro. Speech graphs provide a quantitative measure of thought disorder in psychosis. *Plos ONE*, 7:e34928, 2012.

[46] V. Latora and M. Marchiori. Efficient Behavior of Small-World Networks. *Phys Rev Lett*, 87:198701, 2001.

[47] D. Kim and A. E. Motter. Resource allocation pattern in infrastructure networks. *J Phys A-Math Theor*, 41:224019, 2008.

[48] R. Louf, P. Jensen, and M. Barthelemy. Emergence of hierarchy in cost-driven growth of spatial networks. *P Natl Acad Sci USA*, 110:8824–9, 2013.

[49] X. F. Wang. Complex Networks: Topology, Dynamics and Synchronization. *Int J Bifucart Chaos*, 12:885–916, 2002.

[50] C. Li and G. Chen. Synchronization in general complex dynamical networks with coupling delays. *Physica A*, 343:263–278, 2004.

[51] D. Huber and L. Tsimring. Cooperative dynamics in a network of stochastic elements with delayed feedback. *Phys Rev E*, 71:036150, 2005.

[52] S. N. Dorogovtsev and J. F. F. Mendes. *Evolution of Networks: From Biological Nets to the Internet and WWW*. Oxford University Press, New York, 2003.

[53] M. E. J. Newman. The Structure and Function of Complex Networks. *SIAM Review*, 45:167–256, 2003.

[54] G. Caldarelli. *Scale-Free Networks: Complex Webs in Nature and Technology (Oxford Finance)*. Oxford University Press, New York, 2007.

[55] P. Holme, B. Kim, C. Yoon, and S. Han. Attack vulnerability of complex networks. *Phys Rev E*, 65:056109, 2002.

[56] A. Sydney, C. Scoglio, M. Youssef, and P. Schumm. Characterizing the Robustness of Complex Networks. *IJITST*, 2:291–320, 2010.

[57] H. J. Herrmann, C. M. Schneider, A. A. Moreira, J. S. Andrade Jr, and S. Havlin. Onion-like network topology enhances robustness against malicious attacks. *J Stat Mech*, P01027, 2011.

[58] C. M. Schneider, A. A. Moreira, J. S. Andrade Jr, S. Havlin, and H. J. Herrmann. Mitigation of malicious attacks on networks. *P Natl Acad Sci USA*, 108:3838–3841, 2011.

[59] S. Kirkpatrick, C. D. Gelatt, and Vecchi M. P. Optimization by Simulated Annealing. *Science*, 220:671–680, 1983.

[60] P. Buesser, F. Daolio, and M. Tomassini. Optimizing the Robustness of Scale-Free Networks with Simulated Annealing. In A. Dobnikar, U. Lotrič, and B. Šter, editors, *Adaptive and Natural Computing Algorithms*, volume 6594, pages 167–176. Springer Berlin Heidelberg, 2011.

[61] D. E. Newman, B. Nkei, B. A. Carreras, I. Dobson, V. E. Lynch, and P. Gradney. Risk Assessment in Complex Interacting Infrastructure Systems. In *Proceedings of the 38th Hawaii International Conference on System Sciences*, pages 1–10, 2005.

[62] V. Spyratos, P. S. Bourgeron, and M. Ghil. Development at the wildland-urban interface and the mitigation of forest-fire risk. *P Natl Acad Sci USA*, 104:14272–6, 2007.

[63] Z. Wu and P. Holme. Onion structure and network robustness. *Phys Rev E*, 84:026106, 2011.

[64] I. Alvarez-Hamelin, L. Dall'Asta, A. Barrat, and A. Vespignani. k-core decomposition: a tool for the visualization of large scale networks. *Adv Neur In*, 18(16), 2005.

[65] D. Helbing. *Systemic Risks in Society and Economics*. Paper prepared for IRGC Workshop on Emerging Risks, 2009.

[66] H. Frank and I. T. Frisch. Analysis and Design of Survivable Networks. *IEEE T Commun Techn*, 18:501–519, 1970.

[67] M. Molloy and B. Reed. A critical point for random graphs with a given degree sequence. *Random Struct Algor*, 6:161–179, 2000.

[68] G. Paul, T. Tanizawa, S. Havlin, and H. E. Stanley. Optimization of robustness of complex networks. *Eur Phys J B*, 38:187–191, 2004.

[69] J. Ash and D. Newth. Optimizing complex networks for resilience against cascading failure. *Physica A*, 380:673–683, 2007.

[70] A. A. Moreira, J. S. Andrade Jr, H. J. Herrmann, and J. Indekeu. How to Make a Fragile Network Robust and Vice Versa. *Phys Rev Lett*, 102:018701, 2009.

[71] K. Rokneddin, J. Ghosh, L. Dueñas-Osorio, and J. E. Padgett. Bridge retrofit prioritisation for ageing transportation networks subject to seismic hazards. *Struct Infrastruct E*, DOI:10.1080/15732479.2011.654230, 2012.

[72] *World in figures: Industries Infrastructure*. The Economist. Acessed on 17th of December of 2012. http://www.economist.com/news/21566563-infrastructure.

[73] *Brazil announces construction of 800 airports*. France 24. Acessed on 17th of December of 2012. http://goo.gl/utAfmu.

[74] *Compromise reached in Zurich airport row*. Swiss-info. Acessed on 17th of December of 2012. http://swissinfo.ch/eng/i.html?cid=33027782&sb=twi.

[75] S. Havlin, D. Y. Kenett, E. Ben-Jacob, A. Bunde, R. Cohen, H. J. Herrmann, J. W. Kantelhardt, J. Kertész, S. Kirkpatrick, J. Kurths, J. Portugali, and S. Solomon. Challenges in network science: Applications to infrastructures, climate, social systems and economics. *Eur Phys J-Spec Top*, 214:273–293, 2012.

[76] Z. Jiang, M. Liang, and D. Guo. Enhancing Network Performance By Edge Addition. *Int J Mod Phys C*, 22:1211–1226, 2011.

[77] A. Zeng and W. Liu. Enhancing network robustness against malicious attacks. *Phys Rev E*, 85:066130, 2012.

[78] T. P. Peixoto and S. Bornholdt. Evolution of Robust Network Topologies: Emergence of Central Backbones. *Phys Rev Lett*, 109:118703, 2012.

[79] T. P. Hayes, J. Saia, and A. Trehan. The Forgiving Graph: a distributed data structure for low stretch under adversarial attack. *Distrib Comput*, 25:261–278, 2012.

[80] J. Wang. Robustness of complex networks with the local protection strategy against cascading failures. *Safety Sci*, 53:219–225, 2013.

[81] L. P. Chi and X. Cai. Structural Changes Caused By Error and Attack Tolerance in Us Airport Network. *Int J Mod Phys B*, 18:2394–2400, 2004.

[82] R. Guimerà and L. A. N. Amaral. Modeling the world-wide airport network. *Eur Phys J B*, 38:381–385, 2004.

[83] W. Li and X. Cai. Statistical analysis of airport network of China. *Phys Rev E*, 69:046106, 2004.

[84] L. Donetti, F. Neri, and M. A. Muñoz. Optimal network topologies: expanders, cages, Ramanujan graphs, entangled networks and all that. *J Stat Mech*, P08007, 2006.

[85] Z. Wu, L. Braunstein, V. Colizza, R. Cohen, S. Havlin, and H. E. Stanley. Optimal paths in complex networks with correlated weights: The worldwide airport network. *Phys Rev E*, 74:056104, 2006.

[86] G. Bagler. Analysis of the airport network of India as a complex weighted network. *Physica A*, 387:2972–2980, 2008.

[87] A. Gautreau, A. Barrat, and M. Barthélemy. Microdynamics in stationary complex networks. *P Natl Acad Sci USA*, 106:8847–52, 2009.

[88] N. Pyrgiotis, K. M. Malone, and A. Odoni. Modelling delay propagation within an airport network. *Transport Res C-Emer*, 27:60–75, 2013.

[89] T. Verma, N. A. M. Araújo, and H. J. Herrmann. Revealing the structure of the world airline network. *Scientific Reports*, 4:5638, 2014.

[90] J. Zhang, X. Cao, W. Du, and K. Cai. Evolution of Chinese airport network. *Physica A*, 389:3922–3931, 2010.

[91] M. Yglesias. *China's Sensible Infrastructure Boom*. Slate. Acessed on 4th of December of 2013. http://goo.gl/wBSA0B.

[92] S. Calder. *Shenzhen airport Terminal Three: Vast, shiny, new and empty? China's latest temple to aviation opens*. The Independent. Acessed on 4th of December of 2013. http://goo.gl/XFMr5L.

[93] *ICAO 2012 Air Transport Results*. Accessed on 18th of June of 2013. http://goo.gl/LCgb5f.

[94] *Flight disruptions cost airlines $1.7bn, says IATA*. BBC News. Last modified on 21th of April of 2010. http://news.bbc.co.uk/2/hi/business/8634147.stm.

[95] J. Patokallio. OpenFlights.org, 2014.

[96] M. Newman. Mixing patterns in networks. *Phys Rev E*, 67:026126, 2003.

[97] A. Barrat, M. Barthélemy, R. Pastor-Satorras, and A. Vespignani. The architecture of complex weighted networks. *P Natl Acad Sci USA*, 101:3747–52, 2004.

[98] M. Newman and M. Girvan. Finding and evaluating community structure in networks. *Phys Rev E*, 69:026113, 2004.

[99] S. Erlander and N. F. Stewart. *The Gravity Model in Transportation Analysis*. VSP, Utrecht, 1990.

[100] D. Balcan, V. Colizza, B. Gonc, H. Hu, J. J. Ramasco, and A. Vespignani. Multiscale mobility networks and the spatial. *P Natl Acad Sci USA*, 106:21484–21489, 2009.

[101] G. Krings, F. Calabrese, C. Ratti, and V. D. Blondel. Urban gravity: a model for inter-city telecommunication flows. *J Stat Mech*, L07003, 2009.

[102] J. M. Kleinberg. Navigation in a small world. *Nature*, 406:845, 2000.

[103] G. Li, S. D. S. Reis, A. A. Moreira, S. Havlin, H. E. Stanley, and J. S. Andrade Jr. Towards Design Principles for Optimal Transport Networks. *Phys Rev Lett*, 104:018701, 2010.

[104] G. D'Agostino and A. Scala, editors. *Networks of Networks: The Last Frontier of Complexity*. Springer, Heidelberg, 2014.

[105] S. H. Strogatz, D. M. Abrams, A. McRobie, B. Eckhardt, and E. Ott. Theoretical mechanics: crowd synchrony on the Millennium Bridge. *Nature*, 438:43–44, 2005.

[106] L. Glass. Synchronization and rhythmic processes in physiology. *Nature*, 410(8):277–284, 2001.

[107] M. L. Kringelbach, N. Jenkinson, S. L. F. Owen, and T. Z. Aziz. Translational principles of deep brain stimulation. *Nat Rev Neurosci*, 8:623–35, 2007.

[108] C. C. McIntyre, M. Savasta, L. K. Goff, and J. L. Vitek. Uncovering the mechanism(s) of action of deep brain stimulation: activation, inhibition, or both. *Clin Neurophysiol*, 115:1239–48, 2004.

[109] J. Volkmann, J. Herzog, F. Kopper, and G. Deuschl. Introduction to the Programming of Deep Brain Stimulators. *Movement Disord*, 17:S181–S187, 2002.

[110] S. Floyd and V. Jacobson. Random early detection gateways for congestion avoidance. *IEEE ACM T Network*, 1:397–413, 1993.

[111] Z. Néda, E. Ravasz, T. Vicsek, Y. Brechet, and A. Barabási. Physics of the rhythmic applause. *Phys Rev E*, 61:6987–6992, 2000.

[112] S. Boccaletti, J. Kurths, G. Osipov, D. L. Valladares, and C. S. Zhou. The synchronization of chaotic systems. *Phys Rep*, 366:1–101, 2002.

[113] A. Pikovsky, M. Rosenblum, and J. Kurths. *Synchronization: A universal concept in nonlinear sciences, Vol. 12*. Cambridge Univ. Press, Cambridge, 2003.

[114] S. H. Strogatz. *The Emerging Science of Spontaneous Order*. Hyperion, New York, 2003.

[115] J. Lü and G. Chen. A Time-Varying Complex Dynamical Network Model and Its Controlled Synchronization Criteria. *IEEE T Automat Contr*, 50:841–846, 2005.

[116] A. E. Motter, C. S. Zhou, and J. Kurths. Enhancing complex-network synchronization. *Europhys Lett*, 69:334–340, 2005.

[117] J. A. Acebrón, L. L. Bonilla, C. J. P. Vicente, F. Ritort, and R. Spigler. The Kuramoto model : A simple paradigm for synchronization phenomena. *Rev Mod Phys*, 77:137–185, 2005.

[118] G. Osipov, J. Kurths, and C. Zhou. *Synchronization in oscillatory networks*. Springer Verlag, New York, 2007.

[119] A. Arenas, A. Díaz-Guilera, J. Kurths, Y. Moreno, and C. Zhou. Synchronization in complex networks. *Phys Rep*, 469:93–153, 2008.

[120] S. Boccaletti. *The synchronized dynamics of complex systems*. Elsevier, Amsterdam, 2008.

[121] A. Barrat, M. Barthelemy, and A. Vespignani. *Dynamical Processes on Complex Networks*. Cambridge Univ. Press, Cambridge, 2008.

[122] V. Nicosia, M. Valencia, M. Chavez, A. Díaz-Guilera, and V. Latora. Remote Synchronization Reveals Network Symmetries and Functional Modules. *Phys Rev Lett*, 110:174102, 2013.

[123] B. Lyon et al. The opte project, http://opte.org, 2003.

[124] B. L. Chen, D. H. Hall, and D. B. Chklovskii. Wiring optimization can relate neuronal structure and function. *P Natl Acad Sci USA*, 103:4723–8, 2006.

[125] N. Bhatla et al. Wormweb, http://wormweb.org, 2009.

[126] D. H. Zanette. Synchronization and frustration in oscillator networks with attractive and repulsive interactions. *Europhys Lett*, 72:190–196, 2005.

[127] H. Hong and S. H. Strogatz. Conformists and contrarians in a Kuramoto model with identical natural frequencies. *Phys Rev E*, 84:046202, 2011.

[128] H. Hong and S. H. Strogatz. Kuramoto Model of Coupled Oscillators with Positive and Negative Coupling Parameters: An Example of Conformist and Contrarian Oscillators. *Phys Rev Lett*, 106:054102, 2011.

[129] W. Wang and J. E. Slotine. On partial contraction analysis for coupled nonlinear oscillators. *Biol Cybern*, 92:38–53, 2005.

[130] C. Castillo-Chavez and F. Brauer. *Mathematical Models in Population Biology and Epidemiology*. Springer Verlag, New York, 2001.

[131] J. Gómez-Gardeñes, S. Gómez, A. Arenas, and Y. Moreno. Explosive Synchronization Transitions in Scale-Free Networks. *Phys Rev Lett*, 106:128701, 2011.

[132] S. Assenza, R. Gutiérrez, J. Gómez-Gardeñes, V. Latora, and S. Boccaletti. Emergence of structural patterns out of synchronization in networks with competitive interactions. *Scientific Reports*, 1:99, 2011.

[133] E. Oh, K. Rho, H. Hong, and B. Kahng. Modular synchronization in complex networks. *Phys Rev E*, 72:047101, 2005.

[134] A. Arenas, A. Díaz-Guilera, and C. J. Pérez-Vicente. Synchronization processes in complex networks. *Physica D*, 224:27–34, 2006.

[135] M. Faloutsos, P. Faloutsos, and C. Faloutsos. On Power-Law Relationships of the Internet Topology. *SIGCOMM*, pages 251–262, 1999.

[136] A. Lancichinetti, M. Kivelä, J. Saramäki, and S. Fortunato. Characterizing the community structure of complex networks. *Plos ONE*, 5:e11976, 2010.

[137] Y. Hu, Y. Nie, H. Yang, J. Cheng, Y. Fan, and Z. Di. Measuring the significance of community structure in complex networks. *Phys Rev E*, 82:066106, 2010.

[138] Y. Liu, J. Slotine, and A. Barabási. Controllability of complex networks. *Nature*, 473:167–73, 2011.

[139] G. Yan, J. Ren, Y. Lai, C. Lai, and B. Li. Controlling Complex Networks: How Much Energy Is Needed? *Phys Rev Lett*, 108:218703, 2012.

[140] V. Volman and M. Perc. Fast random rewiring and strong connectivity impair subthreshold signal detection in excitable networks. *New J Phys*, 12:043013, 2010.

[141] V. Volman, M. Perc, and M. Bazhenov. Gap junctions and epileptic seizures - two sides of the same coin? *Plos ONE*, 6:e20572, 2011.

[142] V. M. Eguíluz, D. R. Chialvo, G. A. Cecchi, M. Baliki, and A. V. Apkarian. Scale-Free Brain Functional Networks. *Phys Rev Lett*, 94:018102, 2005.

[143] J. Lorenz, H. Rauhut, F. Schweitzer, and D. Helbing. How social influence can undermine the wisdom of crowd effect. *P Natl Acad Sci USA*, 108:9020–5, 2011.

[144] C. Duke. Prosperity, complexity and science. *Nat Phys*, 2:426–428, 2006.

[145] S. Boccaletti, V. Latora, Y. Moreno, M. Chavez, and D. Hwang. Complex networks: Structure and dynamics. *Phys Rep*, 424:175–308, 2006.

[146] L. K. Gallos, H. A. Makse, and M. Sigman. A small world of weak ties provides optimal global integration of self-similar modules in functional brain networks. *P Natl Acad Sci USA*, 109:2825–2830, 2012.

[147] J. Gao, S. V. Buldyrev, H. E. Stanley, and S. Havlin. Networks formed from interdependent networks. *Nat Phys*, 8:40–48, 2011.

[148] C. M. Schneider, N. Yazdani, N. A. M. Araújo, S. Havlin, and H. J. Herrmann. Towards designing robust coupled networks. *Scientific Reports*, 3:1969, 2013.

[149] C. M. Schneider, N. A. M. Araújo, and H. J. Herrmann. Algorithm to determine the percolation largest component in interconnected networks. *Phys Rev E*, 87:043302, 2013.

[150] S. V. Buldyrev, R. Parshani, G. Paul, H. E. Stanley, and S. Havlin. Catastrophic cascade of failures in interdependent networks. *Nature*, 464:1025–1028, 2010.

[151] C. D. Brummitt, R. M. D'Souza, and E. A. Leicht. Suppressing cascades of load in interdependent networks. *P Natl Acad Sci USA*, 109:E680–E689, 2011.

[152] C. Li, W. Sun, and J. Kurths. Synchronization between two coupled complex networks. *Phys Rev E*, 76:046204, 2007.

[153] F. Sorrentino and E. Ott. Network synchronization of groups. *Phys Rev E*, 76:056114, 2007.

[154] X. Wu, W. X. Zheng, and J. Zhou. Generalized outer synchronization between complex dynamical networks. *Chaos*, 19:013109, 2009.

[155] Y. Shang, M. Chen, and J. Kurths. Generalized synchronization of complex networks. *Phys Rev E*, 80:027201, 2009.

[156] X. Mao. Stability switches, bifurcation, and multi-stability of coupled networks with time delays. *Appl Math Comput*, 218:6263–6274, 2012.

[157] N. A. M. Araújo, H. Seybold, R. M. Baram, H. J. Herrmann, and J. S. Andrade Jr. Optimal Synchronizability of Bearings. *Phys Rev Lett*, 110:064106, 2013.

[158] A. Cardillo, J. Gómez-Gardeñes, M. Zanin, M. Romance, D. Papo, F. D. Pozo, and S. Boccaletti. Emergence of network features from multiplexity. *Scientific Reports*, 3:1344, 2013.

[159] S. Gómez, A. Díaz-Guilera, J. Gómez-Gardeñes, C. J. Pérez-Vicente, Y. Moreno, and A. Arenas. Diffusion Dynamics on Multiplex Networks. *Phys Rev Lett*, 110:028701, 2013.

[160] H. G. Schuster and P. Wagner. Mutual Entrainment of Two Limit Cycle Oscillators with Time Delayed Coupling. *Prog Theor Phys*, 81:939–945, 1989.

[161] M. K. Yeung and S. H. Strogatz. Time Delay in the Kuramoto Model of Coupled Oscillators. *Phys Rev Lett*, 82:648, 1999.

[162] M. Y. Choi, H. J. Kim, D. Kim, and H. Hong. Synchronization in a system of globally coupled oscillators with time delay. *Phys Rev E*, 61:371–381, 2000.

[163] T. Dahms, J. Lehnert, and E. Schöll. Cluster and group synchronization in delay-coupled networks. *Phys Rev E*, 86:016202, 2012.

[164] C. R. S. Williams, T. E. Murphy, R. Roy, F. Sorrentino, T. Dahms, and E. Schöll. Experimental Observations of Group Synchrony in a System of Chaotic Optoelectronic Oscillators. *Phys Rev Lett*, 110:064104, 2013.

[165] A. Takamatsu, T. Fujii, and I. Endo. Time delay effect in a living coupled oscillator system with the plasmodium of Physarum polycephalum. *Phys Rev Lett*, 85:2026, 2000.

[166] A. Takamatsu, E. Takaba, and G. Takizawa. Environment-dependent morphology in plasmodium of true slime mold Physarum polycephalum and a network growth model. *J Theor Biol*, 256:29–44, 2009.

[167] M. Amiel, G. Mélançon, and C. Rozenblat. Réseaux multi-niveaux: l'exemple des échanges aériens mondiaux de passagers. *Mappemonde*, 79:1–12, 2005.

[168] Q. Zhou and J.W. Bialek. Approximate Model of European Interconnected System as a Benchmark System to Study Effects of Cross-Border Trades. *IEEE T Power Syst*, 20:782–788, 2005.